A COUPLED MODEL FOR RING DYNAMICS, GAS FLOW, AND OIL FLOW THROUGH THE RING GROOVES IN IC ENGINES

by

Ke Jia

B.S. Mechanical Engineering
Huazhong University of Science and Technology, 2006

Submitted to the Department of Mechanical Engineering
in Partial Fulfillment of the Requirements for the Degree of

Master of Science in Mechanical Engineering

at the

MASSACHUSETTS INSTITUTE OF TECHNOLOGY

January 2009

Signature of the Author.....
Department of Mechanical Engineering
January 2009

Certified by.....
Tian Tian
Principal Research Engineer, MIT Energy Initiative
Thesis Supervisor

Accepted by.....
David E. Hardt
Chairman, Department Committee on Graduate Studies

(This page was intentionally left blank)

A COUPLED MODEL FOR RING DYNAMICS, GAS FLOW, AND OIL FLOW THROUGH THE RING GROOVES IN IC ENGINES

by

Ke Jia

Submitted to the Department of Mechanical Engineering
on January, 2009 in Partial Fulfillment of the Requirements for the
Degree of Master of Science in Mechanical Engineering

ABSTRACT

Oil flows through ring/groove interface play a critical role in oil transport among different regions the piston ring pack of internal combustion engines. This thesis work is intended to improve the understanding and modeling capability on this important oil transport mechanism for better analysis in engine oil consumption. A model incorporating ring dynamics, gas flow, and oil flow was developed to study oil transport in the piston ring-pack system. The major new element of this new model is adaptation of a mass conserved two phase oil/gas flow sub-model. Doing so, the present model can describe the oil flows through the ring/groove interface in a consistent manner.

The model was applied to a heavy duty diesel engine at maximum power condition and to a SI engine at engine-braking and moderate load conditions. In the diesel application, the model demonstrates that oil can be released through the second ring/groove interface during second ring flutter and ring/groove interface plays positive role in reducing oil consumption and oil residence time. On the other hand, oil can be pumped up into the top ring groove and combustion chamber through the top ring/groove interface at engine braking conditions in the SI engine. Both applications show that oil flow rate through ring/groove interface is most prominent during the period of the engine cycle when the ring motion and gas pressure exhibit dynamic behaviors, and thus show that the coupling of the ring dynamics and gas/oil flows in the present model is essential to predict the oil pumping through ring/groove interface.

Thesis Supervisor: Tian Tian
Title: Principal Research Engineer, MIT Energy Initiative

(This page was intentionally left blank)

Acknowledgements

First, I would like to express my deepest thanks to my lovely wife Xin Sun and my parents for their support, sacrifice, patience, and most of all, their love throughout these years. Their encouragement has always been the motivation for me to continue my academic journey in this institution.

I would also like to give special thanks to my advisor, Dr. Tian Tian, who contributed to every aspect of my Master and helped me to achieve what I wished for from the entire experience. Dr. Tian Tian, who not only gave me the opportunity to conduct my master studies in MIT, but also supported and guided me consistently through his insightful and broad knowledge. I enjoyed and will remember every single discussion with him, which helped me to solve the problems I encountered and eventually leaded to the achievement of my thesis work. Tian was more than just an advisor, and I consider him a great friend. Furthermore, I would like to thank Professor John B. Heywood, Professor C.C. Mei, Professor Mikic, Borivoje B., Professor Ahmed F. Ghoniem, Dr. Aslan Kasimov and Dr. Matthew Hancock for the course study at MIT. Additionally, I would like to express my gratitude to Leslie Reagan for the tremendous help she provides.

Additionally, I would like to use this opportunity to thank some of the people from the industry sponsors of this project. First of all, I would like to Yoann LeBaratoux from Ferrari. The other sponsors are members of the Consortium on Lubrication in Internal Combustion Engines at MIT. The consortium's current members include: Volvo AB, Mahle GmBh, Renault SA, and PSA Peugeot Citroen. I'd like to thank the representatives from these companies: Remi Rabute, Randy Lunsford, Dr. Rolf-Gerhard Fiedler, Dr. Eduardo Tomanik, Bengt Olson, Fredrik, Stromstedt, and Gabrielle Cavallaro for their input and patience.

The solid engineering background I obtained in Huazhong University of Science and Technology has helped me to confront the difficulties I encountered in the courses and research at MIT. I would therefore be very grateful to the professors I met while attending school here: Professor Sheng Liu, Professor Honghai Zhang, Professor Tielin Shi, and Dr. Yinzhi Gan. Specifically, I sincerely thank Professor Gang Chen, Dr Xiaoman Duan, and Dr. Yuhai Mei for leading me to MIT.

Furthermore, I could not have made it through the past four years without the help of the friends I made while at MIT. First, I should thank Eric Senzer for his effort in my thesis work. My Chinese friends Shen Sheng, Min Xu, Xingyun Ma, Bin Pan, Yajun Fang, Na An, and Ming Dao, were always there when I needed help. My groupmates Jeff Wang, Yong Li, Steve Przesmitzki, Haijie Chen, Fiona McClure, and Dongfang Bai and officemates Yinchun Wang, Lynette Cheah, Vince Costanzo, and Nate Anderson were always there for support and we enjoyed many good times together. Thane Dewitt, Nancy Cook, and Janet Maslow are thanked for various reasons.

Ke Jia 2008

(This page was intentionally left blank)

Table of Contents

List of Figures

List of Tables

(This page was intentionally left blank)

1. Introduction

1.1 Oil Consumption and Blowby and Their Importance

Development of modern automotive engines is driven by three major factors: fuel economy, pollutant engine-out emission, and customer satisfaction [1]. In respect to the growing concern about the environmental impact and energy resource depletion, governments have introduced stricter emission regulations and invested more manpower and funds to improve the fossil fuel utilization and new energy resources development. To meet these requirements, advanced technologies need to be developed for all aspects of engines, including lubrication oil, fuel, and engine components. One such method is the controlling of oil consumption in engines

Reduction of oil consumption is required. Unburned or partially burned oil in the exhaust gases contributes directly to hydrocarbon and particulate emissions of the engines. Moreover, chemical compounds in oil additives can poison and destroy exhaust systems and severely reduce their conversion efficiency and pollutant reducing effectiveness. As one of the most complicated problems in the power cylinder system, oil consumption is still the least understood area although a great deal of effort has been made. Among several paths for oil, the paths along the liner and along the piston are two major ones to consider. Oil transport along the liner is largely determined by the ring-pack lubrication effectiveness, while oil transport along the piston is mainly controlled by the ring dynamics and blow-by gas flow. The demonstration of the interaction between ring performance and oil and gas transport can help to understand the oil transport mechanism and lead to effective ways of reducing the oil consumption.

The oil transport along the ring-pack system is driven by the motion of the piston and piston rings. Sometimes, oil is entrained in blow-by gases, transporting within the ring-pack. There are two major ways for oil to transport along the ring-pack system and be emitted by the engine: oil consumption in the combustion chamber and oil transport under the shear effect of blowby gas. Both are significant sources of engine emissions.

There are two major functions of piston-ring-pack system in internal combustion engines. First, the ring-pack seals the gases in the combustion chamber, thereby minimizing energy losses and emissions. Second, the ring-pack assists in oil transport along the cylinder bore, trading off before providing sufficient oil to reduce friction while keeping oil consumption at a minimum [2]. Therefore the piston-ring-pack is one of the most critical components in the power cylinder system of an internal combustion engine. A typical ring pack is made up of two or three rings, in which the top one or two rings keeps sealing the combustion chamber, and the lowest ring acts as the oil control ring, as shown in Figure 1-1.

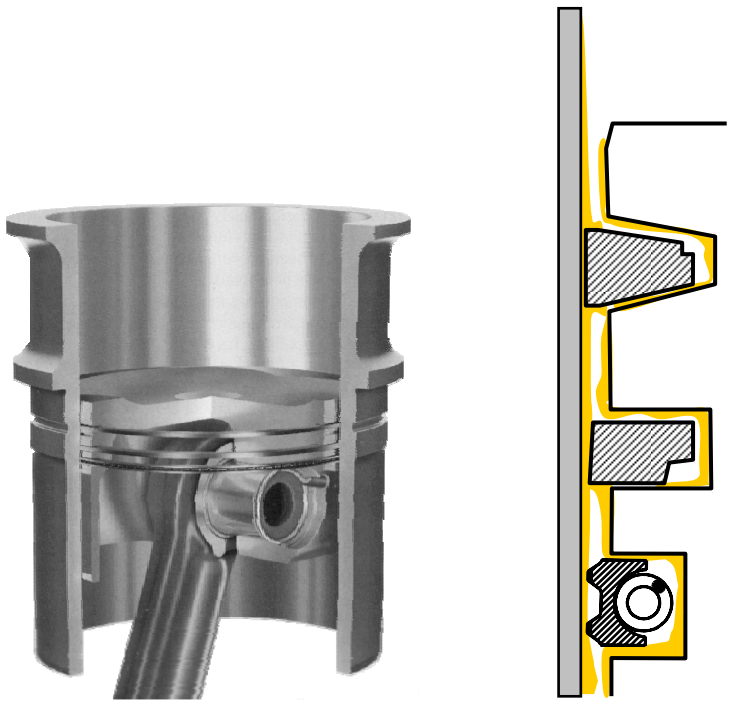

Figure 1-1 Power cylinder system and ring-pack system

Blowby gas flow refers to the undesired gas flow from the combustion chamber to the crankcase. It reduces the efficiency of the engine, and contaminates oil with the combustion products present in the gases. The ring-pack system serves as a channel for blowby gases. As a result, it is important for engine manufacturers and lubricant suppliers to optimize ring-pack system to take into account in controlling oil consumption resulting from blowby gases. Such research pursues to decrease the amount of blow-by gas flow while upholding sufficient lubrication and minimum friction.

Understanding the interaction between ring dynamics and oil and gas transport in ring-pack systems is crucial and needs to be imperatively studied. Extensive studies have been conducted by numerical simulation [3-11] due to the complex nature of oil transport within this system, and the inaccessibility for experimental observation. It is always difficult to accurately observe the oil transport within ring pack, especially in the ring grooves. Among the efforts to investigate the piston ring-pack performance, numerical simulation has been advancing in many aspects and plays a very important role. In the ring-pack system throughout 4-stroke cycle, the following considerations need to present:

- the ring motion and oil and gas transport within the ring grooves
- gas leakage from the ring gaps
- the variation of oil film thickness
- The oil reserved inside the ring grooves and piston lands

It is imperative to develop more comprehensive and quantitative model for the numerical simulation.

1.2 Ring-Pack Systems

The design of ring-pack systems is committed to improving gas sealing ability and oil consumption while factoring in effects on friction loss, wear, and oil degradation. It is increasingly challenging to meet the demands for required performance of the piston ring-pack systems with demands of modern engines. Such demands on the piston, rings, and lubricating oil increase with the specific power output of new engines via higher engine speeds and higher cylinder pressures. Additionally, in the use of lighter materials for components new mechanical and thermal stresses appear, making the ring pack lubrication and sealing performance even more critical.

There is a great desire to continuously decrease the friction and wear in the ring pack [15, 16]. This contrasts with the demand in oil consumption, since a drop in oil consumption can cause higher friction and excessive component wear. The simplest and most effective way to limit both friction and wear is to provide sufficient, but not excessive oil to the critical contact areas, such as the ring running surfaces and ring grooves. However, oil consumption requirements effectively limit the amount of oil supplied to these cars. The ring friction is typically inversely correlated to the ring sealing ability [17], and hence reduced friction may result in increased oil consumption. While sufficient oil is desired, any excess oil may contribute to unnecessary consumption, or result in oil degradation if the oil is exposed to excessive temperatures or contaminants. Thus, demands strive to reach a balance between sufficient lubrication and minimum oil consumption. But before such optimum design changes can be made for engines, a comprehensive understanding of oil’s behavior and interaction with the piston and ring-pack system is necessary.

The first function of the piston rings is to seal the combustion chamber from the crankcase, especially under high combustion gas pressures and the gas pressures on the various lands. There are competing flows at work in oil's transport - blowby gases dragging the oil back down to the crankcase and inertia drawing it up to the combustion chamber [18], as shown in Figure 1-2. Top ring lift-off occurs during the end of the compression and early part of the expansion strokes, throwing oil into the combustion chamber. The ring groove flow area is affected not only by the ring's position, but by the piston tilt varying the clearance between the ring and groove. In doing so, larger flow areas are created for oil or blowby gas, depending on the stroke [19].

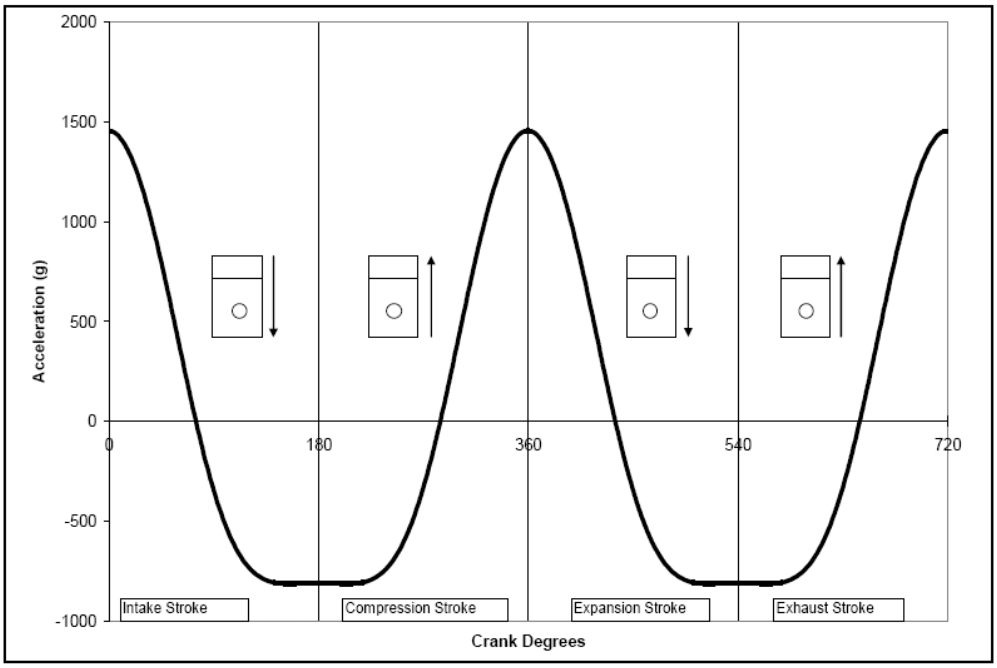

Figure 1-2 Acceleration in G forces as a function of crank position for a Spark-Ignited engine

Typical 2nd rings of Spark-Ignited engines are Napier/Scraper rings that have rectangular base shapes, as shown in Figure 1-3. The purpose is to seal the lower outer periphery and upper inner side of the 2nd ring groove. Both types of rings have a taper face to prevent top edge contact due to a negative dynamic twist. The Napier ring has a positive static twist to control oil pumping into and out of the groove [20], while the Scraper ring with a negative static twist helps induce flutter. The flutter of the 2nd ring has little effect on blowby, but decreases oil consumption. It releases the 2nd land gas to the 3rd land, thus decreasing 2nd land pressure. Although blowby is higher, the design has proven better for oil consumption/control.

Figure 1-3 Design of a Napier/Scraper ring

The OCR controls the liner oil film thickness for lubrication of the top ring running surface. There are three traditional designs for the OCR as shown in Figure 1-4: U-Flex, 2-piece, and 3-piece. The 2-piece OCR releases a large amount of oil at one location on the piston circumference (near its gap) while the U-Flex gaps release a small quantity of

oil at about 50 evenly spaced locations around the circumference of the 3rd land, giving a better oil distribution [21]. Drainage holes in the back of the groove assist in emptying the pools of oil that have accumulated in the groove to the back of the piston and into the crankcase [22]. The OCR experiences a higher pressure on its face profile when compared to the top two rings; it has high ring tension and therefore never experiences radial collapse. However, the OCR can flutter within its groove, causing large quantities of oil to flow towards the top two rings, especially during light load and transient loading conditions [19]. The 3rd land pressure drops quickly when the OCR is pushed down and an upward force from inertia and friction can bring the OCR up again [23].

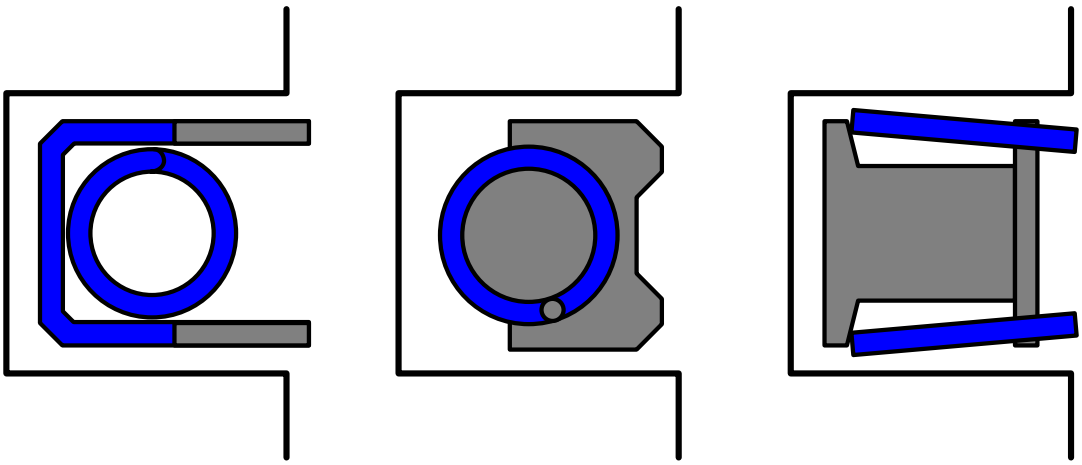

(A) (B) (C)

Figure 1-4 Design of an oil control ring: (A) U-Flex, (B) 2-piece, and (C) 3-piece

1.3 Importance of Oil Transport in Ring-Grooves

The most critical aspect in analyzing oil transport is how much oil is present in the different regions of the ring-pack system. Numerous oil transport processes occur within and between the various regions of the ring-pack systems, such as the piston lands, the ring grooves, and the liner [13].

There are multiple potential driving forces for oil transport between the different regions of the piston ring pack. These driving forces include: 1) Pressure gradients, 2) Inertia forces, 3) Shear stress from gas flow, and 4) Mechanical transport, such as ring/liner and ring/groove relative motion [21,24], which add even more complexity to the system. Pressure gradients and the resulting gas flows greatly vary in amplitude and direction with engine load. Consequently, oil transport is expected to exhibit great variations over the range of potential engine operating conditions.

With a large range of driving forces, oil transport on the piston ring pack becomes very complex and dynamic as the engine operating conditions are changed. The variation of these forces by orders of magnitude creates a situation where small changes in geometry of the rings, grooves, relative angles, piston lands, running surfaces, and thermal deformations all have a significant impact on oil transport and oil consumption. The oil flow and transport in different regions depends on the amount of oil present, and

the amount of oil in different regions is determined by the exchange between regions.

There are three types of pressure forces present in the ring grooves: gas pressure, oil pressure, and asperity contact force. The rings are dynamic in their grooves, moving both axially and circumferentially, as well as having various degrees of twist and waviness [13]. When the ring is away from the piston flank and oil film, there is a pressure driven gas flow between the ring ID and OD. The corresponding pressure distribution can be calculated based on the assumption of fully developed, quasi-steady and locally-parallel flow (Poiseuille flow) [32]. When the ring is in contact with the oil film, the gas flow stops and the oil pressure is generated.

While the ring gaps are permanent paths for gas and oil transport, the channel between the flanks of the rings and grooves can become additional and sometimes predominant paths for gas and oil transport. Understanding the oil and gas transport along the ring and groove clearance needs to resolve several critical processes. First, the ring is moving inside the groove mainly in axial direction with certain amount of dynamic twist. Doing so, the channel between ring and groove flanks vary drastically within a cycle. Second, there is a presence of both gas and oil in the ring/groove clearance channel and one need to resolve a two phase flow for predicting the gas and oil flow rates. Third, all the pressures surrounding the ring/groove clearance, gas/oil flows, and ring dynamics are coupled. The last and the most difficult challenge is to know the oil availability at the boundaries of the ring/groove clearance channel.

The existing model [13] is able to provide a fairly realistic reaction force between the flanks of the rings and grooves as well as the gas mass conservation. However, it is not able to maintain oil mass conservation in the ring/groove clearance. The present work is to adapt a mass conserved two phase flow model for the oil and gas flows in the channel between the flanks of rings and grooves and couple it with ring dynamics and gas flows through other paths. The connection between the oil volume on lands and goove and the BC for oil supply are still not connected due to the complex fluid mechanics involved.

1.4 Objectives of the Thesis Work

As discussed in previous sections, the existing ring-pack system model has some limitations when the oil film thickness in the ring groove has a significant influence on the ring dynamics, and the oil and gas transport. In this study, a coupled model of ring dynamics, oil flow, and gas flow will be created to reveal the interaction between ring motion and two-phase flow. The … understanding of such would therefore provide the direction of engine tests and measurement. The oil film variation in a cycle and its interaction with gas flows will be considered in this model. The quantitative characteristics of the coupled model can demonstrate oil transport in the ring grooves more realistically.

This model is valid for any piston ring-pack system of an internal combustion engine. For this research, it will be applied to a heavy duty diesel engine to show how oil transport through the ring grooves affects the ring dynamics and how the piston and ring parameters influence the oil film thickness and therefore the ring dynamics, oil consumption, and blowby. Another application of this model is the steady and transient analysis under low load in SI engines to understand the physics behind the oil transport inside the ring grooves, which can not be observed by experiments. Both the steady and transient analysis are conducted to demonstrate oil transport inside the ring grooves with different sources of oil supply and oil amount inside the ring grooves, both of which affect oil consumption and blowby

The more detailed understanding of oil transport mechanisms explained in this study should decrease reliance on trial and error design changes. Doing so would allow for more intelligent design choices, and the understanding of engine friction, wear, and oil degradation. With this understanding, improvements can be made.

(This page was intentionally left blank)

2. Modeling Ring-Pack Dynamics and Gas and Oil Flow

2.1 Introduction

The goal of this chapter is to develop an integrated ring pack model that handles the oil flow through the ring/groove interface in a consistent manner. A coupled 2-D ring dynamics and gas and oil transport is adopted to describe the two phase flow (oil and gas) and its influence on ring dynamics and vice verse. This model includes a typical piston ring-pack system with two compression rings and one OCR. This design is typical of most diesel engines and gasoline engines.

The model output includes:

- ring axial and angular positions
- forces and moments on the rings
- oil and gas flow rates between different adjacent regions
- pressure distribution in ring grooves
- Oil film thickness (OFT) distribution in ring grooves
- oil filling speed inside ring grooves
- blowby

In the following sections, the model formulation will be discussed first. Then, the normalized and discretized forms of the governing equations are derived along with boundary condition and other considerations.

2.2 Model Development

2.2.1 Model Formulation

Ring motion is driven by the gas and oil pressure generated in the ring-pack systems and inertia with the reciprocating motion of the piston. The motion is limited by the geometry of piston, grooves, and liner. The force and moment generated on a ring throughout the cycle can be cataloged as:

- pressure of gas and oil two phase flow in the ring grooves
- asperity contact pressure between ring and piston flanks
- friction along the rings and liners
- pressure generated around the ring corners
- inertia force of the rings due to acceleration/deceleration
- moment generated from the radial pressure on the ring running surfaces

The sum of forces acting on each ring is formulated as:

$$\sum F = \int_{x_a}^{x_b} p_{mix} dx + \sum F_{asp} + \sum F_{corner} + F_f + F_{iner} \tag{2.1}$$

Where p_{mix} is the pressure generated from the oil and gas transport in ring grooves, x_a and x_b are the horizontal position of the ring ends, F_{asp} is the asperity contact force between the ring and the upper or lower side of piston flanks, F_{corner} is the force due to the pressure inside the ring grooves and on the piston lands, F_f is the friction force between the ring and liner, and F_{iner} is the inertial force of the ring, as shown in Figure 2-1.

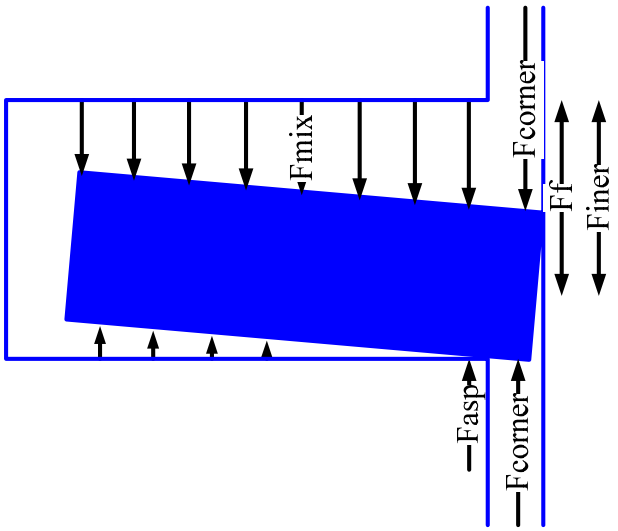

Figure 2-1 Forces acting on a ring

For the moments,

$$\sum M = \int_{x_a}^{x_b} x p_{mix} dx + \sum M_{asp} + \sum M_{corner} + M_f + M_{face} \tag{2.2}$$

where M_{face} is the moment generated from the radial pressure on the ring running surfaces

The two-phase flow in the ring-pack system is through the ring grooves and via the ring gaps. Figure 2-2 demonstrates the schematic for the oil and gas transport in the top ring groove. The oil and gas transport in the second ring groove and oil control ring groove are handled in the same way.

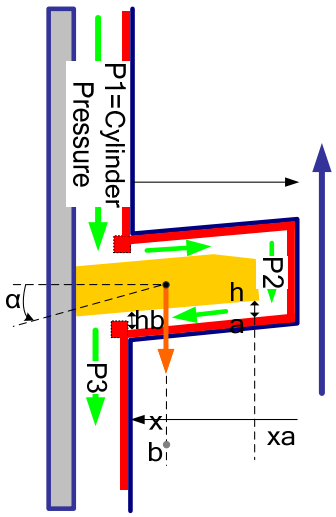

Figure 2-2 Schematic for the oil and gas transport in top ring groove and the definition of coordinate

The ring motion and gas and oil transport are inter-related and they are solved simultaneously

2.2.1.1 Oil inside the Ring Grooves and on the Lands

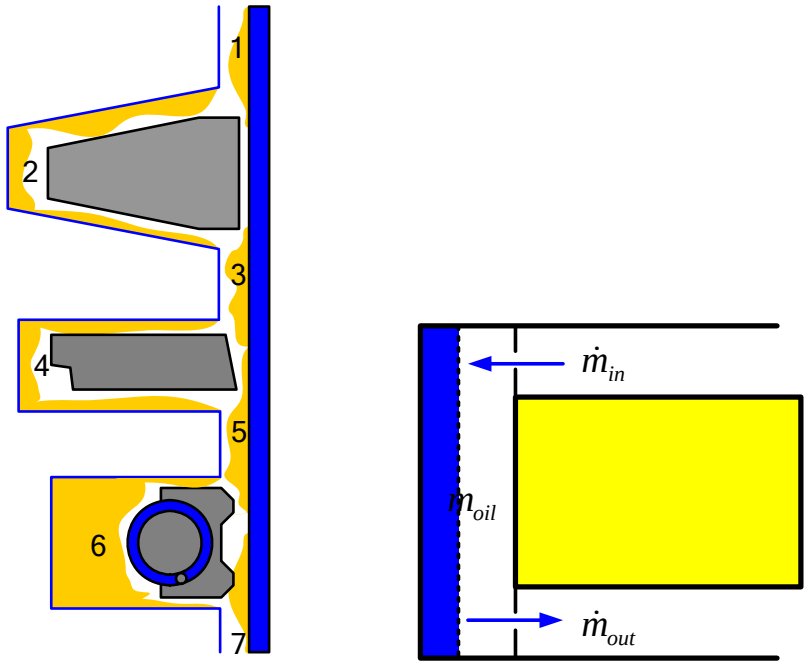

Figure 2-3 Oil in the ring-pack system and transported inside a ring groove

The regions inside the ring groove (2, 4, and 6 as shown in Figure 2-2) and on the piston lands (1, 3, 5, and 7 as shown in Figure 2-3) directly affect the pressure distribution in the whole ring-pack system, and therefore the oil and gas transport and ring dynamics. Each region has presence of both oil and gas, and the change of oil and gas amount in different regions are through transport between regions. As can be detected, the oil inside the ring groove and on the piston lands determines the flow path for the gas transport. The expansion of the bore and piston also changes the volume of these regions.

The oil inside the ring grooves comes from oil transport through the ring grooves and gap flow. The leakage of oil between the ring and liner is one of the major sources of oil present on the piston lands. If the oil flow rate is known, the change rate of the oil volume inside each region can be derived. However, the opposite is not true, i.e., if the amount of oil in each region is known, By applying mass conservation, the variation of oil mass inside the ring groove and on the piston lands is expressed easily, such as the oil transport inside a ring groove:

$$\frac{dm_{oil}}{dt} = \dot{m}_{in} - \dot{m}_{out} \tag{2.3}$$

The variation of both the oil and gas flow through the ring gap is shown,

$$m_{oil} = \rho_{oil} V_{oil} \tag{2.4}$$

$$V_{oil} = V_{region} - V_{gas} + dV_{region} \tag{2.5}$$

The whole volume V_{region} inside the ring groove is divided into region reserves gas and oil separately. For the equations, the oil inside the ring groove is related to the gas transport through the grooves and gap. dV_{region} is the variation of the whole volume after considering the bore expansion effect.

When the engine is running under high load and speed, oil transport in the ring grooves is major source for the oil inside the ring grooves and on the piston lands. Under low load and speed, gap flow plays an important role. However, if the ring collapses due to the lower pressure inside ring grooves and higher land pressure, the leakage of oil flow between the ring and liner becomes the major oil source.

2.2.1.2 Oil Pumping between a Ring and Its Groove

The influence of the radial motion of the rings is neglected compared with the lift and twist motion of the rings, therefore the Reynolds equation

$$\frac{\partial h}{\partial t} = \frac{1}{12\mu}\frac{\partial}{\partial x}\left(h^3 \frac{\partial P}{\partial x}\right) \tag{2.6}$$

is modified to extend its applications to two phase flow in the ring grooves, as shown in Figure 2-4. In this work, it is assumed that the oil in the partial film region evenly attaches to both the surface of upper and lower flanks of the piston grooves. The shear force applied by the gas flow on the oil film is also taken into account, as shown in Figure 2-5.

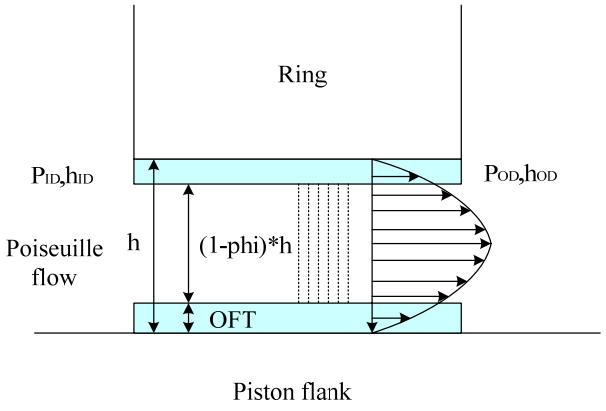

Figure 2-4 Schematic of two phase flow in a ring groove

To describe the two phase flow in the ring grooves, an extra parameter, ϕ, is introduced to represent the volume ratio of the oil in the ring grooves [39].

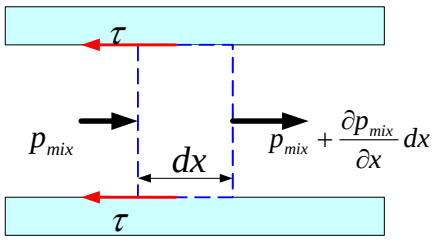

Figure 2-5 Schematic of gas dragging effect on oil film

For oil

$$\frac{\partial(\phi h\rho_{oil})}{\partial t} = \frac{\partial}{\partial x}[\frac{1}{12\mu_{oil}}\rho_{oil}(\phi h)^3\frac{\partial p_{mix}}{\partial x} - \frac{\tau(\phi h)^2}{4\mu_{oil}}] \tag{2.7}$$

where

$$\tau = -\frac{(1-\phi)h\rho_{oil}}{2}\frac{\partial p_{mix}}{\partial x} \tag{2.8}$$

From equations (2.7) and (2.8), we obtain

$$\frac{\partial(\phi h\rho_{oil})}{\partial t} = \frac{\partial}{\partial x}[\frac{1}{24\mu_{oil}}\phi^2(3-\phi)h^3\rho_{oil}\frac{\partial p_{mix}}{\partial x}] \tag{2.9}$$

The form of (2.9) can be simplified into

$$\frac{\partial(\phi h\rho_{oil})}{\partial t} = \frac{\partial}{\partial x}[\frac{1}{12\mu_{oil}}\phi_c h^3\rho_{oil}\frac{\partial p_{mix}}{\partial x}] \tag{2.10}$$

where $\phi_c = \frac{1}{2}\phi^2(3-\phi)$

For the gas, the Reynolds equation is modified into

$$\frac{\partial[(1-\phi)h\rho_{air}]}{\partial t} = \frac{\partial}{\partial x}[\frac{1}{12\mu_{air}}\rho_{air}(\phi h)^3\frac{\partial p_{mix}}{\partial x}] \tag{2.11}$$

Combined with the idea gas equation

$$\rho_{air} = \frac{p_{mix}}{RT} \tag{2.12}$$

The final equation of the gas transport in the ring grooves is

$$\frac{\partial[(1-\phi)hp_{mix}]}{\partial t} = \frac{\partial}{\partial x}[\frac{1}{12\mu_{air}}p_{mix}(1-\phi)^3h^3\frac{\partial p_{mix}}{\partial x}] \tag{2.13}$$

2.2.1.3 Asperity Contact between Ring and Piston Flanks

When a ring approaches the piston flank sufficiently enough, there is an asperity contact force on the ring and the piston flank, as shown in Figure 2-6.

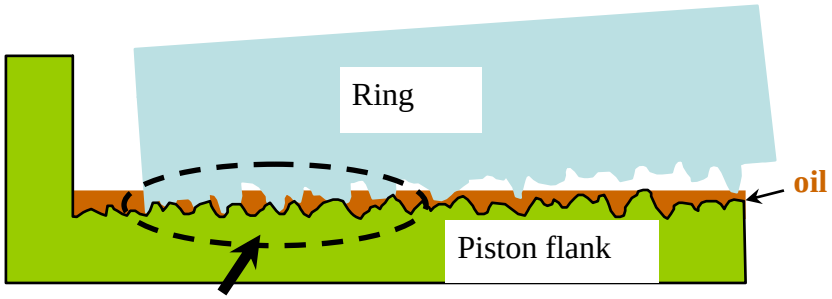

Figure 2-6 Asperity contact between ring and groove

With Greenwood & Tripp's method [34], the asperity contact pressure between the ring and piston flank is computed. The horizontal position of both ends of the contact region, x_{c1} and x_{c2}, are derived from the lift of the ring center and ring twist angle as following:

$$\begin{cases} x_{c1} = X_1 \\ x_{c2} = \min\left(\dfrac{4\sigma - h_0}{\alpha}, X_2\right) \end{cases} \quad \text{if} \quad \alpha > 0 \tag{2.14a}$$

$$\begin{cases} x_{c1} = \max\left(\dfrac{4\sigma - h_0}{\alpha}, X_1\right) \\ x_{c2} = X_2 \end{cases} \quad \text{if} \quad \alpha < 0 \tag{2.14b}$$

Where X_1 and X_2 are the horizontal positions of the ring ends in the coordinate shown in Figure 2-2, α is the ring twist angle, h_0 is the normal clearance between a ring and the groove it approaches to, and σ is the combined surface roughness.

The force and moment generated by asperity contact pressure are expressed with the fitting formula of Hu, et al. [35] and with the Gaussian distribution assumed:

$$F^{asp} = K_C \int_{x_{c1}}^{x_{c2}} \left(4 - \frac{h_0 + \alpha x}{\sigma}\right)^z dx \tag{2.15}$$

$$M^{asp} = K_C \int_{x_{c1}}^{x_{c2}} x\left(4 - \frac{h_0 + \alpha x}{\sigma}\right)^z dx \tag{2.16}$$

Where K_C is a parameter related to material properties and contact form of the rings and piston flanks.

2.2.1.4 Gas Flow through a Ring Gap

Complex flow phenomena happen around the ring gap, especially when the oil flow is blocked in the ring grooves. Since it rarely happens with the model of the two phase oil and gas flow in the ring grooves, the criteria for the oil blockage is set by the ratio between the oil and gas in the ring grooves, ϕ, and the real clearance for the two phases to go through in the ring grooves.

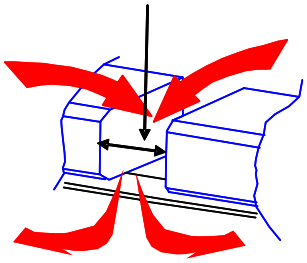

Figure 2-7 Illustration of the ring gap

A simplified model is applied for the gas flow through a ring gap because the detail fluid analysis is beyond the scope of this study. The geometry of the gap and flow between the ring groove and piston lands through the gap are shown in Figure 2-7. The pressure inside the gap is assumed the same as that inside the ring grooves. The mass flow rates of the gas transport between the regions of groove and piston lands through the gaps can be expressed by isentropic orifice flow [36]:

$$\dot{m}_{gap} = \frac{C_D A_{gap} p_U}{\sqrt{RT_U}} f_m \tag{2.17}$$

where

$$f_m = \begin{cases} \gamma^{\frac{1}{2}} \left(\frac{2}{\gamma+1} \right)^{\frac{\gamma+1}{2(\gamma-1)}} & \frac{p_D}{p_U} \le \left(\frac{2}{\gamma+1} \right)^{\frac{\gamma}{\gamma-1}} \\ \left(\frac{p_D}{p_U} \right)^{\frac{1}{\gamma}} \left\{ \frac{2\gamma}{\gamma-1} \left[1 - \left(\frac{p_D}{p_U} \right)^{\frac{\gamma-1}{\gamma}} \right] \right\}^{\frac{1}{2}} & \frac{p_D}{p_U} > \left(\frac{2}{\gamma+1} \right)^{\frac{\gamma}{\gamma-1}} \end{cases} \tag{2.18}$$

and

$$C_D = 0.85 - 0.25 \left(\frac{p_D}{p_U} \right)^2 \tag{2.19}$$

As mentioned, the gap flow influences the pressure in different regions in the ring-pack system, and therefore the ring dynamics and oil and gas transport in the ring

grooves.

2.2.1.5 Other Considerations

The detailed geometric configuration of the ring and piston are considered, such as keystone and tilt of the ring and piston flanks, hook, chamfer, and cut of the corner on both the ring and piston flank. When the engine is in operation, the bore size and piston size may vary with their axis motion due to thermal stress and deformation [13], which is different from that under cold condition. Consequently, the clearance between the ring and its piston flanks, the ring gap areas, and the volume inside the ring grooves and on the piston lands may vary from the cold geometry accordingly. The influence of these considerations will be shown in Chapters 3 and 4.

2.2.2 Governing Equations

Based on mass conservation and Newton's second law, equations are formulated for $p_2, p_3, p_4, p_5, h_{r,i}, \alpha_{r,i}, \dot{h}_{r,i}, \dot{\alpha}_{r,i}, \dot{m}^l_{oil,i}, \dot{m}^u_{oil,i}, \phi^l_{i,j}, \phi^u_{i,j}, p^l_{mix,i,j}, p^u_{mix,i,j}$

$$\frac{V_2}{\pi BRT_2}\frac{dp_2}{dt} = \dot{m}_{12} - \dot{m}_{23} \tag{2.20a}$$

$$\frac{V_3}{\pi BRT_3}\frac{dp_3}{dt} = \dot{m}_{13} + \dot{m}_{23} - \dot{m}_{35} - \dot{m}_{34} \tag{2.20b}$$

$$\frac{V_4}{\pi BRT_4}\frac{dp_4}{dt} = \dot{m}_{34} - \dot{m}_{45} \tag{2.20c}$$

$$\frac{V_5}{\pi BRT_5}\frac{dp_5}{dt} = \dot{m}_{35} + \dot{m}_{45} - \dot{m}_{56} \tag{2.20d}$$

$$\begin{aligned}&\frac{m_{r,i}}{\pi B}\frac{d^2h_{r,i}}{dt^2} = \sum_{j=1}^{N} p^u_{mix,i,j}\Delta x + \int p^u_{asp,i}dx + C_{dyn}p^u_{dyn} + F_{rl,i} \\ &- \sum_{j=1}^{N} p^l_{mix,i,j}\Delta x - \int p^l_{asp,i}dx - C_{dyn}p^l_{dyn} + F_{iner,i}\end{aligned} \tag{2.20e}$$

$$\begin{aligned}&\frac{I_{r,i}}{\pi B}\frac{d^2\alpha_{r,i}}{dt^2} = \sum_{j=1}^{N} x_j p^u_{mix,i,j}\Delta x + \int xp^u_{asp,i}dx + C_{dyn}\int xp^u_{dyn}dx \\ &+ \sum_{j=1}^{N} x_j p^l_{mix,i,j}\Delta x + \int xp^l_{asp,i}dx + C_{dyn}\int xp^l_{dyn}dx + F_{rl,i}d_i \\ &+ M_{face,i} - T_{r,i}\left(\alpha_{r,i} - \alpha_{0,i}\right)\end{aligned} \tag{2.20f}$$

$$\dot{h}_{r,i} = \frac{dh_{r,i}}{dt} \tag{2.20g}$$

$$\dot{\alpha}_{r,i} = \frac{d\alpha_{r,i}}{dt} \tag{2.20h}$$

$$\dot{m}^l_{oil,i} = \frac{dm^l_{oil,i}}{dt} \tag{2.20i}$$

$$\dot{m}^u_{oil,i} = \frac{dm^u_{oil,i}}{dt} \tag{2.20j}$$

$$\frac{\partial\left[\phi^l_{i,j}h^l_{r,i,j}\rho^l_{oil,i}\right]}{\partial t} == \frac{\partial}{\partial x}\left[\frac{1}{12\mu_{oil}}\phi^l_{c,i,j}{h^l_{r,i,j}}^3\rho^l_{oil,i}\frac{\partial p^l_{mix,i,j}}{\partial x}\right] \tag{2.20k}$$

$$\frac{\partial\left[\phi^u_{i,j} h^u_{r,i,j} \rho^u_{oil,i}\right]}{\partial t} == \frac{\partial}{\partial x}\left[\frac{1}{12\mu_{oil}} \phi^u_{c,i,j} h^{u\ 3}_{r,i,j} \rho^u_{oil,i} \frac{\partial p^u_{mix,i,j}}{\partial x}\right] \quad (2.20l)$$

$$\frac{\partial[(1-\phi^l_{i,j}) h^l_{r,i,j} p^l_{mix,i,j}]}{\partial t} = \frac{\partial}{\partial x}\left[\frac{1}{12\mu_{air}} p^l_{mix,i,j} (1-\phi^l_{i,j})^3 h^{l\ 3}_{r,i,j} \frac{\partial p^l_{mix,i,j}}{\partial x}\right] \quad (2.20m)$$

$$\frac{\partial[(1-\phi^u_{i,j}) h^u_{r,i,j} p^u_{mix,i,j}]}{\partial t} = \frac{\partial}{\partial x}\left[\frac{1}{12\mu_{air}} p^u_{mix,i,j} (1-\phi^u_{i,j})^3 h^{u\ 3}_{r,i,j} \frac{\partial p^u_{mix,i,j}}{\partial x}\right] \quad (2.20n)$$

Table 2-1 Nomenclature of governing equations

$\phi^l_{i,j}$	the ratio between oil and air in two-phase flow of the lower ring/groove clearance of the *ith* ring at the *jth* grid point, $i = 1,2,3$, $j = 1, N$
$\phi^u_{i,j}$	the ratio between oil and air in two-phase flow of the upper ring/groove clearance of the *ith* ring at the *jth* grid point, $i = 1,2,3$, $j = 1, N$
$h^l_{r,i,j}$	height of the lower ring/groove clearance of the *ith* ring at the *jth* grid point, $i = 1,2,3$, $j = 1, N$
$h^u_{r,i,j}$	height of the upper ring/groove clearance of the *ith* ring at the *jth* grid point, $i = 1,2,3$, $j = 1, N$
$p^l_{mix,i,j}$	two-phase flow pressure acting on the lower flank of the *ith* ring at the *jth* grid point, $i = 1,2,3$, $j = 1, N$
$p^u_{mix,i,j}$	two-phase flow pressure acting on the upper flank of the *ith* ring at the *jth* grid point, $i = 1,2,3$, $j = 1, N$
B	engine bore size
$F_{iner,i}$	inertia force of the *ith* ring due to piston acceleration/deceleration, $i = 1,2,3$
$F_{rl,i}$	friction on the *ith* ring running surface between ring and liner, $i = 1,2,3$

$h_{r,i}$	lift of the ith ring's center of gravity, $i=1,2,3$
$I_{r,i}$	moment of inertia of the ith ring, $i=1,2,3$
$M_{face,i}$	moment on ith ring from the radial pressure on the inside and outside surfaces, $i=1,2,3$
$\dot{m}_{Di(i+1),i}$	mass flow rate into the ring/groove clearance between region i and $(i+1)$ from region i, $i=1,6$
$\dot{m}_{Di(i+1),(i+1)}$	mass flow rate into the ring/groove clearance between region i and $(i+1)$ from region $(i+1)$, $i=1,6$
$\dot{m}_{ij}$	mass flow rate from region i to region j, $i=1,6$, $j=2,7$
$m_{r,i}$	mass of the ith ring, $i=1,2,3$
p_i	gas pressure of region i, $i=1,7$
p_{oil}	pressure generated in the oil between a ring and its groove
$p^{l}_{gas,i}$	gas pressure acting on the lower flank of the ith ring, $i=1,2,3$
$p^{l}_{oil,i}$	oil pressure acting on the lower flank of the ith ring, $i=1,2,3$
$p^{l}_{asp,i}$	asperity contact pressure acting on the lower flank of the ith ring, $i=1,2,3$
$p^{u}_{gas,i}$	gas pressure acting on the upper flank of the ith ring, $i=1,2,3$
$p^{u}_{oil,i}$	oil pressure acting on the upper flank of the ith ring, $i=1,2,3$
$p^{u}_{asp,i}$	asperity contact pressure acting on the upper flank of the ith ring, $i=1,2,3$
T_i	average temperature of region i, $i=1,7$
$T_{i,j}$	average temperature of the ring/groove clearance between region i and j, $i,j=1,7$
$T_{r,i}$	torsional resistance of the ith ring, $i=1,2,3$

V_i	volume of region i, $i=1,7$
$\alpha_{r,i}$	twist angle of the ith ring, $i=1,2,3$
$\alpha_{0,i}$	static twist angle of the ith ring, $i=1,2,3$

The height of the clearance between ring and its piston flanks in every discretized grid is related to the lift of the ring center as following. For the clearance between both the ring surface and lower piston flank

$$h^{l}_{r,i,j} = h_{r,i} - h_{ring,i}/2 + \alpha_{r,i} x_j \tag{2.21}$$

For the clearance between both the ring surface and upper piston flank

$$h^{u}_{r,i,j} = h_{groove,i} - h_{ring,i}/2 - h_{r,i} - \alpha_{r,i} x_j \tag{2.22}$$

(N is the number of grid points at respectively upper and lower ring/groove clearances of both rings, and N_j is the jth one, then

$$x_j = \frac{(x_b - x_a)N_j}{N} - \frac{x_b - x_a}{2} = \frac{(x_b - x_a)(2N_j - 1)}{2N} \tag{2.23}$$

where $j = 1, N$)

The bounds of the integrals are determined by the instantaneous positions and the moving directions of the rings as described of the rings. The torsional stiffness $T_{r,i}$ for a section of a ring is expressed as:

$$T_{r,i} = E_i b_i^3 \ln\left(\frac{D_{O,i}}{D_{I,i}}\right) \Big/ 3\left(D_{O,i} + D_{I,i}\right) \tag{2.24}$$

Where

Table 2-2 Nomenclature of torsional stiffness computation

b_i	width of the ith ring, $i=1,2,3$
$D_{O,i}$	outer diameter of the ith ring, $i=1,2,3$
$D_{I,i}$	inner diameter of the ith ring, $i=1,2,3$
E_i	elastic modulus of the ith ring, $i=1,2,3$

2.3 Computation Algorithm

2.3.1 Normalization of the System

Variables and governing equations are normalized as the following:

$$p_i, (i = 1,5),\ p_{mix} \sim p_0$$

$$h_{r,i}, (i = 1,2,) \sim h_{ref}$$

$$x \sim x_{ref}$$

$$\alpha_{r,i}, (i = 1,2,3) \sim \alpha_{ref} = \frac{h_{ref}}{d_{ref}}$$

$$\delta t \sim t_0$$

$$\dot{h}_{r,i}, (i = 1,2,3) \sim \frac{h_{ref}}{t_0}$$

$$\dot{\alpha}_{r,i}, (i = 1,2,3) \sim \frac{\alpha_{ref}}{t_0}$$

2.3.2 Discretization of the Ring Grooves and Boundary Conditions

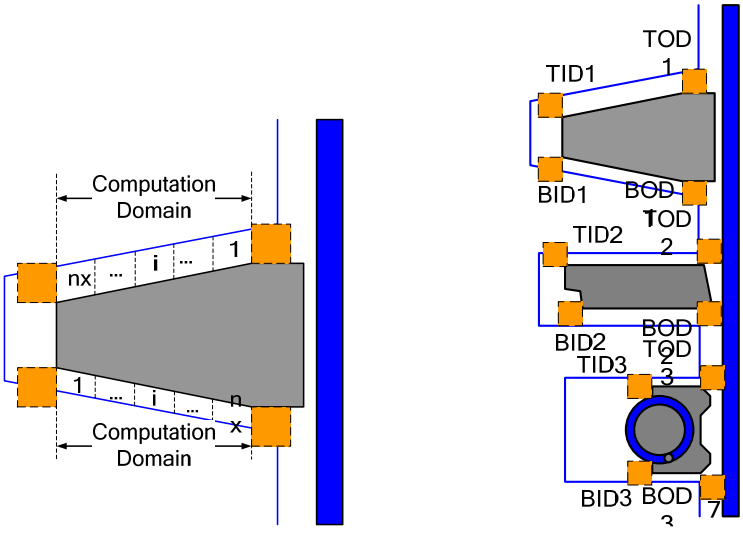

Figure 2-8 Discretization of the ring groove and boundary conditions

The control volume method was used to discretize the channel between the flanks of the ring and groove as shown in Figure 2-8. Then, boundary conditions have to be established to prescribe the available oil and gas at the boundaries. As discussed earlier,

in reality, the boundary condition is related to the oil and gas amount as well as their flows inside the ring grooves and on the piston lands. However, further work is needed to make this connection and it is not in the scope of the present work. In this work, the oil film thickness in the axial direction at the boundaries is specified as the input. Although inside the model this oil film thickness boundary condition does not have to be a constant within a cycle, the following calculations use constant film thickness for simplicity. Four square oil reservoirs are placed as the oil sources from inside ring grooves or on the piston lands. The reservoirs located at the inner and outer end of both upper and lower ring grooves are denoted as TID, TOD, BID and BOD, respectively. The boundary condition distribution in the whole ring-pack system is shown in Figure 2-8.

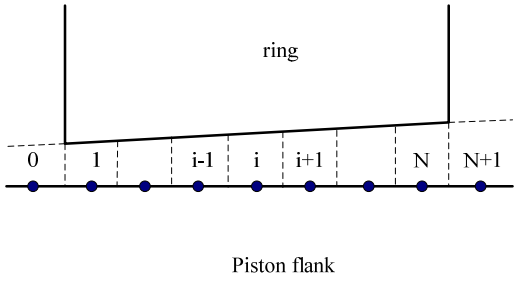

Figure 2-9 Schematic of the a ring groove discretized

After the region in the ring groove is dicretized as shown in Figure 2-9, the mass flow rate of both the gas and oil flow between the adjacent three grids (1, 2, and 3) can be expressed in the following forms with respect to the pressure difference between these grid

$$m_{oil,12} = C_{\mu,oil} C_{\phi 1} h_{lhs} \Delta p_{12}, \qquad C_{\mu,oil} = \frac{p_0 t_0}{12 \mu_{oil} \Delta x} \tag{2.25a}$$

$$m_{air,12} = C_{\mu,air} \Delta \phi_1^3 p_1^t h_{lhs} \Delta p_{12}, \qquad C_{\mu,air} = \frac{p_0 t_0}{12 \mu_{air} \Delta x} \tag{2.26a}$$

when $p_2 < p_1$,

$$m_{oil,12} = C_{\mu,oil} C_{\phi 2} h_{lhs} \Delta p_{12} \tag{2.25b}$$

$$m_{air,12} = C_{\mu,air} \Delta \phi_2^3 p_2^t h_{lhs} \Delta p_{12} \tag{2.26b}$$

when $p_2 \geq p_1$,

$$m_{oil,23} = C_{\mu,oil} C_{\phi 2} h_{rhs} \Delta p_{23} \tag{2.27a}$$

$$m_{air,23} = C_{\mu,air} \Delta \phi_2^3 p_2^t h_{rhs} \Delta p_{23} \tag{2.28a}$$

when $p_3 < p_2$,

$$m_{oil,23} = C_{\mu,oil} C_{\phi 3} h_{rhs} \Delta p_{23} \tag{2.27b}$$

$$m_{air,23} = C_{\mu,air} \Delta \phi_3^3 p_3^t h_{rhs} \Delta p_{23} \tag{2.28b}$$

when $p_3 \geq p_2$, where $C_{\mu,oil}$ is the viscous coefficient of oil flow, $C_{\mu,air}$ is the viscous coefficient of air flow, h_{lhs} is the average clearance height of grids 1 and 2, h_{rhs} is the average clearance height of grids 2 and 3, Δp_{12} is the pressure difference between grids 1 and 2, Δp_{23} is the pressure difference between grids 2 and 3, and $C_{\phi 1}$, $C_{\phi 2}$, and $C_{\phi 3}$ are the coefficient derived from equations (2.10) and (2.13).

The difference equations for the forces and moments integrated from the gas and oil pressure in the upper and lower ring grooves of a ring are:

$$F_{mix,i}^l = \sum_{j=1}^{N} p_{mix,i,j}^l \Delta x \tag{2.29}$$

$$F_{mix,i}^u = \sum_{j=1}^{N} p_{mix,i,j}^u \Delta x \tag{2.30}$$

$$M_{mix,i}^l = \sum_{j=1}^{N} x_j p_{mix,i,j}^l \Delta x \tag{2.31}$$

$$M_{mix,i}^u = \sum_{j=1}^{N} x_j p_{mix,i,j}^u \Delta x \tag{2.32}$$

The extension of grids from 1 to *nx* at the both ends to 0 and nx+1 is used to connect the end grids in a ring groove and the boundary conditions. The specific setup is written in the following way:
at TOD

$$p_{1,0} = p_{vol1}, hx_{1,0} = hx_{1,1}, \phi_{1,0} = \min\left(1, \frac{h_{bound\,1[1]}}{hx_{1,1}}\right) \tag{2.33}$$

at TID

$$p_{1,nx+1} = p_{vol2}, hx_{1,nx+1} = hx_{1,nx}, \phi_{1,nx+1} = \min\left(1, \frac{h_{bound\,2[1]}}{hx_{1,nx}}\right) \tag{2.34}$$

at BID

$$p_{2,0} = p_{vol2}, hx_{2,0} = hx_{2,1}, \phi_{2,0} = \min\left(1, \frac{h_{bound1[2]}}{hx_{2,1}}\right) \tag{2.35}$$

at BOD

$$p_{2,nx+1} = p_{vol3}, hx_{2,nx+1} = hx_{2,nx}, \phi_{2,nx+1} = \min\left(1, \frac{h_{bound2[2]}}{hx_{2,nx}}\right) \tag{2.36}$$

Where $h_{bound1[1]}$, $h_{bound2[1]}$, $h_{bound1[2]}$, and $h_{bound2[2]}$ are the height of the oil reservoirs at the four different locations.

2.3.4 Algorithm

After discretization, a set of non-linear algebra equations are formed for ring axial and angular positions, gas pressures of different land and groove regions, and the pressure and oil occupancy (ϕ) at all the node points of the ring/groove interface. The numerical algorithm used to solve the governing 2nd order partial differential equations is based on Newton's iteration with a globally-convergent scheme [33] and the SuperLU package developed by James W. Demmel, et al [37].

2.3.4.1 Newton's Globally-Convergent Scheme

To reduce the running time and make the computation more robust, Jacobians for Newton's iteration were derived analytically.

$$G_{Di}\left(y_1, y_2, \cdots, y_N\right) = 0 \tag{2.38}$$

where *N* is the matrix dimension.

$$G_{Di}\left(y_1^{j-1}, y_2^{j-1}, \cdots, y_{16+8N}^{j-1}\right) + \sum_{k=1}^{N} \frac{G_{Di}^{j-1}}{Dy_k}\left(y_k^j - y_k^{j-1}\right) = 0 \quad i = 1, N \tag{2.39}$$

where j represents the iteration step and $\frac{G_{Di}^{j-1}}{Dy_k}$ are Jacobians at the previous iteration step $j-1$.

Convergence is achieved at iteration step n if

$$\max_{k=1,N}\left(\left|y_k^n - y_k^{n-1}\right|\right) < \varepsilon \quad \text{or} \quad \max_{k=1,N}\left(G_{Di}\left(y_1^n, y_2^n, \cdots, y_N^n\right)\right) < \varepsilon \tag{2.40}$$

Then the variable values at time t are

$$y_k(t) = y_k^n \qquad k = 1, N \tag{2.41}$$

As shown by all of the system's governing equations, there are a large number of variables and equations, which need a great deal of effort for the derivations. In these normalized and discretized governing equations, only the top ring grooves has been

shown. Similar methods were under taken for the second ring and oil control ring.

2.3.4.2 The LU factorization of Jacobian Matrix

The jacobian matrix for solving the governing equations is a sparse matrix. As shown in Figure 2-10. The distribution of non-zero elements in the jacobian matrix is a combination of two parts: 1) the first several rows and columns in a band matrix, which are used to solve the pressure and the ratio between the oil and the gas in ring grooves; and 2) the non-zero elements at the right bottom corner and along the right and bottom sides indicating the interaction between the ring dynamics and the variables solved in the band portion.

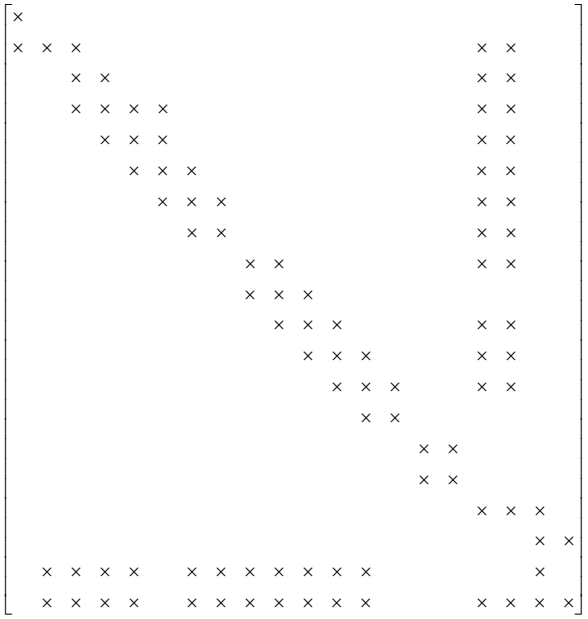

Figure 2-10 The element distribution in the Jacobian matrix

SuperLU [37] is applied to factorize the Jacobian matrix, which is a general purpose library for the direct solution of large, sparse, non-symmetric systems of linear equations on high performance machines. Its preordering subroutines for sparsity and working precision iterative refinement subroutines guarantee the computation speed and stability of the solutions. Typically, the running time is 15~20 minutes for one engine cycle on a PC with a Pentium Dual Core 2.4 GHz Processor.

2.4 Conclusion

In this chapter, a 2-D coupled ring dynamics and gas and oil transport model is presented. In this model, a mass conserved two-phase model was applied to describe the gas and oil flow in the channels between the flanks of the rings and grooves. The corresponding gas and oil flow rates as well as the pressure generated on the flanks of the rings are coupled with mass flows among different regions and ring dynamics. The oil and gas inside the ring grooves and on the lands, oil pumping between a ring and its groove, asperity contact between ring and piston flanks, gas flow through a ring gaps, and other specifications interactions for piston and ring design are considered.

After the introduction of boundary conditions and discretization of the ring grooves, Newton's globally-convergent scheme is applied to solve the normalized and discretized governing equations and the SuperLU package is used for LU factorization of the Jacobian matrix.

In the following, the model is applied to both diesel and gasoline engines, particularly in the situation where the oil transport through ring/groove interface is important.

(This page was intentionally left blank)

3. The Application of the Coupled Model in a HD Diesel Engine

A heavy duty diesel engine was chosen to analyze its ring dynamics, force and moment balance of rings, and the gas and oil transport by using the coupled model. For the analysis, emphasis was placed on the oil film thickness, ring static twist, ring gap, groove tilt, and bore expansion and their influence on the ring dynamics and the oil and gas transport in the ring-pack system.

The direct effects of the oil film thickness and oil inside the ring grooves on ring dynamics and oil and gas transport in the ring-pack system are discussed. Additionally, the influence of the oil film variation in the ring grooves on ring dynamics and oil and gas transport in the ring-pack system are analyzed.

3.1 The Baseline Case

In this chapter, the coupled model is applied to a HD diesel engine with about 2.6 liter/cylinder displacement. Running condition studied is 1800RPM/full-load. The boundary conditions shown in Figure 2-8 are set up in Table 3-1 Boundary conditions for the baseline case. Under such boundary conditions, a relative dry situation in the ring grooves is demonstrated. Figure 3-1 Cylinder pressure for the baseline case is the measured cylinder pressure at 1800 rpm under firing at full load conditions. The crankcase pressure remains near atmospheric pressure under all conditions.

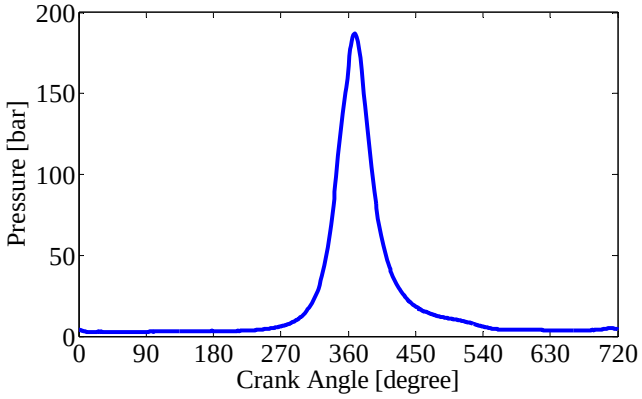

Figure 3-1 Cylinder pressure for the baseline case

Table 3-1 Boundary conditions for the baseline case

Boundary Conditions	Value (um)
TOD1	10
TID1	10
BID1	10
BOD1	10
TOD2	10
TID2	10
BID2	10
BOD2	10
TOD3	5
TID3	5
BID3	5
BO3	5

3.1.1 Oil Film Distribution and Ring Dynamics of the First Ring

The clearance between the lower flank of the top ring and groove is shown in Figure 3-2 The lift of the 1st ring. It can be seen that the top ring stays in the vicinity of the lower flank over the entire cycle (the nominal axial ring/groove clearance is about 150μm). This clearance is due to the magnitude of the top ring lift. The nadir of the ring lift at every node is located between the compression stroke and expansion stroke, which corresponds to the peak cylinder pressure. The added height of both lower and upper ring grooves is about 170um, but the zenith of the 1st ring lift is less than 6um. The 1st ring always stays on the oil film present on the lower piston flank of the 1st ring groove. The oil film thickness at the TID1 and TOD1 is comparable to the ring lift for most of the cycle, as shown in Figure 3-3. Similarly, the oil film thickness at BID1 and BOD1 is also shown in Figure 3-4. Notice that the oil film thickness at TOD1 is less than that at TID1 during the later compression stroke and the earlier expansion stroke. This is due to the difference between the high cylinder pressure and the pressure inside the 1st ring groove, thus driving oil from TOD1 to TID1. Due to the design of the ring (keystone, ring cut, and ring tilt) should be stressed that the position of IDs and ODs are at different positions in x direction as shown in Figure 2-2. That is why the clearance at TOD1 is less than at TID1 in Figure 3-3 as well as the clearance at BOD1 is less than at BID1 at the same time.

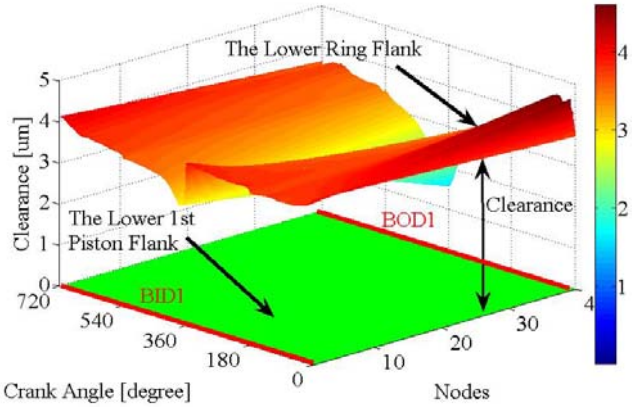

Figure 3-2 The lift of the 1st ring

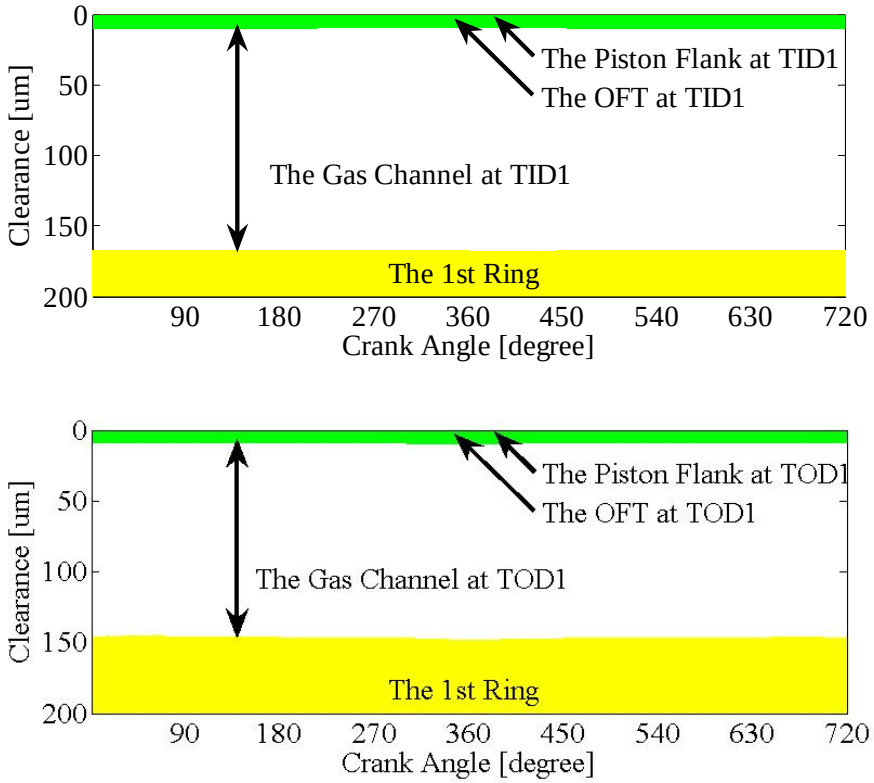

Figure 3-3 Clearance and OFT in 1st upper ring groove (BCs are 10um)

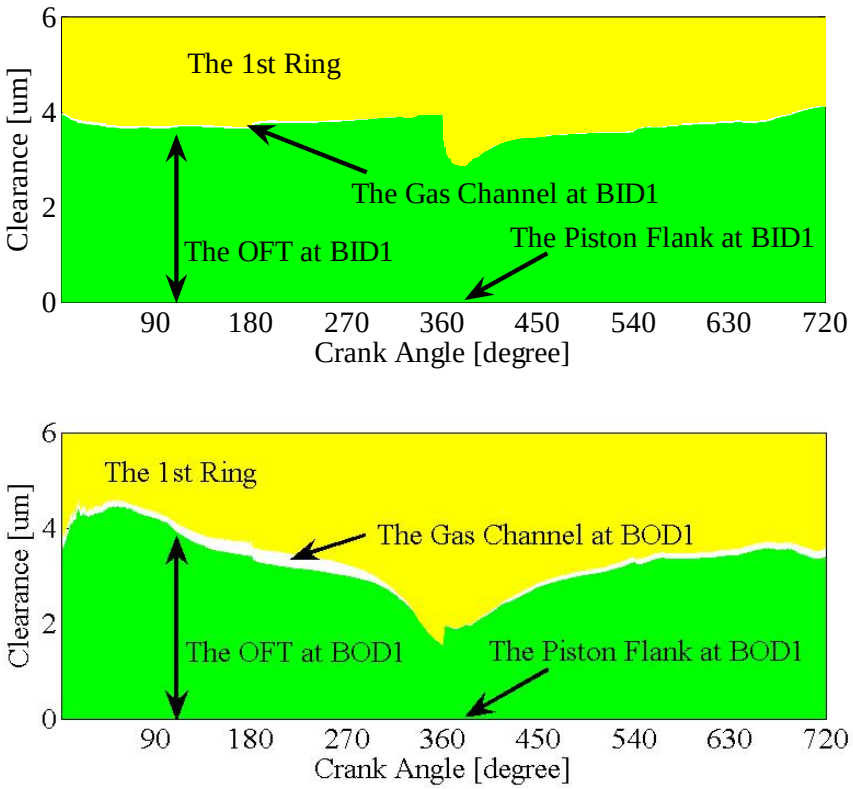

Figure 3-4 Clearance and OFT in 1st lower ring groove (BCs are 10um)

3.1.2 Force and Moment Balance of the First Ring

Figure 3-5 shows the oil and gas pressure distribution in the 1st ring groove. Because the 1st ring always stays on the lower oil film, there is a large clearance between the upper flank of the ring and groove. As the result, the pressure is fairly uniform across the ring/groove clearance on the upper flank. However, in the lower 1st ring groove, the pressure reduces smoothly from BID1 to BOD1 corresponding to the peak cylinder pressure, which also proves the importance of the top ring on blowby gas control. The forces generated by the oil and gas pressure in the upper and lower 1st ring groove are shown in Figure 3-6. Both of these forces generate the primary driving force for the 1st ring. The asperity contact pressure force in the lower groove and the pressure force due to the exposed region on the top ring in the clearance between piston and liner are also very important for the ring lift. These forces, as well as the moment generated by 1st running face, also dominate the dynamic twist of the 1st ring shown in Figure 3-7.

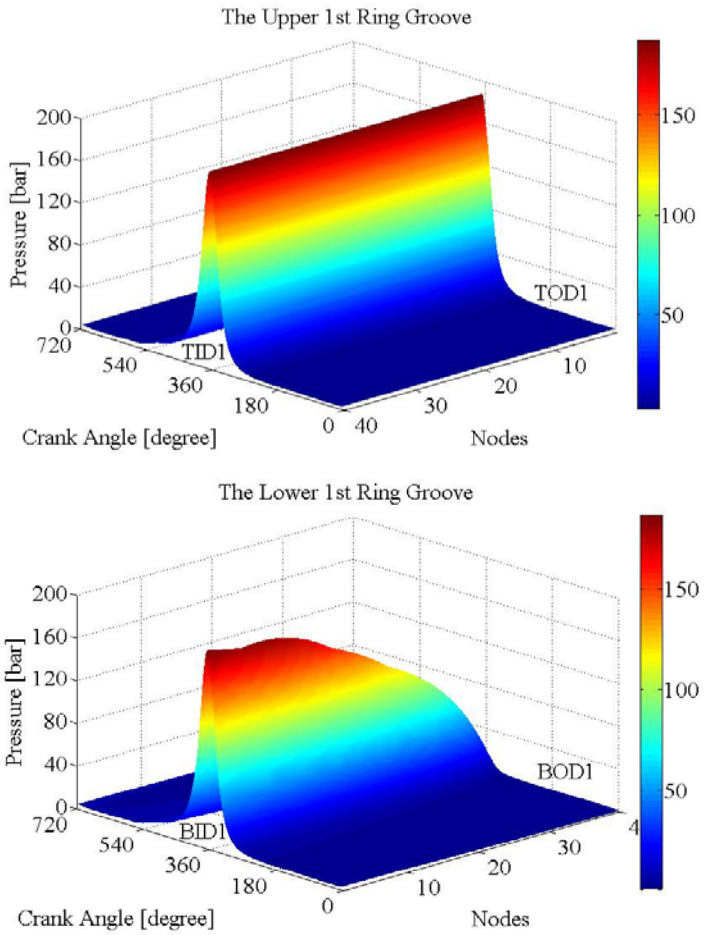

Figure 3-5 Oil and gas pressure distribution in the 1st ring grooves

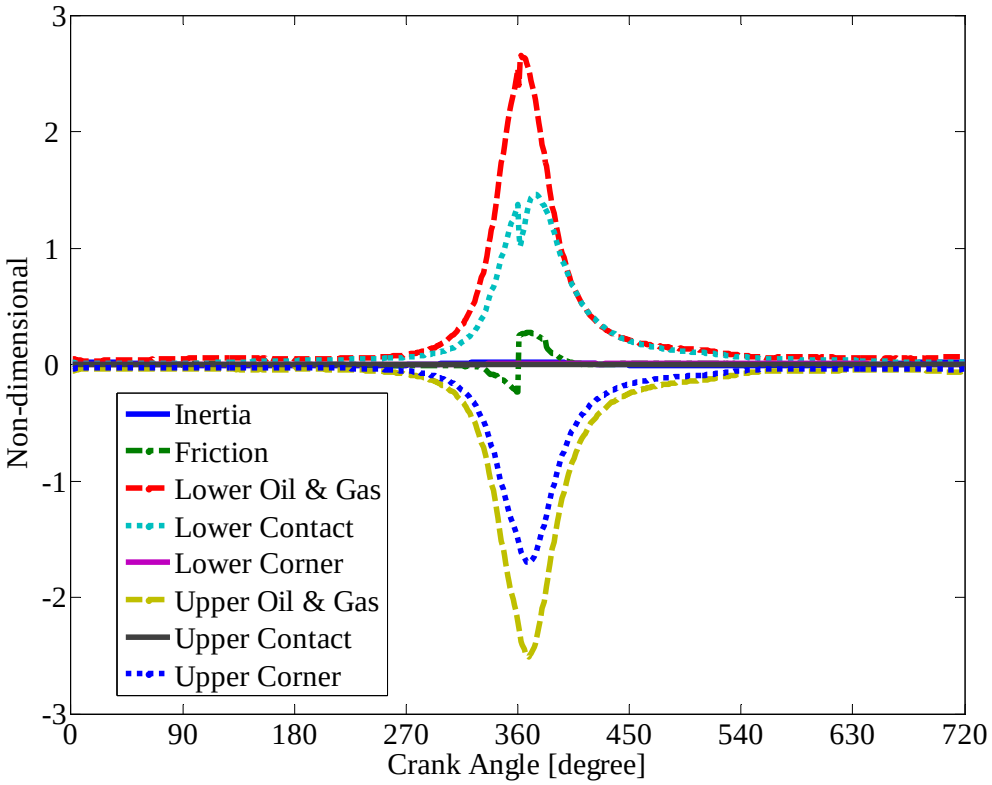

Figure 3-6 Force balance for the 1st ring

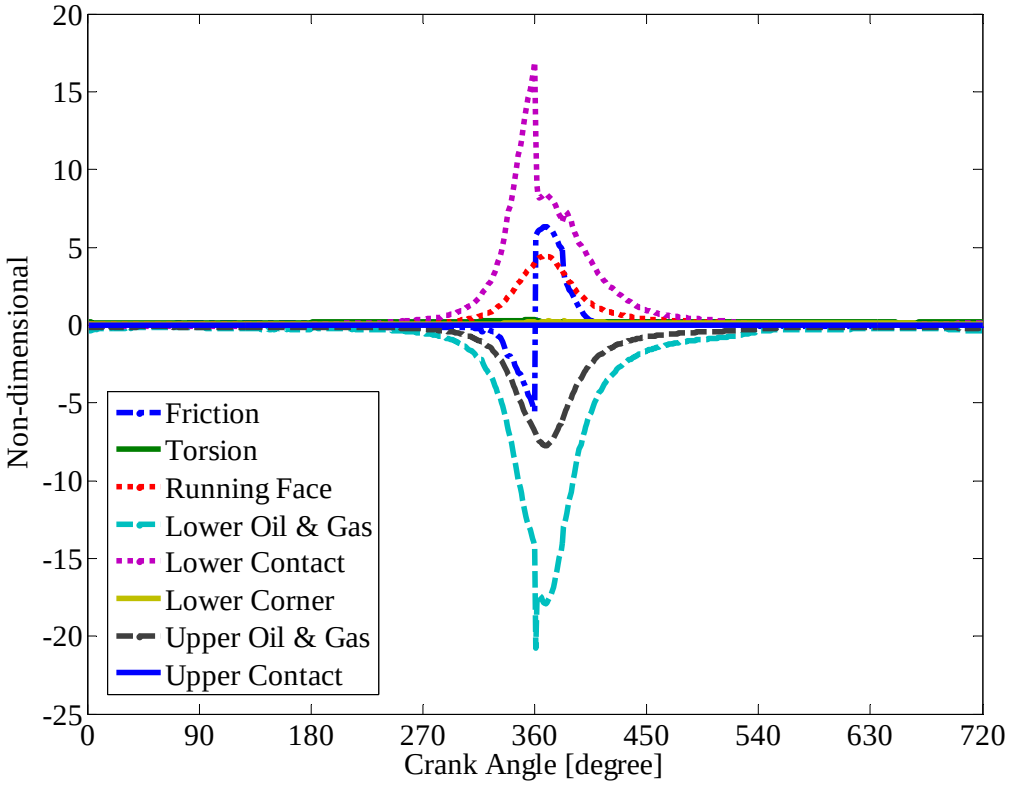

Figure 3-7 Moment balance for the 1st ring

3.1.3 The Second Ring

As shown in Figure 3-8, unlike the top ring, the 2nd ring moves up and down inside the groove due to lack of a dominant force in one direction. The 2nd ring lifts upwards in the early intake stroke, late compression stroke, early expansion stroke, and late exhaust stroke. Figure 3-9 and Figure 3-10 provide the details of the influence of ring dynamics on the oil film thickness and clearance at TOD2, TID2, BID2, and BOD2. The impact of the 2nd ring on the upper oil film causes a different oil film thickness at TOD2 and TID2. The OFT at TID2 is always less then 10um. This suggests that the oil is not able to move to TOD2 to TID2. The same explanation can be applied to the oil film attached on the lower 2nd ring groove. Furthermore, the variation of oil film thickness from 10um at BOD2 to 2um at the nodes in the vicinity of BOD2 demonstrates the oil pumping phenomena due to the reverser pressure differential between the 2nd ring groove and 3rd land pressure.

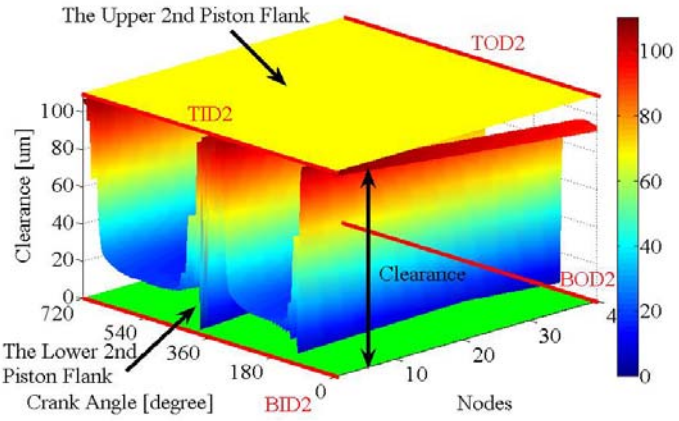

Figure 3-8 The lift of the 2nd ring

The gas and oil pressure distribution in both the upper and lower 2nd ring groove are shown in Figure 3-11. The force and moment balances shown in Figure 3-12 and Figure 3-13 demonstrate their competition with one another, resulting in 2nd ring flutter.

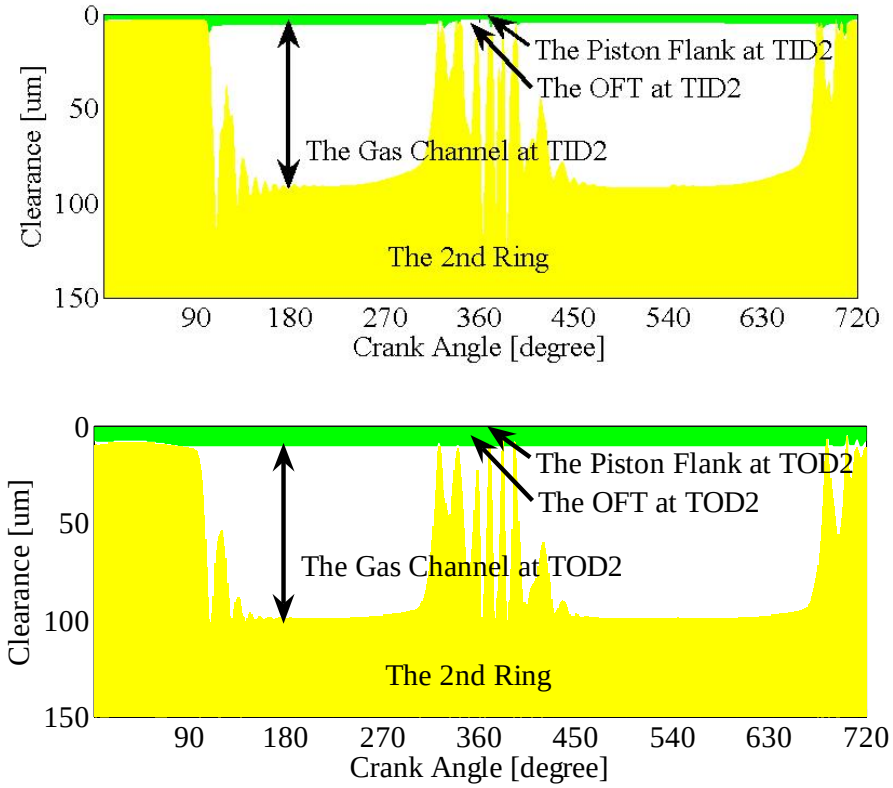

Figure 3-9 Clearance and OFT in upper 2nd ring groove (BCs are 10um)

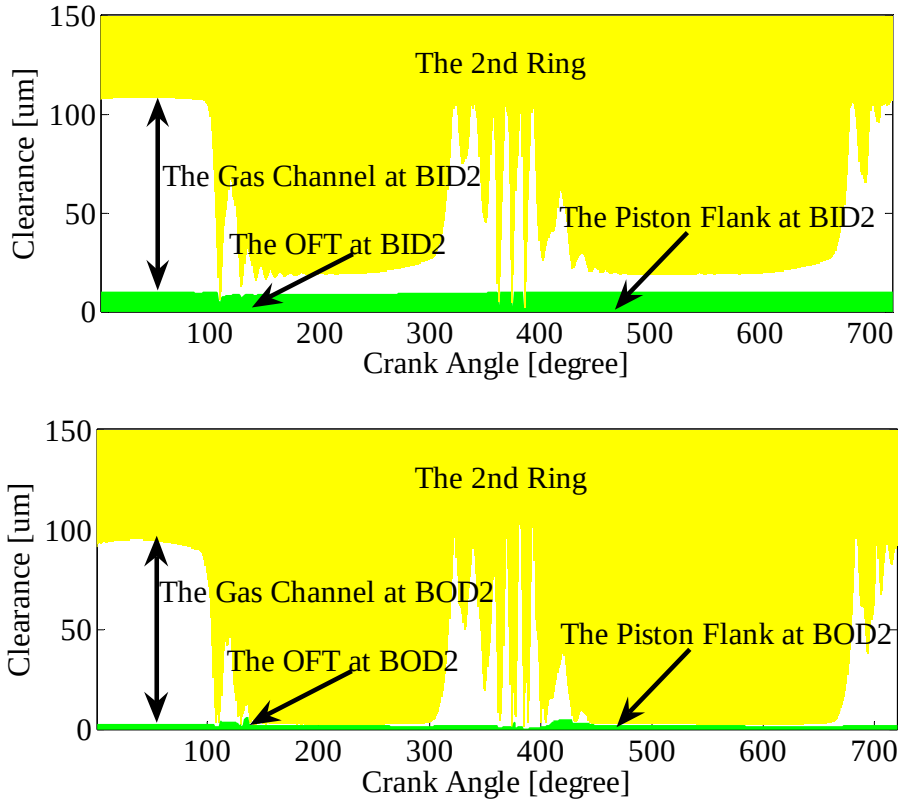

Figure 3-10 Clearance and OFT in lower 2nd ring groove (BCs are 10um)

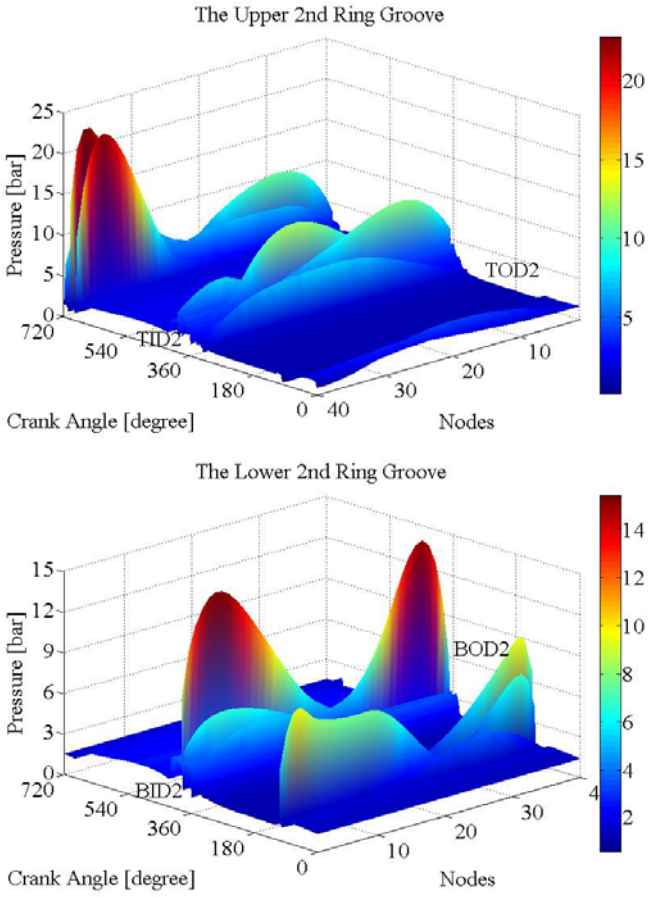

Figure 3-11 Pressure distribution in the 2nd ring grooves

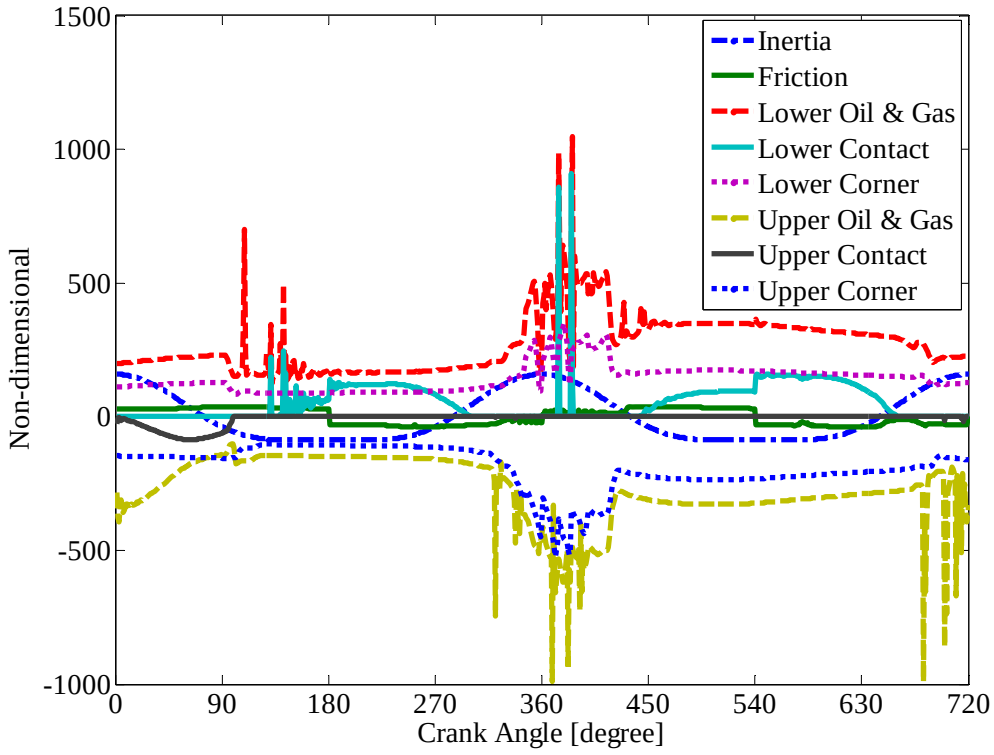

Figure 3-12 Force balance for the 2nd ring

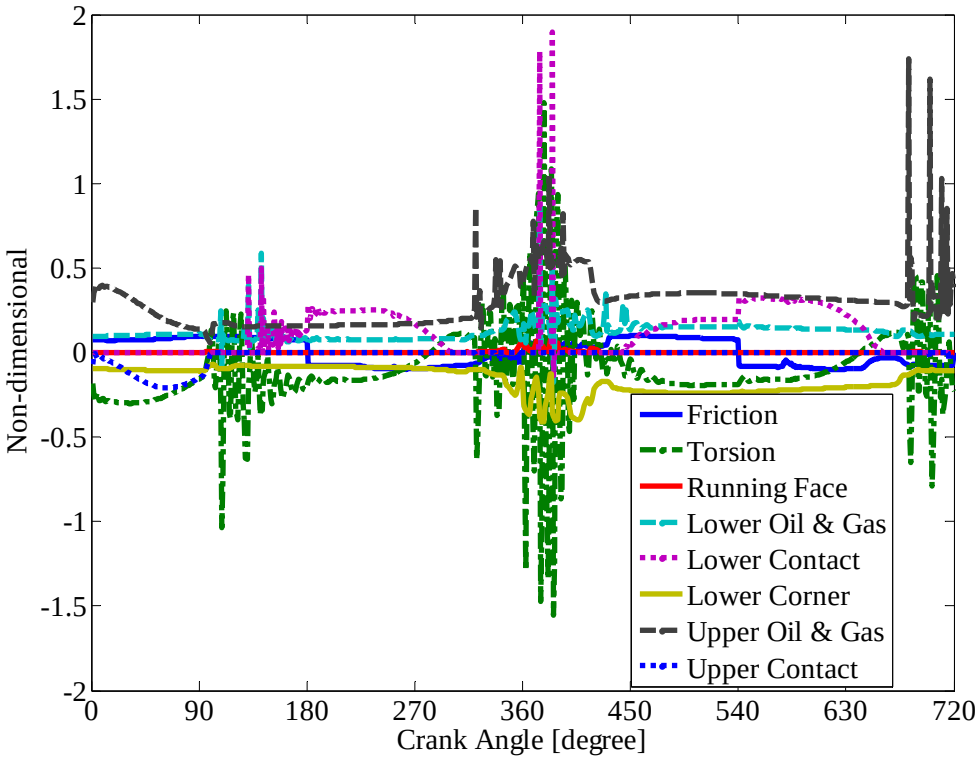

Figure 3-13 Moment balance for the 2nd ring

3.1.4 Pressure Distribution in Sub-regions

Figure 3-14 shows the pressure distribution in the sub-regions of the ring-pack system. As discussed earlier, the pressure inside the 1st ring groove is basically the same as the cylinder pressure. However, the pressures on the 2nd piston land, inside the 2nd ring groove, and on the 3rd piston land are much lower. These pressures oscillate at late compression stroke, early expansion stroke, and late exhaust stroke due to the flutter of the 2nd ring.

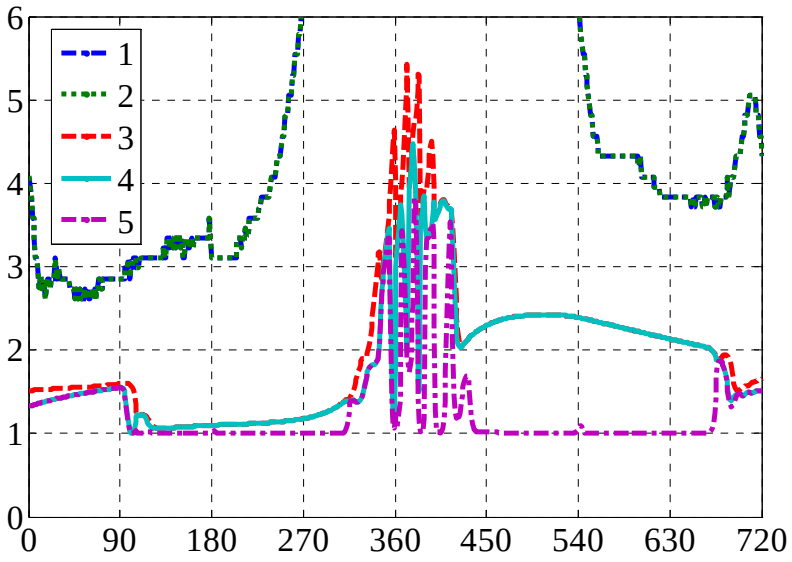

Figure 3-14 Pressure distribution in sub-regions of ring-pack system

3.2 The Effects of Oil Supply for the 2nd Ring Groove

Because the 1st ring is severely affected by the peak cylinder pressure and always stays on the oil film of the lower 1st ring groove as discussed earlier, the effect of oil film thickness on the 1st ring is not as explicit as that on the 2nd ring. In this section, the effects of oil film thickness on the 2nd ring will be discussed.

The instability of gas flow in the ring groove and the competition of forces and moments induce 2nd ring flutter. Conversely, the 2nd ring flutter has a direct impact on the gas flow and oil transport between the ring and its piston flanks. In the case of the engine used in this study, without the effects of the variation of oil film thickness, ring flutter can not be influenced because the effect of the compression of the ring ends on oil film is neglected throughout the engine cycle. To study oil transport in the 2nd ring groove, it is crucial to include the variation of the oil film thickness. Other ring-pack system models [13] cannot account for the effects of ring motion by assuming that the oil film thickness is invariable. The limitation is obvious since the variations of oil film thickness and hence the ring dynamic lift and twists are totally neglected. The ability to address the oil film thickness effects more accurately is the major advantage of this coupled model.

The boundary conditions shown in Figure 3-15: BOD2 and TOD2 vary from 20um to 80um respectively to study their effect on oil film thickness, the 2nd ring motion, and oil flow rates in the 2nd ring groove.

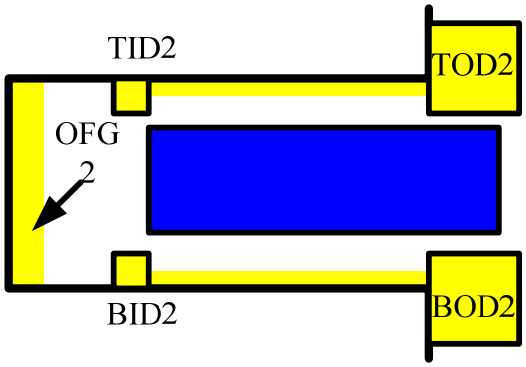

Figure 3-15 Schematic of boundary conditions in the second ring groove

3.2.2 The Effects of the Oil Supply at the BOD2

In this section, the boundary condition BOD2 is set as 20um, 40um, 60um, and 80um separately. Figure 3-16 and Figure 3-17 show there is no obvious effect of BOD2 on the 2nd ring motion, due to its irregularity during the early expansion stroke. However, the oil film thickness at BOD2 varies from 20um to 80um corresponding to BOD2 when the 2nd ring lifts up as shown in Figure 3-18. When the oil is pumped into the lower 2nd ring groove, whether it may reach the BID2 or not depends on the oil supply at the BOD2. Figure 3-19 shows that only 80um supply at BOD2 can result in an oil inflow into the 2nd ring groove. The pumping in mainly occurs at the intake stroke. Unless there is sufficient oil supply at BOD2, oil cannot be pumped into the 2nd ring groove. Once 2nd

ring groove gets sufficient oil, it can also be pumped out through the lower flank.

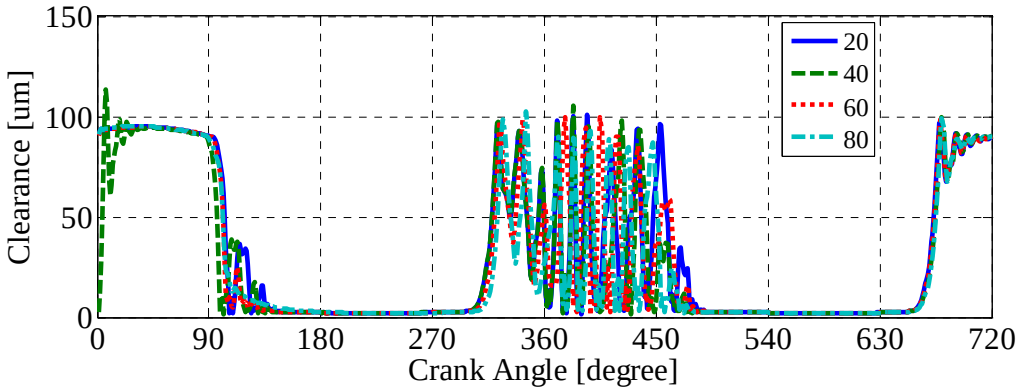

Figure 3-16 Clearance at the BOD2 (BOD2=20um~80um)

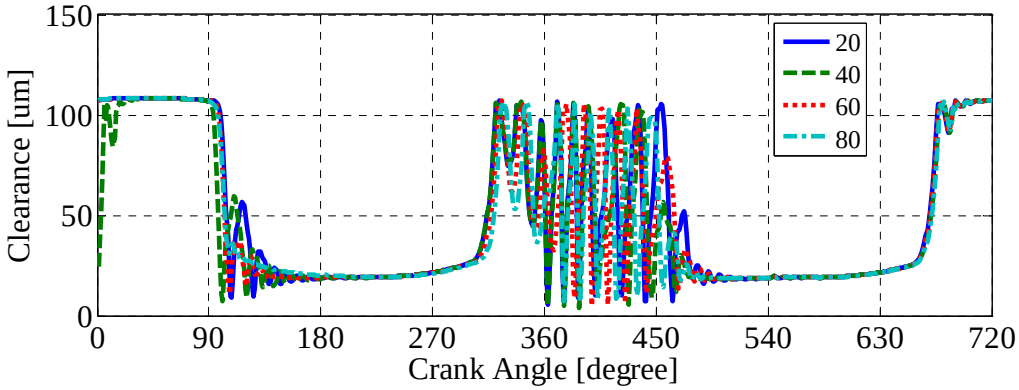

Figure 3-17 Clearance at the BID2 (BOD2=20um~80um)

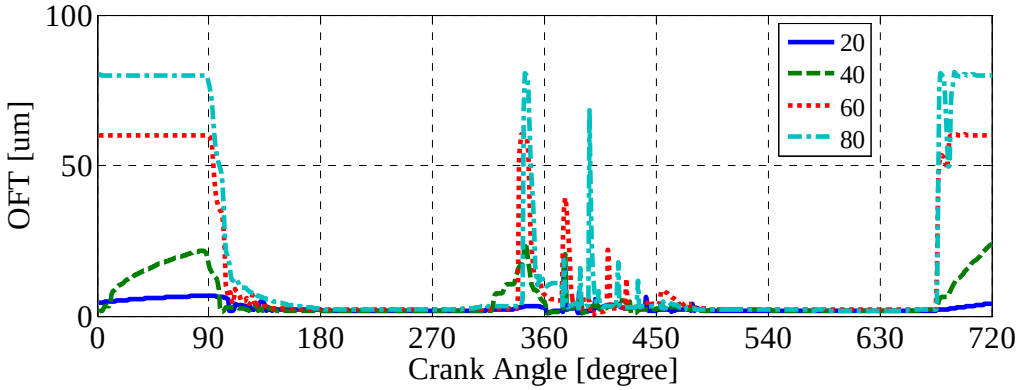

Figure 3-18 The oil film thickness at the BOD2 (BOD2=20um~80um)

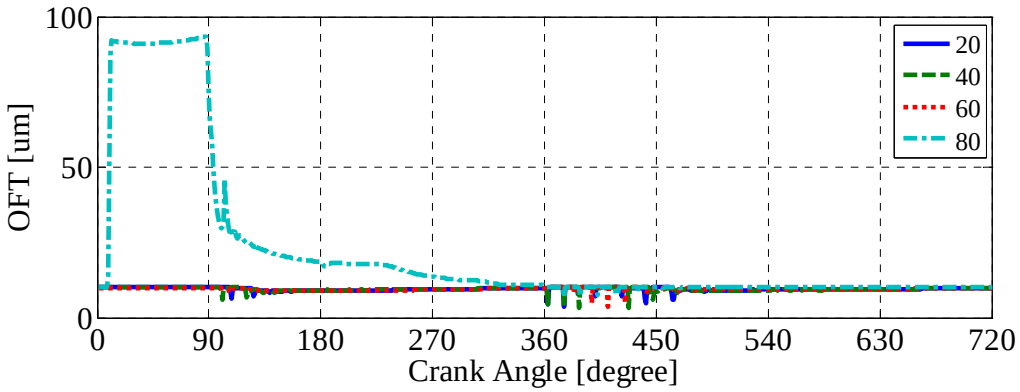

Figure 3-19 The oil film thickness at the BID2 (BOD2=20um~80um)

In the following, the evolution of the lower oil film in the 2nd ring groove at several timeslots of one cycle is compared for various BOD2. In the following figures of this section, the yellow region is the 2nd ring, the green is the oil film, and the white is the gas channel. The vertical arrow at the top center indicates the direction of the 2nd ring motion, the horizontal arrow at the bottom left corner shows the direction of the oil at BID2, and the horizontal arrow at the bottom right corner shows the direction of the oil at BOD2.

At 45 CAD, when BOD2 is 20um, 60um, and 80um, the ring moves downwards, and the oil is flows into the lower 2nd ring groove from the BOD2. The 80um BOD2 makes the oil to reach the BID2. However, the 2nd ring motion for 40um BOD2 is different. This is may caused by the oil flow in the upper 2nd ring groove. The difference between the pressure on the 2nd land and the groove pressure drives the oil flows from the TOD2 to the ring groove, but the oil supply BOD2 forces the oil to flow from the ring groove to the TOD2. These two totally different driven directions may reach a balance when BOD2 is 40um, which is indicated by the accumulated oil flow rate at TOD2 as shown in Figure 3-58.

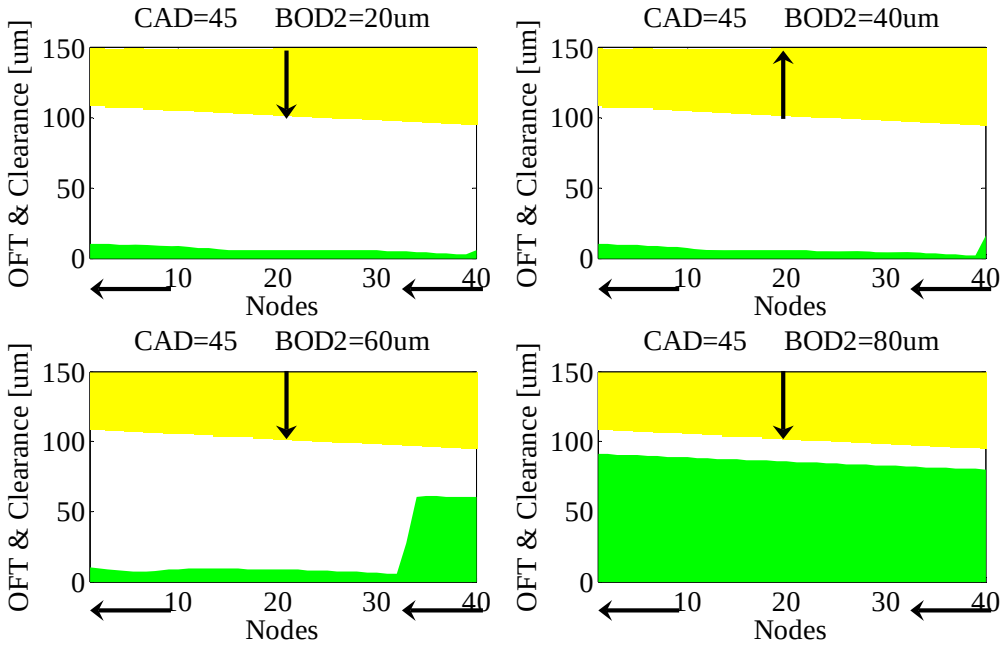

Figure 3-20 The oil film in the lower 2nd ring groove at CAD=45 (BOD2=20~80um)

From Figure 3-21 (CAD=90) to Figure 3-34 (CAD=120), the ring flutter and its effect on the lower oil film are demonstrated. When BOD2 is 20um and 40um, the 2nd ring moves up and down, and touches on the lower oil film occasionally. For 60um BOD2, the large amount of oil at the BOD2 is shown in Figure 3-21~23. For 80um BOD2, because of the sufficient oil supply, the oil can be pumped into the lower groove and even reaches the BID2. However, the flutter is not as frequent as for other BOD2 boundary conditions due to the thicken oil film.

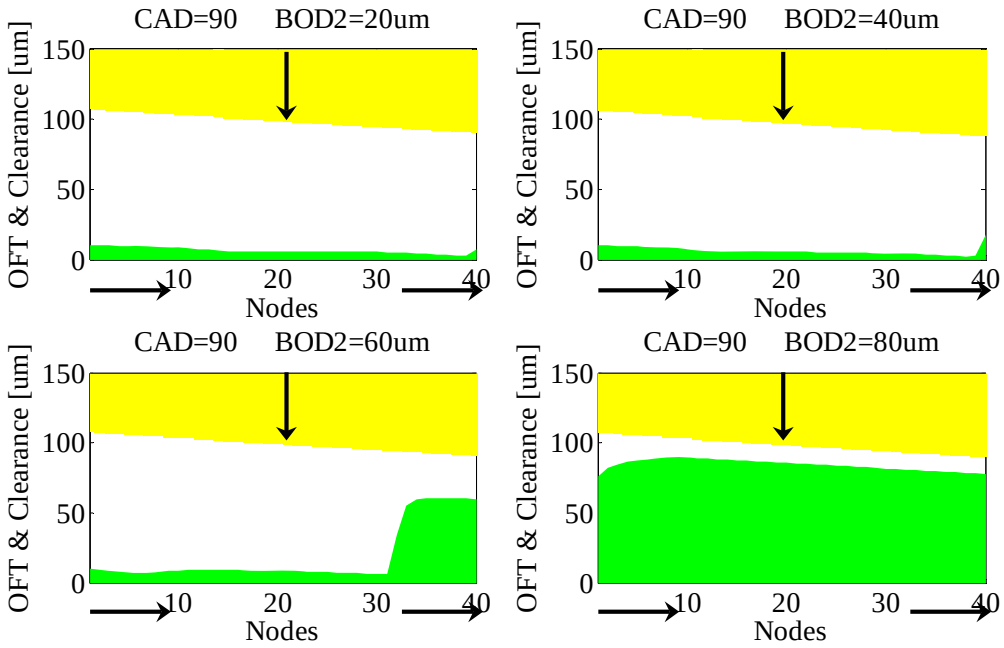

Figure 3-21 The oil film in the lower 2nd ring groove at CAD=90 (BOD2=20~80um)

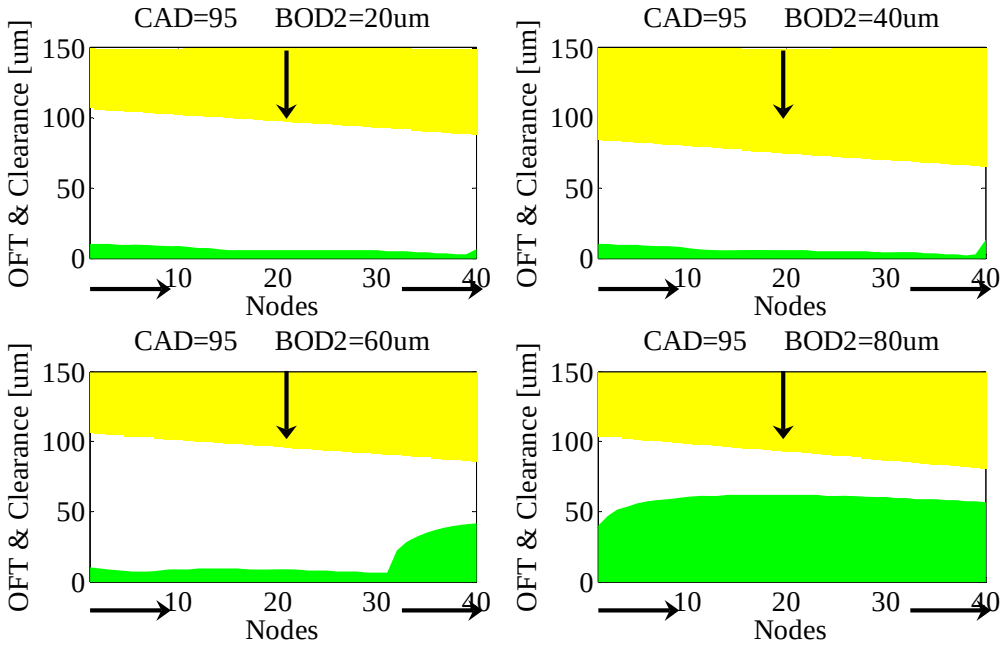

Figure 3-22 The oil film in the lower 2nd ring groove at CAD=95 (BOD2=20~80um)

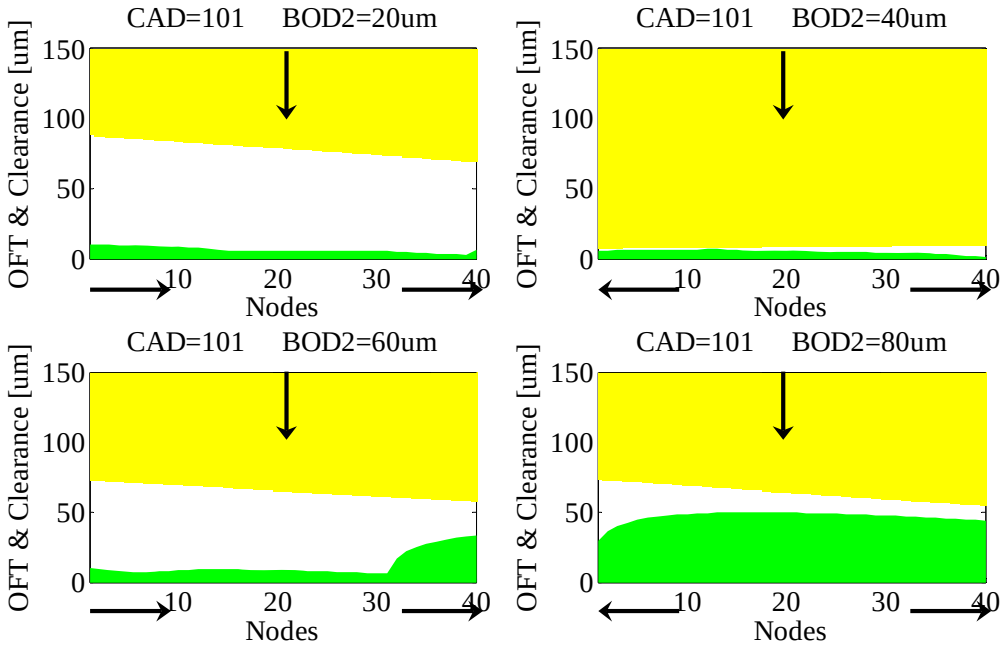

Figure 3-23 The oil film in the lower 2nd ring groove at CAD=101 (BOD2=20~80um)

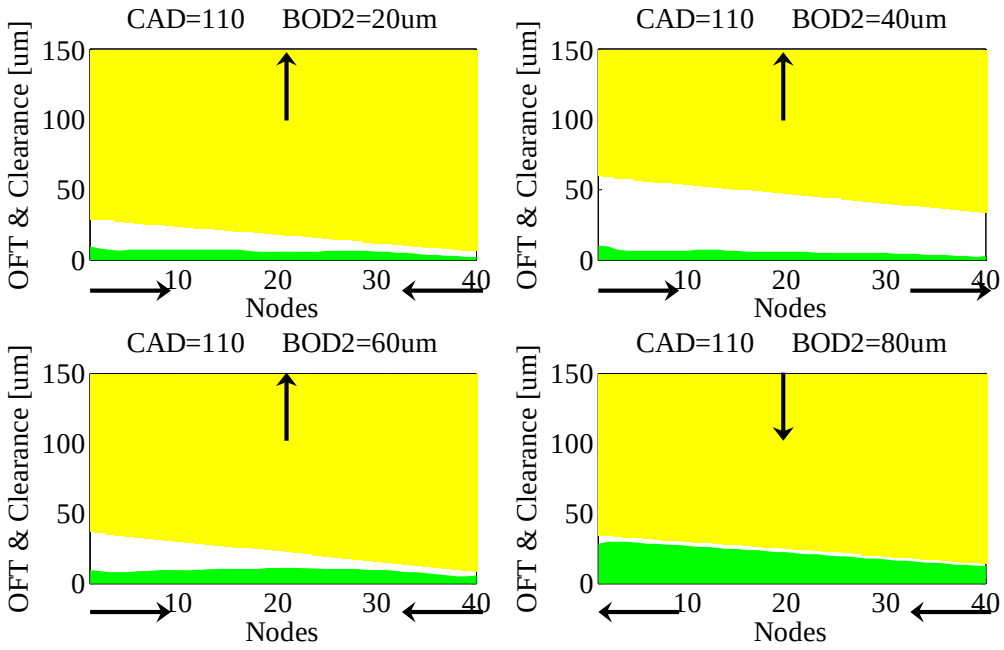

Figure 3-24 The oil film in the lower 2nd ring groove at CAD=110 (BOD2=20~80um)

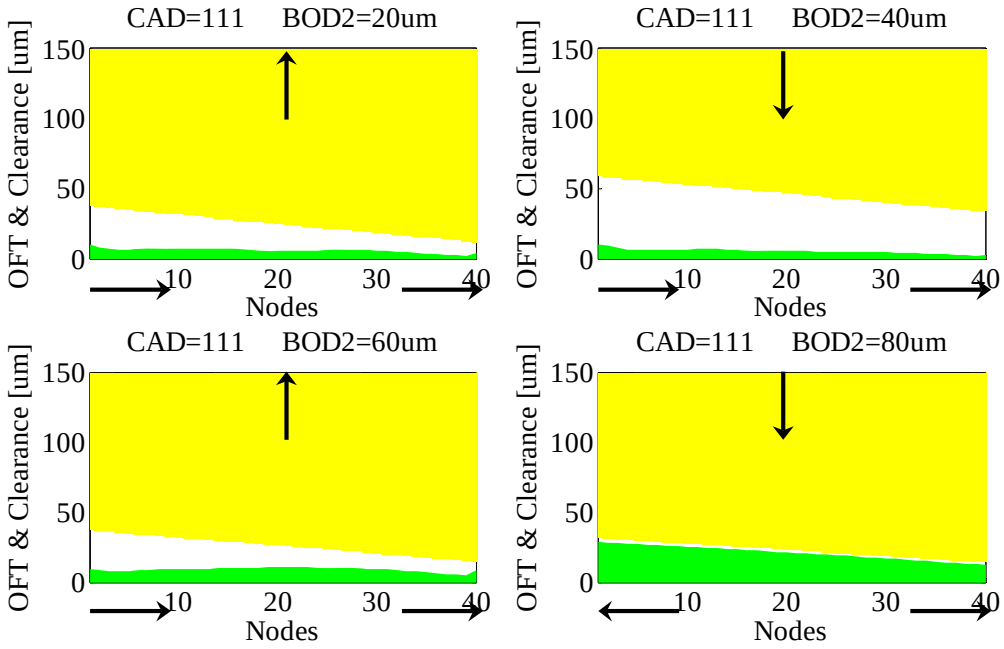

Figure 3-25 The oil film in the lower 2nd ring groove at CAD=111 (BOD2=20~80um)

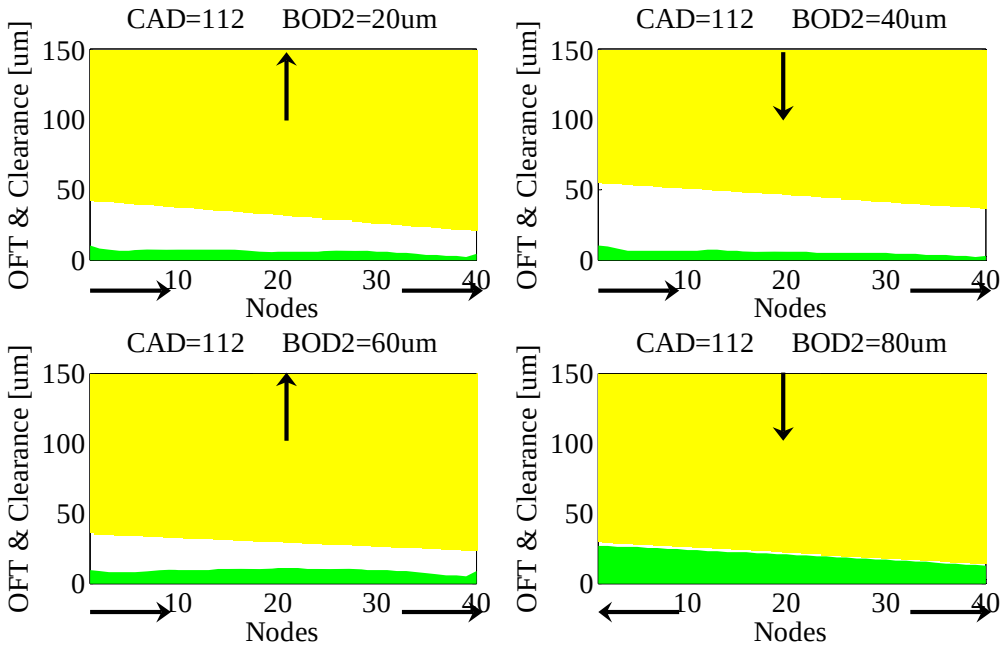

Figure 3-26 The oil film in the lower 2nd ring groove at CAD=112 (BOD2=20~80um)

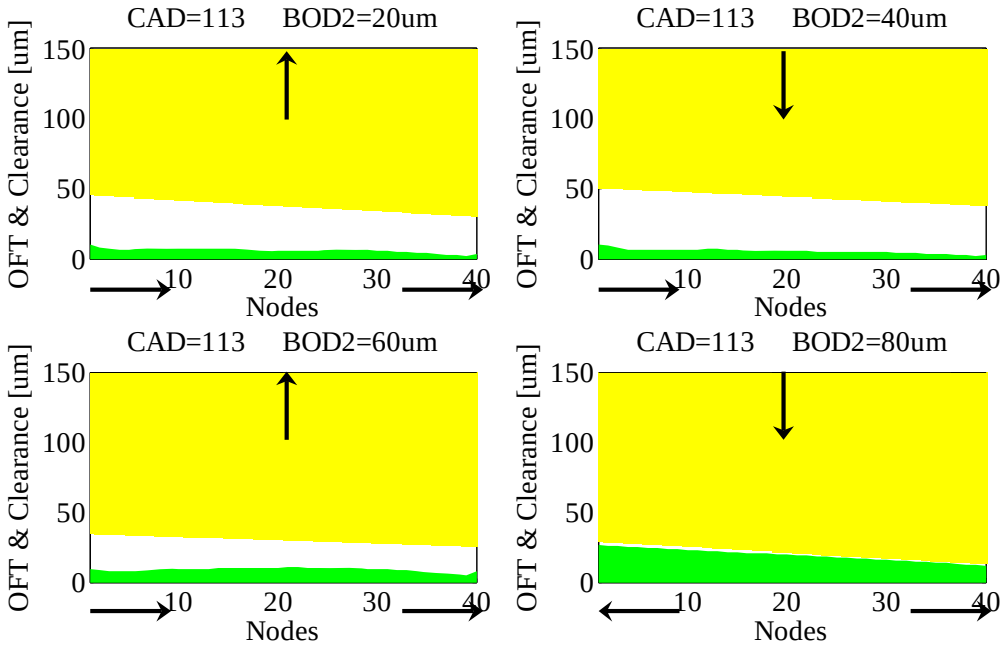

Figure 3-27 The oil film in the lower 2nd ring groove at CAD=113 (BOD2=20~80um)

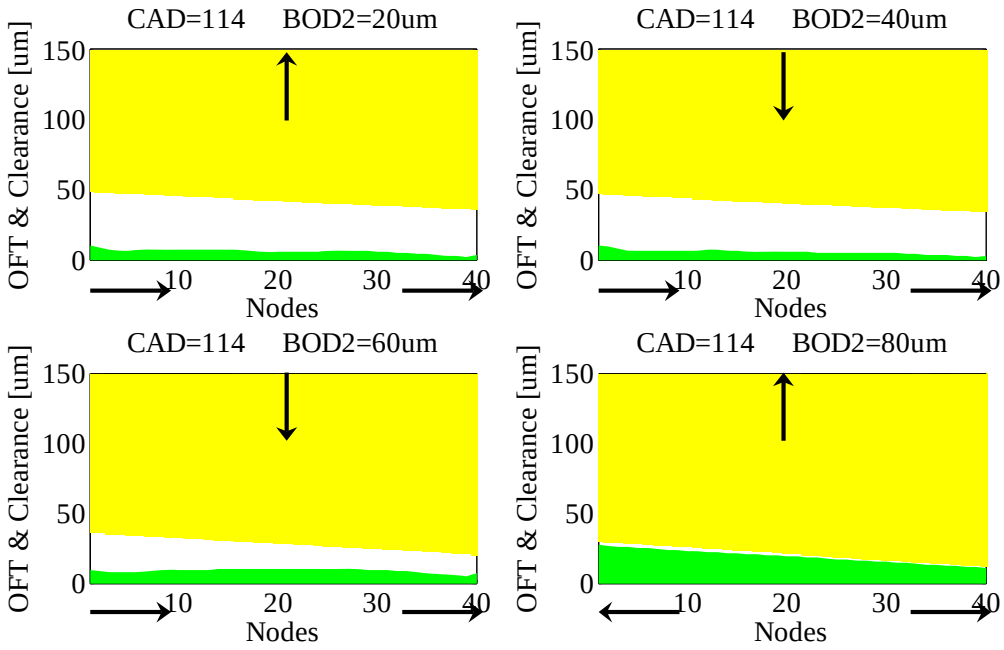

Figure 3-28 The oil film in the lower 2nd ring groove at CAD=114 (BOD2=20~80um)

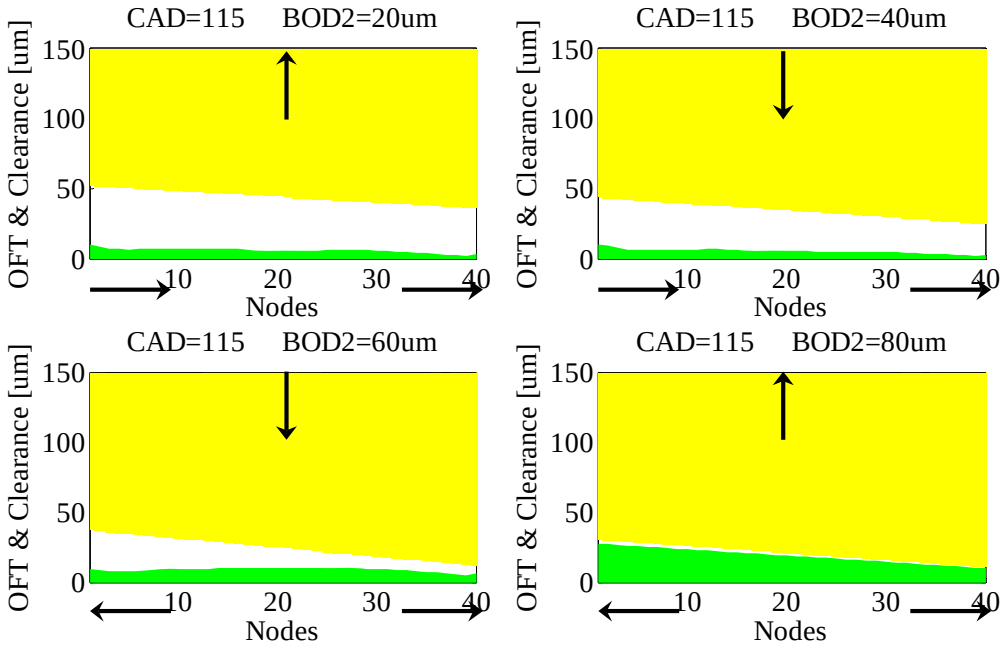

Figure 3-29 The oil film in the lower 2nd ring groove at CAD=115 (BOD2=20~80um)

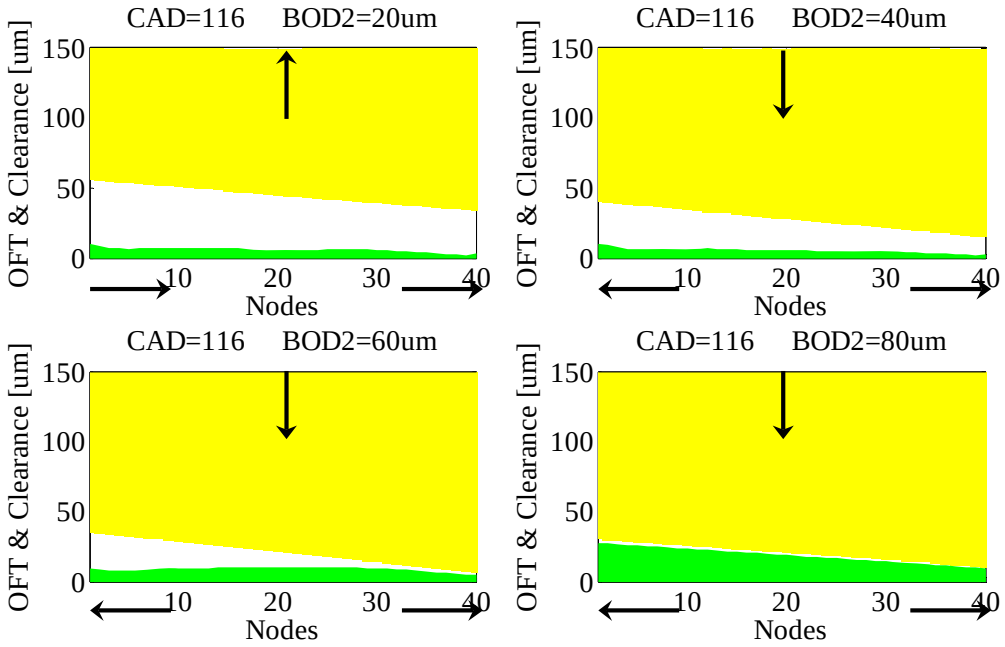

Figure 3-30 The oil film in the lower 2nd ring groove at CAD=116 (BOD2=20~80um)

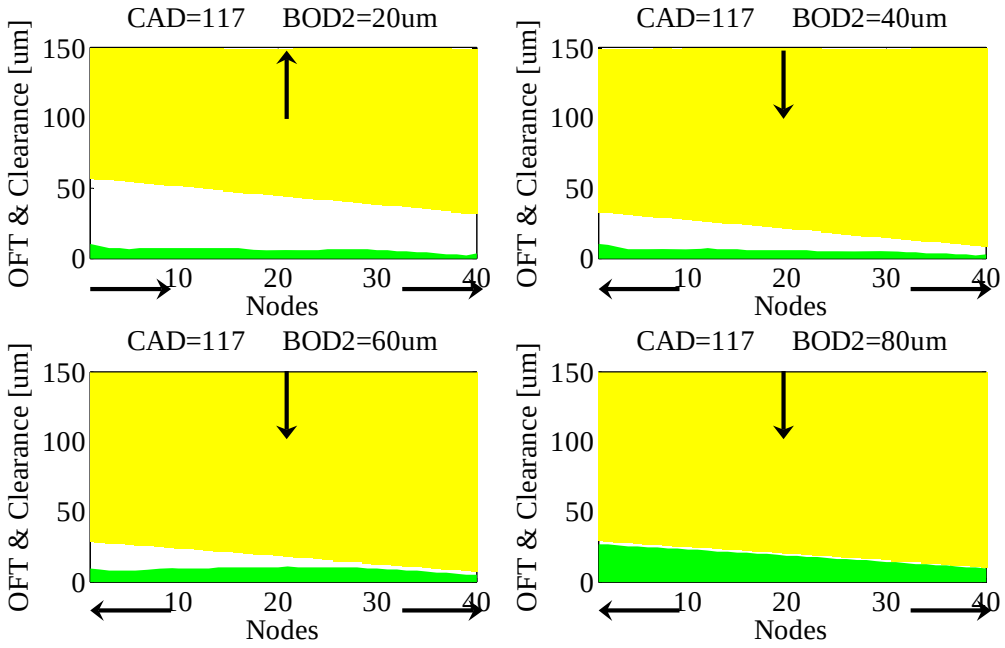

Figure 3-31 The oil film in the lower 2nd ring groove at CAD=117 (BOD2=20~80um)

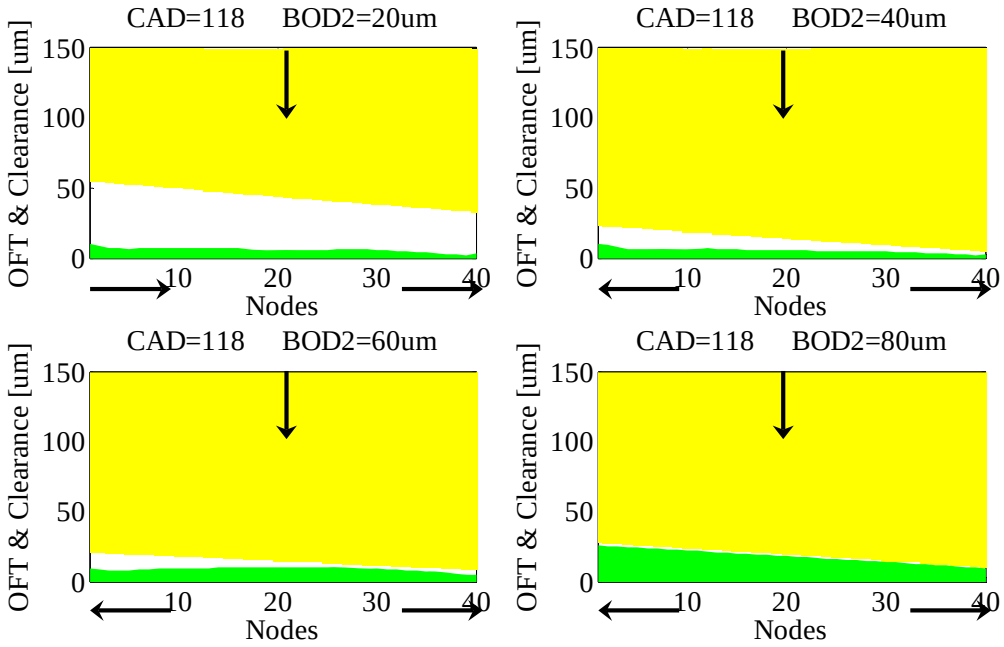

Figure 3-32 The oil film in the lower 2nd ring groove at CAD=118 (BOD2=20~80um)

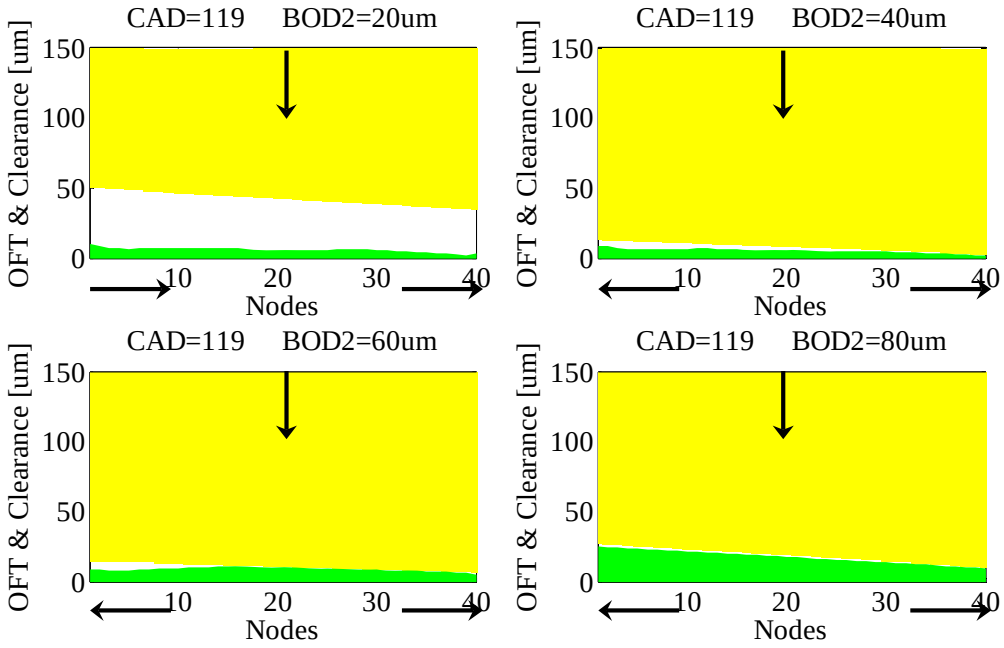

Figure 3-33 The oil film in the lower 2nd ring groove at CAD=119 (BOD2=20~80um)

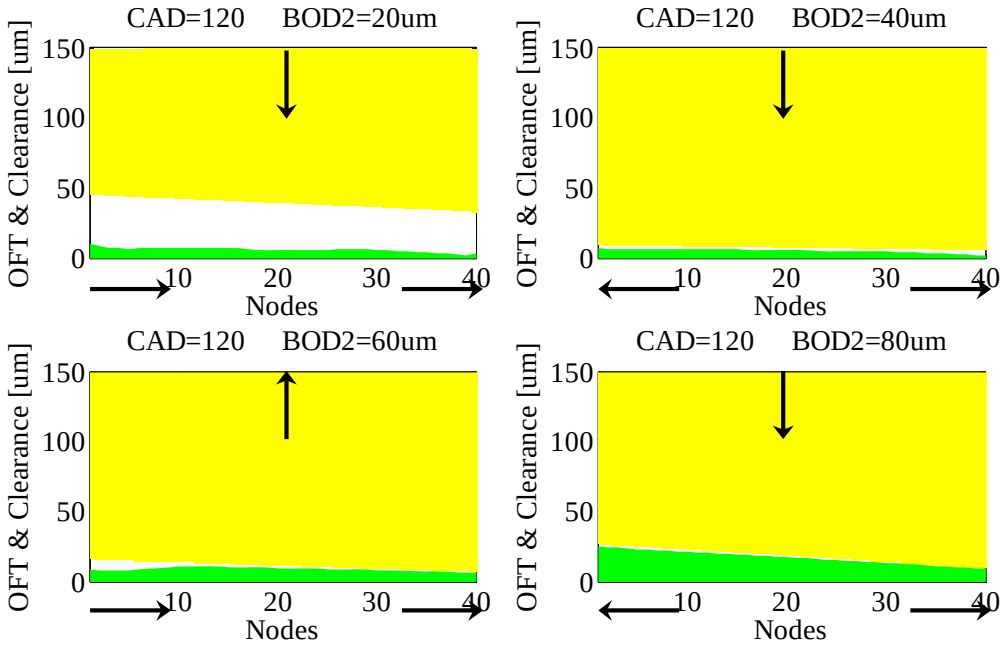

Figure 3-34 The oil film in the lower 2nd ring groove at CAD=120 (BOD2=20~80um)

The same explanation for Figure 3-30 is also suitable to Figure 3-35 for the unique ring motion and oil flow when BOD2 is 40um.

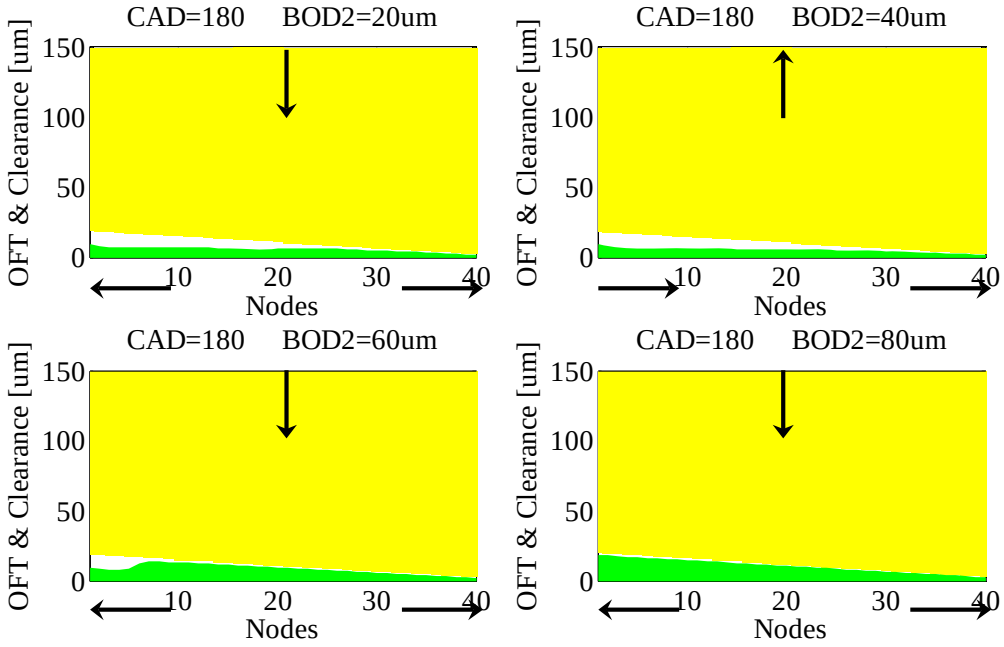

Figure 3-35 The oil film in the lower 2nd ring groove at CAD=180 (BOD2=20~80um)

In Figure 3-36, the large oil supply for 60um BOD2 and 80um BOD2 changes the direction of the oil flow, but the change of the 2nd ring motion is delay for 60um BOD2 because the less oil supply than 80um BOD2.

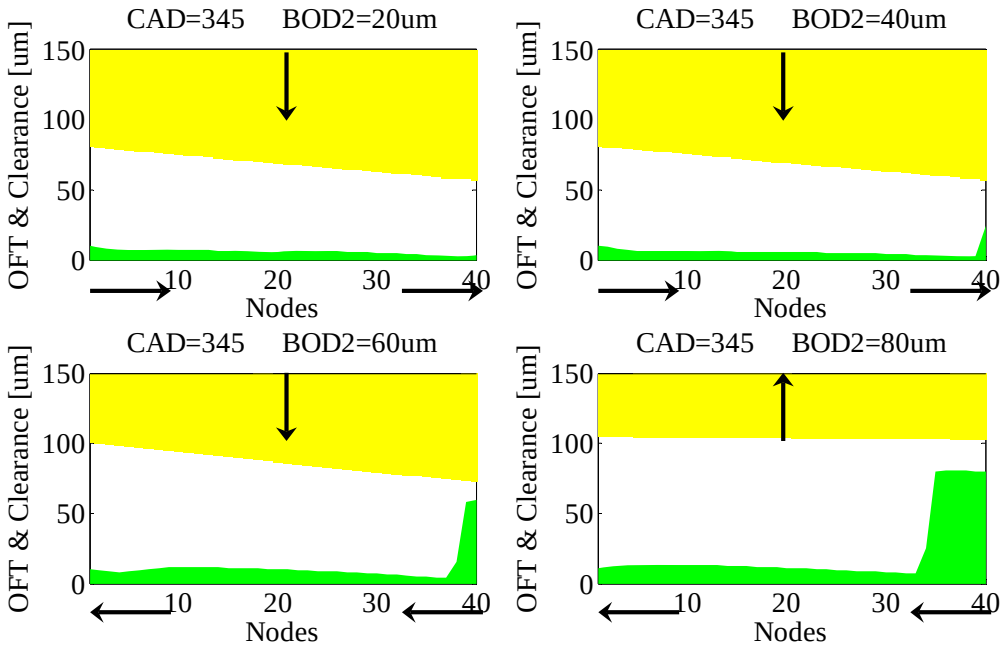

Figure 3-36 The oil film in the lower 2nd ring groove at CAD=345 (BOD2=20~80um)

From Figure 3-37 (CAD=390) to Figure 3-52 (CAD=405), the oil pumping process in the 2nd ring groove is demonstrated. For 20um BOD2, the process is as following:

a) the 2nd ring lifts upwards and the ring flank attaches on the oil film at BOD2, and the oil flows from BID2 to BOD2, as shown in Figure 3-37;
b) the 2nd ring remains to lift upwards and the ring flank separates from the oil film, and the oil flows from BID2 to BOD2, as shown in Figure 3-38~40;
c) the 2nd ring remains to lift upwards, but the oil fills the lower groove from both the BOD2 and the BID2, as shown in Figure 3-41;
d) the 2nd ring starts to move downwards, the oil is pumped into the lower 2nd ring groove from the BOD2, as shown in Figure 3-42~43;
e) the 2nd ring keeps to move down, the oil may flow out of the lower groove from both the BID2 and the BOD2 or flows from the BID2 to the BOD2, which depends on the competitive effects of both the ring dynamics and the pressure difference, as shown in Figure 3-44~48;
f) in Figure 3-49~52, the 2nd ring lifts upwards and negative twists, and the oil flows from BID2 to BOD2, which returns back the step a);

The similar process also happens for 20um BOD2 at other time in a whole engine cycle and for other boundary conditions as well. The magnitude and timing of the 2nd ring lift and twist vary with the boundary conditions and the oil also reserved in the lower groove.

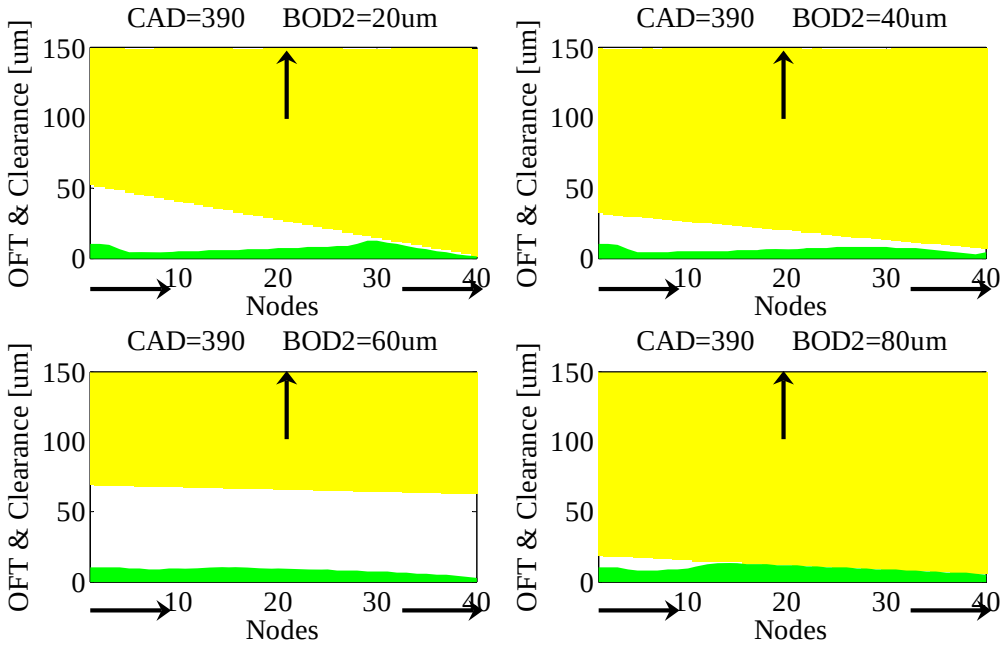

Figure 3-37 The oil film in the lower 2nd ring groove at CAD=390 (BOD2=20~80um)

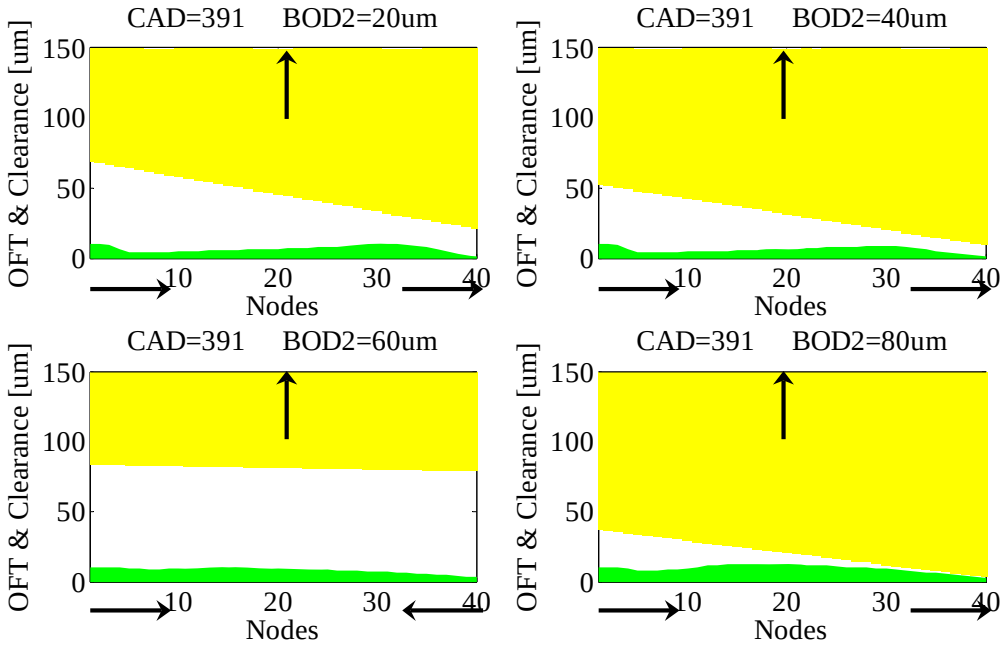

Figure 3-38 The oil film in the lower 2nd ring groove at CAD=391 (BOD2=20~80um)

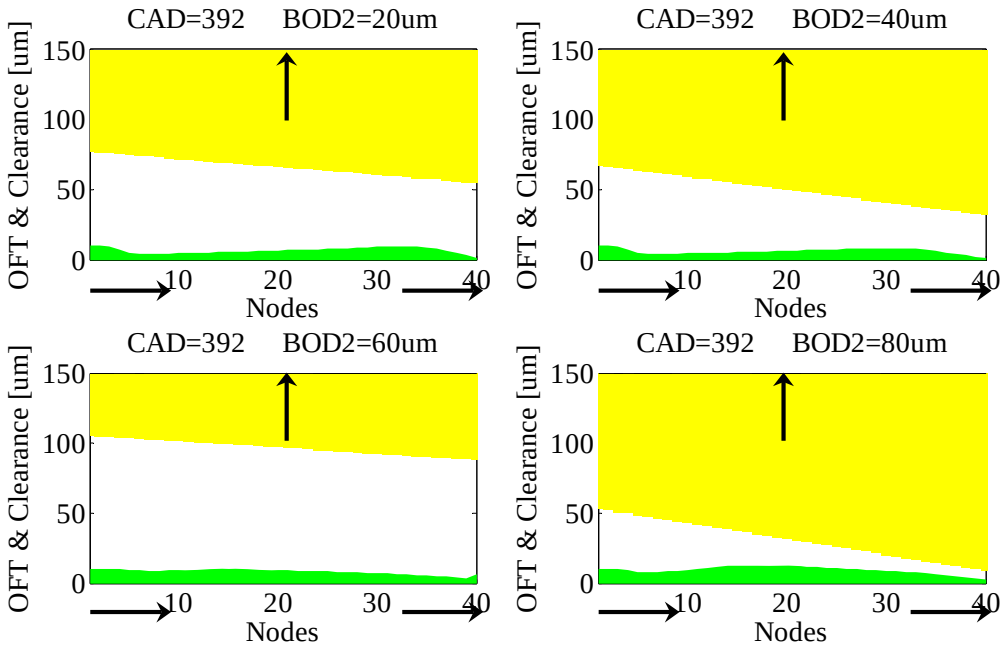

Figure 3-39 The oil film in the lower 2nd ring groove at CAD=392 (BOD2=20~80um)

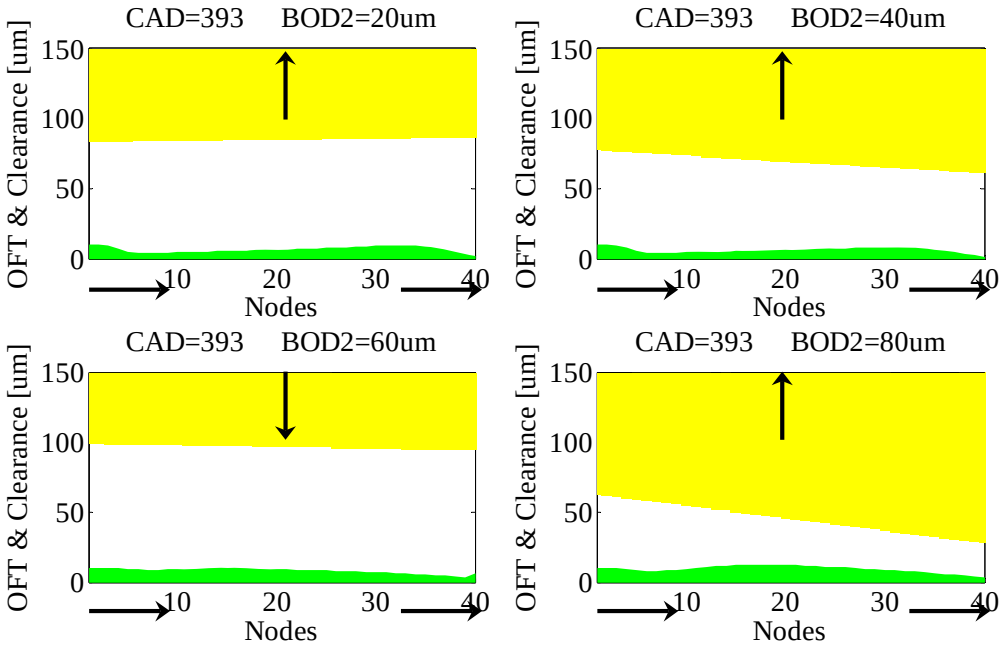

Figure 3-40 The oil film in the lower 2nd ring groove at CAD=393 (BOD2=20~80um)

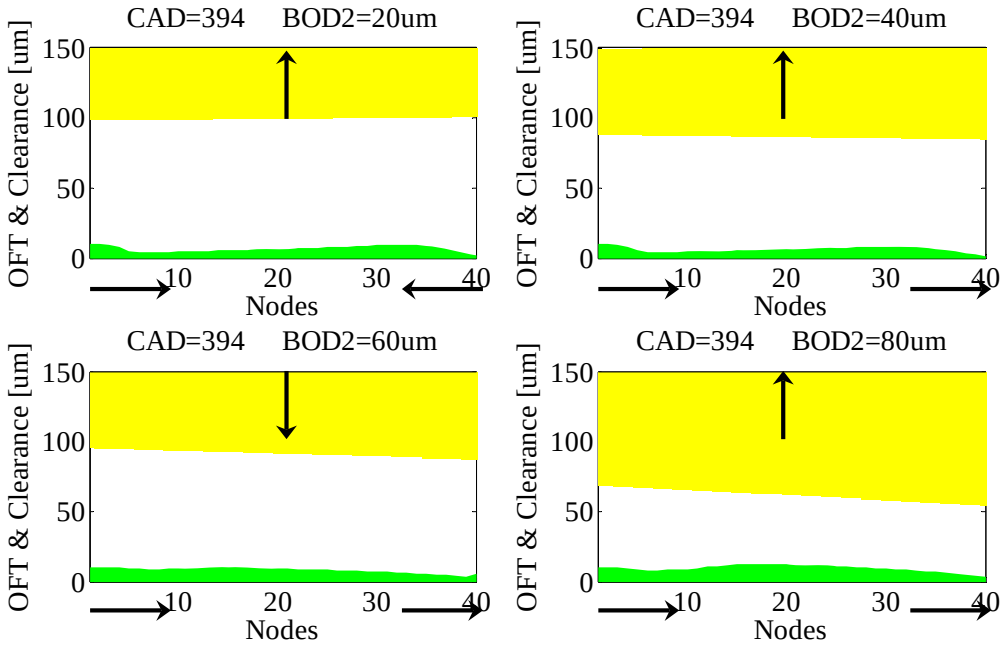

Figure 3-41 The oil film in the lower 2nd ring groove at CAD=394 (BOD2=20~80um)

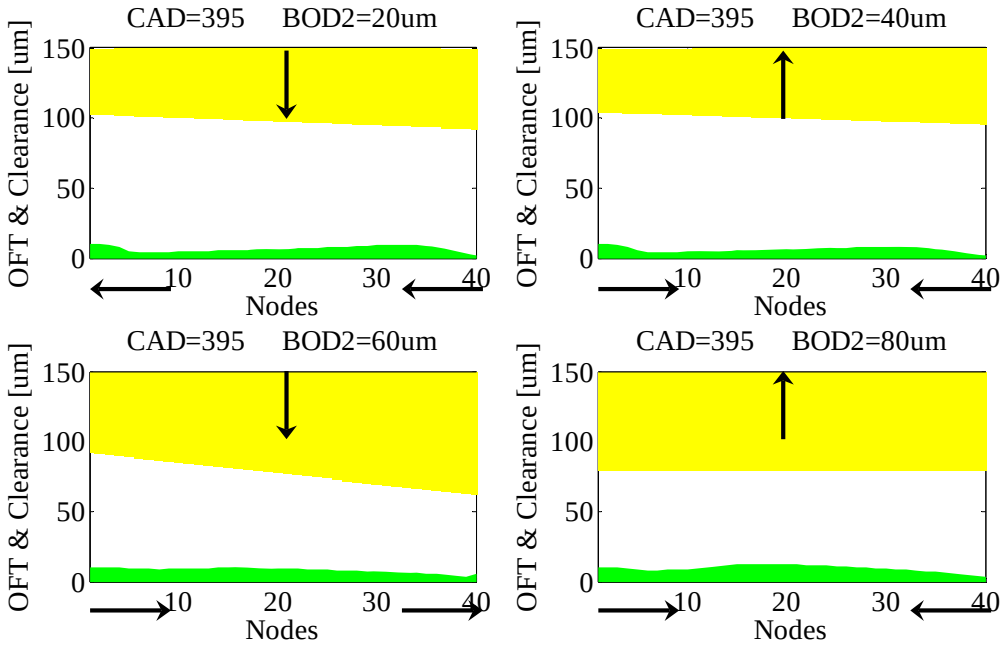

Figure 3-42 The oil film in the lower 2nd ring groove at CAD=395 (BOD2=20~80um)

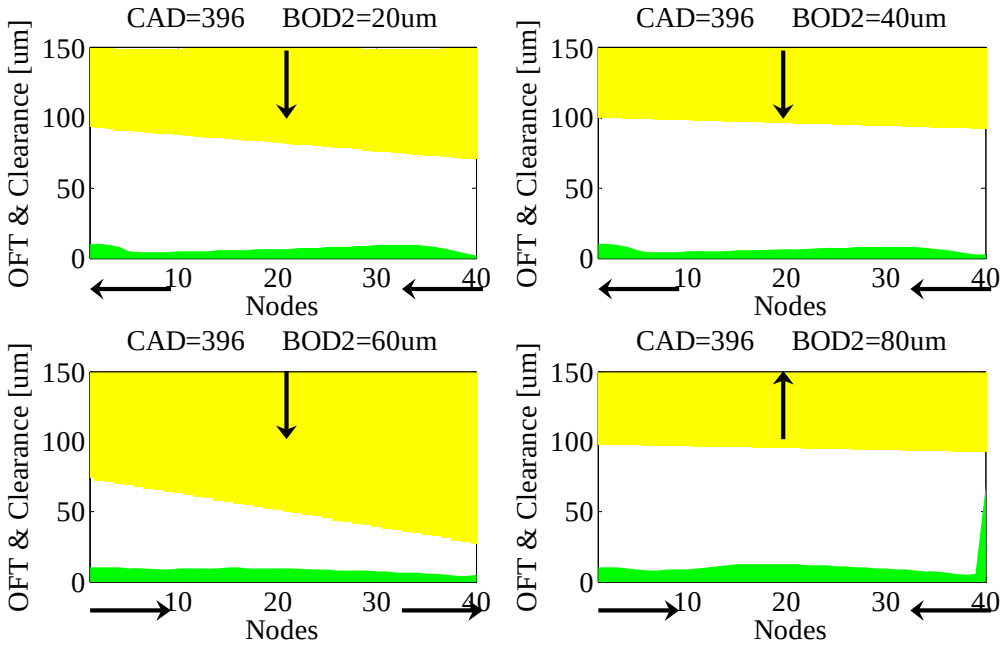

Figure 3-43 The oil film in the lower 2nd ring groove at CAD=396 (BOD2=20~80um)

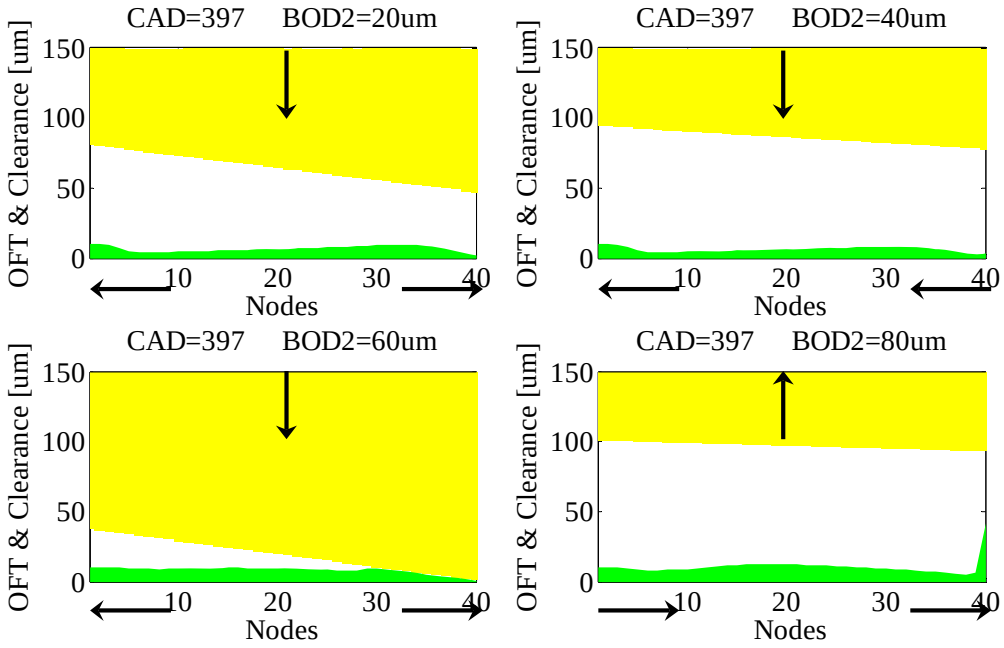

Figure 3-44 The oil film in the lower 2nd ring groove at CAD=397 (BOD2=20~80um)

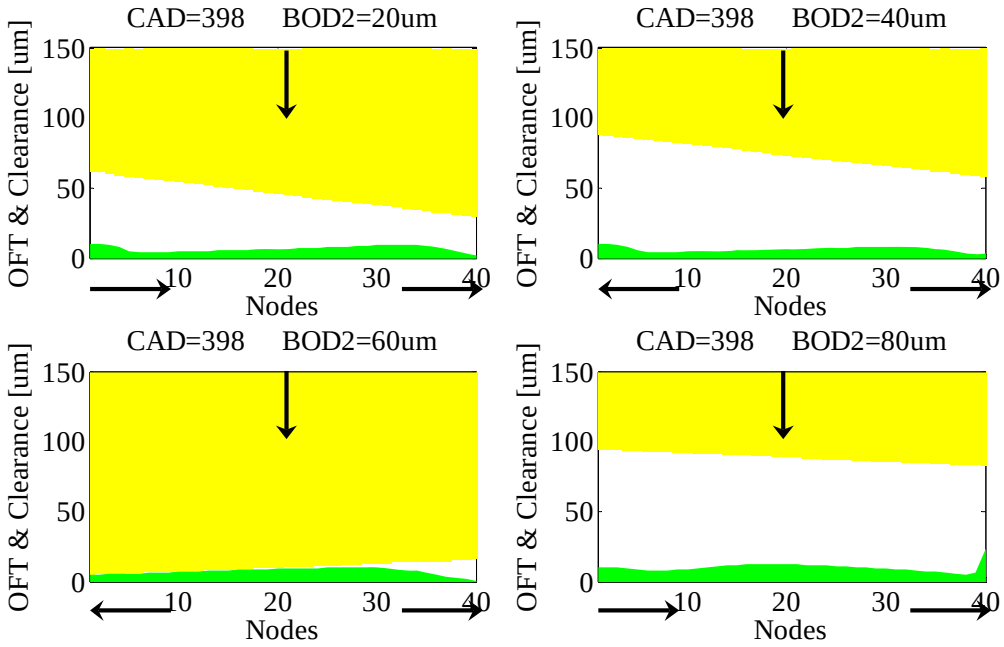

Figure 3-45 The oil film in the lower 2nd ring groove at CAD=398 (BOD2=20~80um)

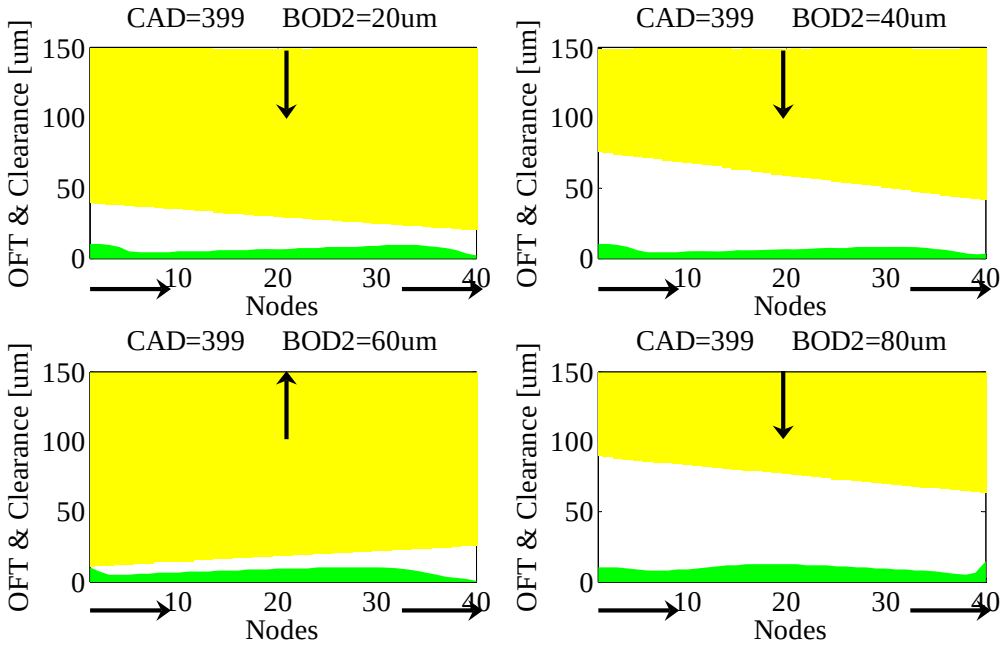

Figure 3-46 The oil film in the lower 2nd ring groove at CAD=399 (BOD2=20~80um)

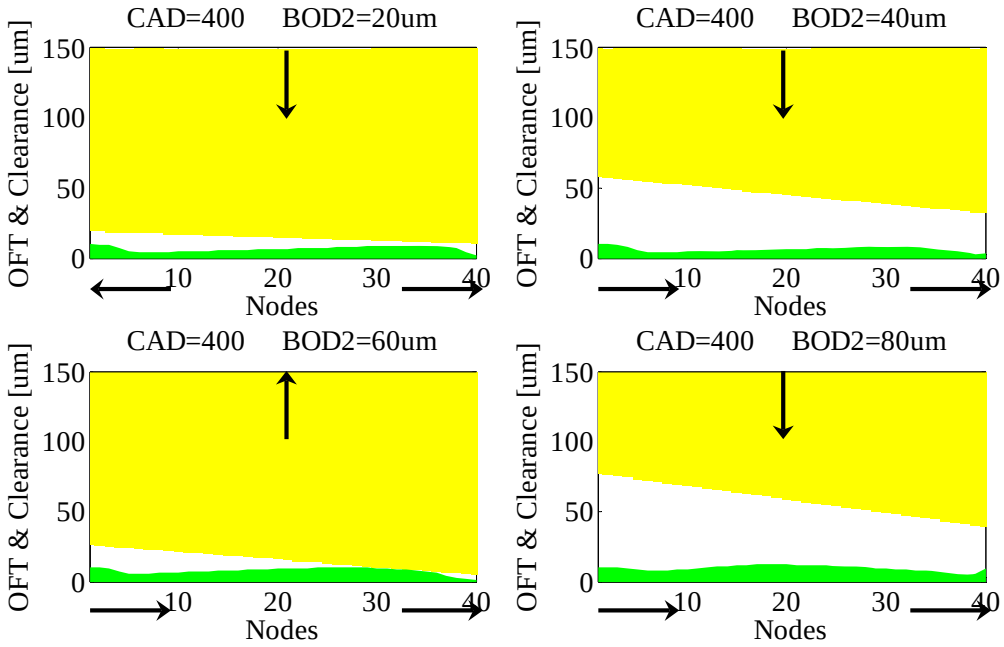

Figure 3-47 The oil film in the lower 2nd ring groove at CAD=400 (BOD2=20~80um)

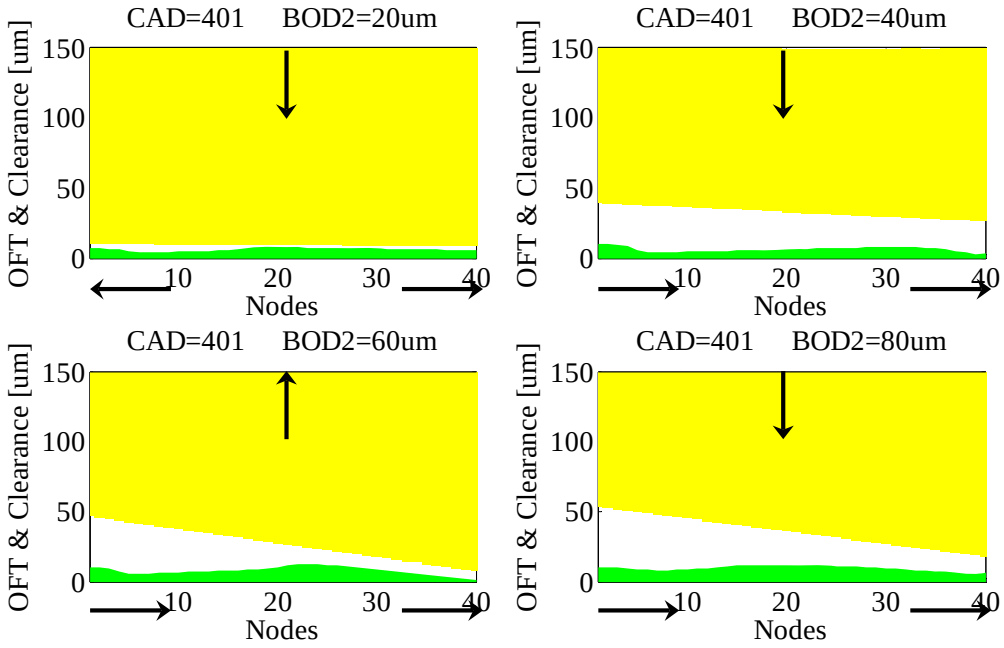

Figure 3-48 The oil film in the lower 2nd ring groove at CAD=401 (BOD2=20~80um)

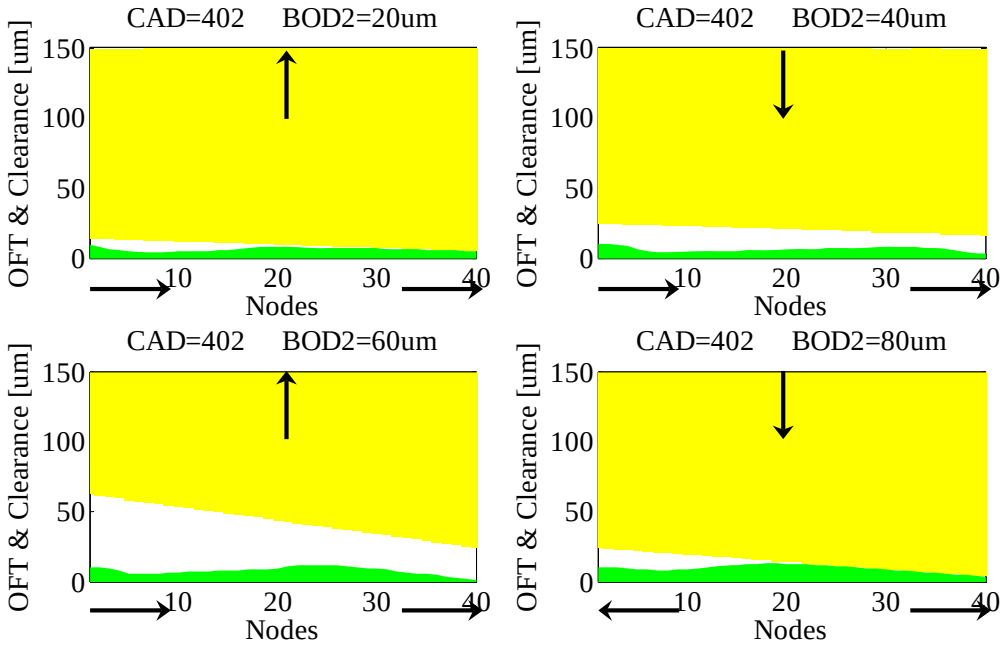

Figure 3-49 The oil film in the lower 2nd ring groove at CAD=402 (BOD2=20~80um)

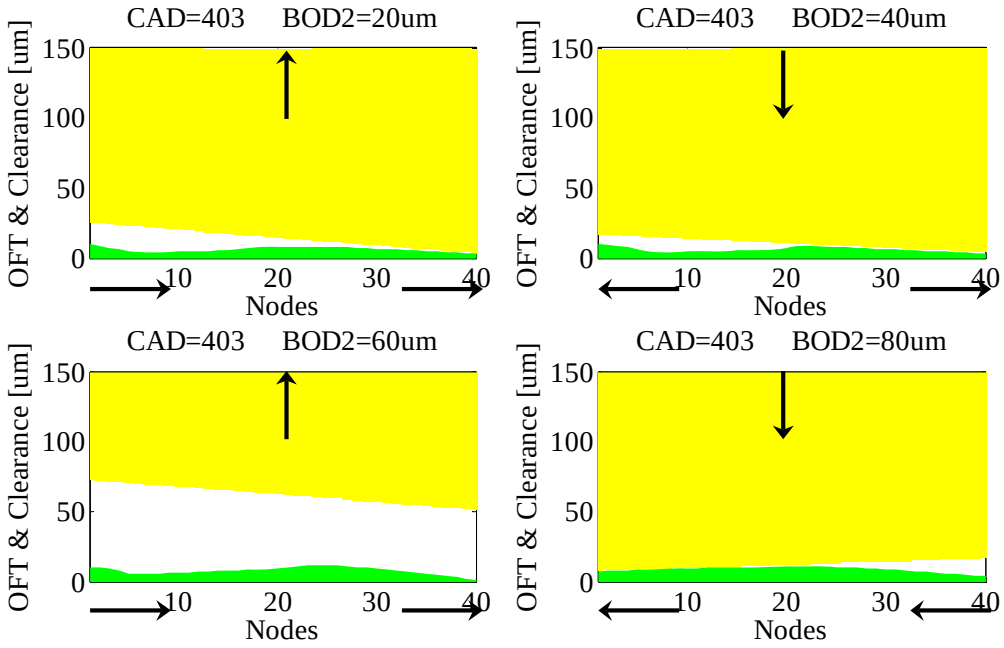

Figure 3-50 The oil film in the lower 2nd ring groove at CAD=403 (BOD2=20~80um)

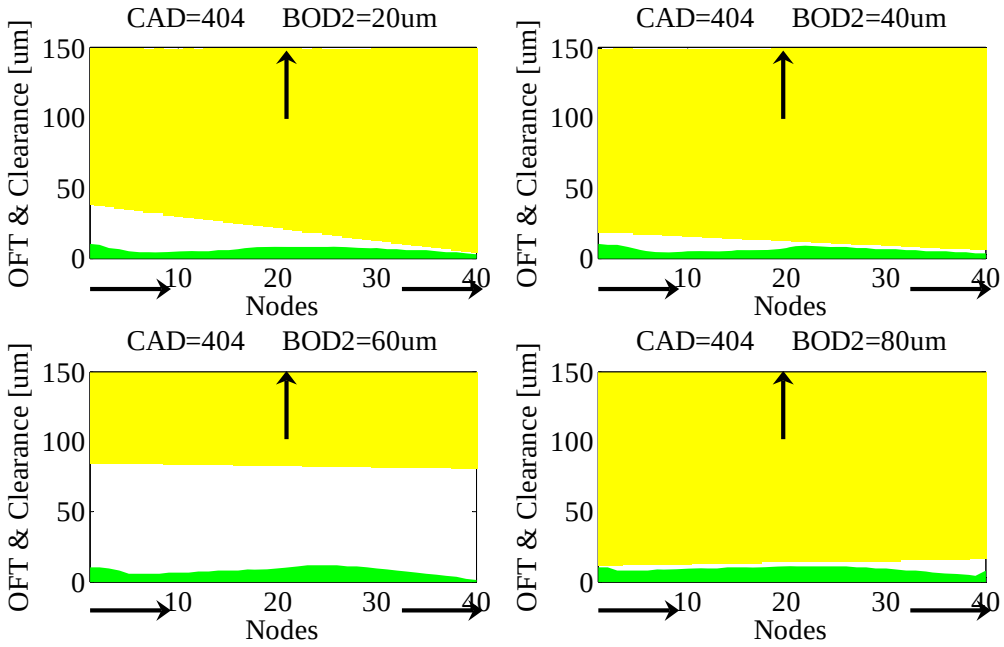

Figure 3-51 The oil film in the lower 2nd ring groove at CAD=404 (BOD2=20~80um)

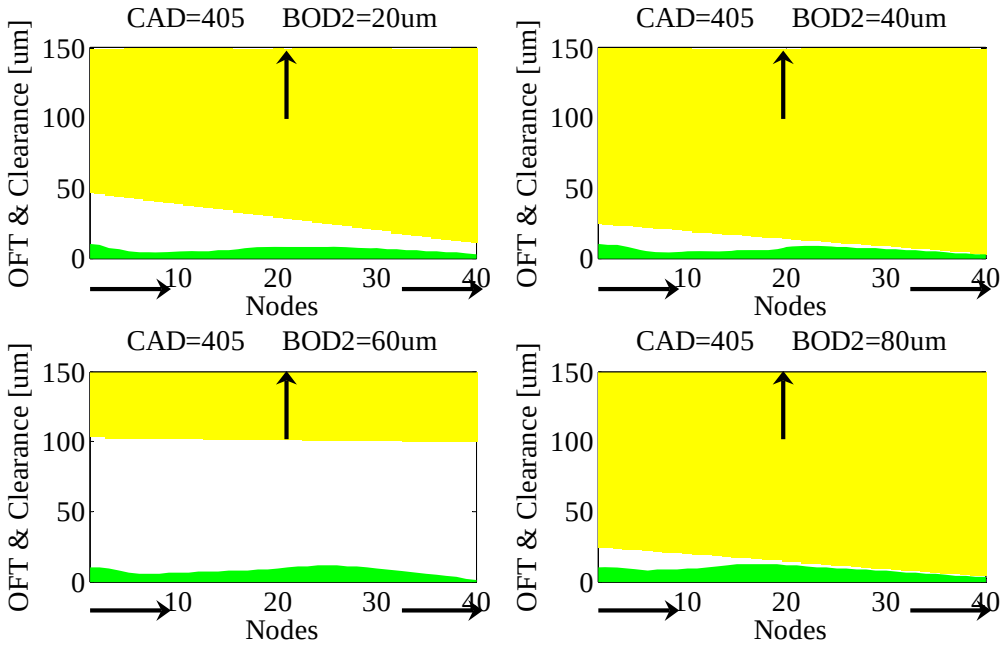

Figure 3-52 The oil film in the lower 2nd ring groove at CAD=405 (BOD2=20~80um)

In the following, the evolution of the 2nd ring motion and the lower oil film in the groove at several timeslots at the exhaust stroke is shown in Figure 3-53~57. The oil pumping phenomenon demonstrated in the intake stroke and the expansion stroke also happens from 680 CAD to 690 CAD

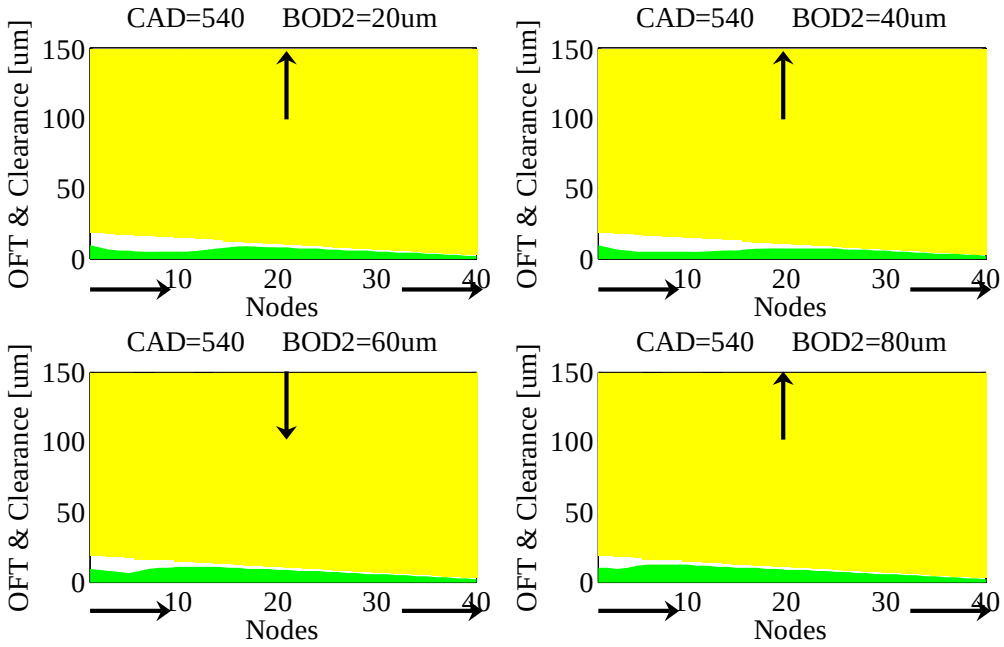

Figure 3-53 The oil film in the lower 2nd ring groove at CAD=540 (BOD2=20~80um)

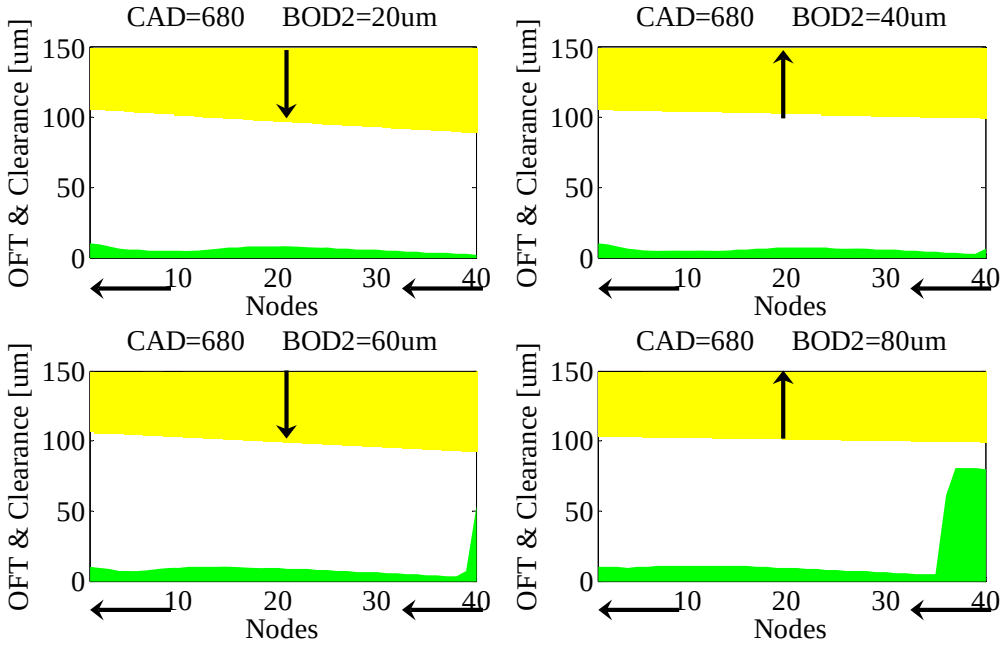

Figure 3-54 The oil film in the lower 2nd ring groove at CAD=680 (BOD2=20~80um)

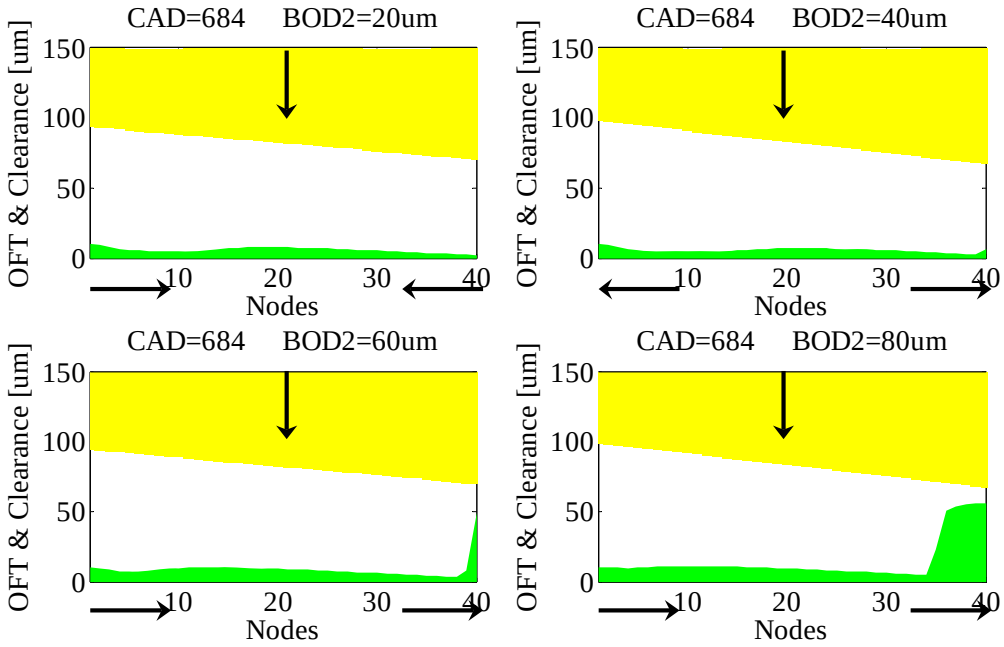

Figure 3-55 The oil film in the lower 2nd ring groove at CAD=684 (BOD2=20~80um)

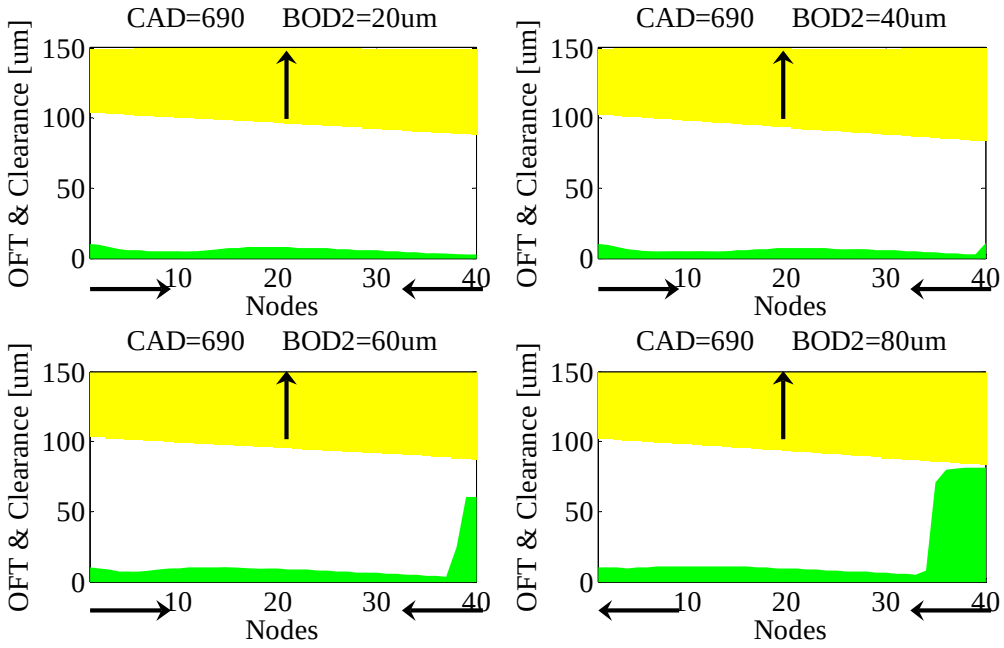

Figure 3-56 The oil film in the lower 2nd ring groove at CAD=690 (BOD2=20~80um)

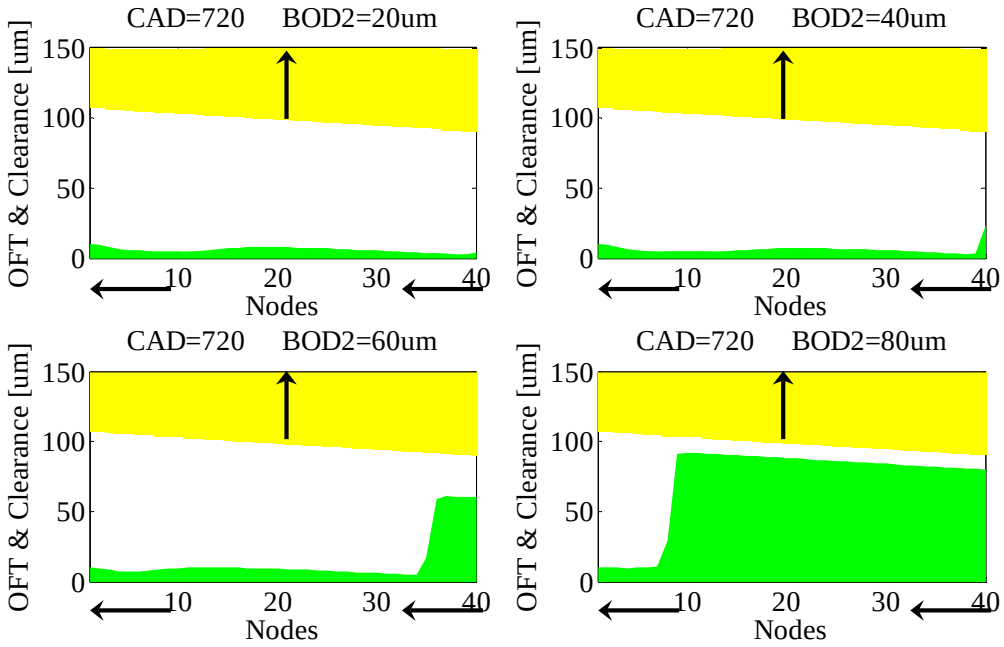

Figure 3-57 The oil film in the lower 2nd ring groove at CAD=720 (BOD2=20~80um)

Figure 3-58 shows the accumulated oil flow rates at the BOD2 (BOD2=20um~80um). The direction of the accumulated oil flow rate is from the 3rd land region to the inside of the 2nd ring groove, and the oil flow rate increases with the increase of the BID2. This is because more oil is pumped into the lower 2nd ring groove mainly at the early expansion stroke.

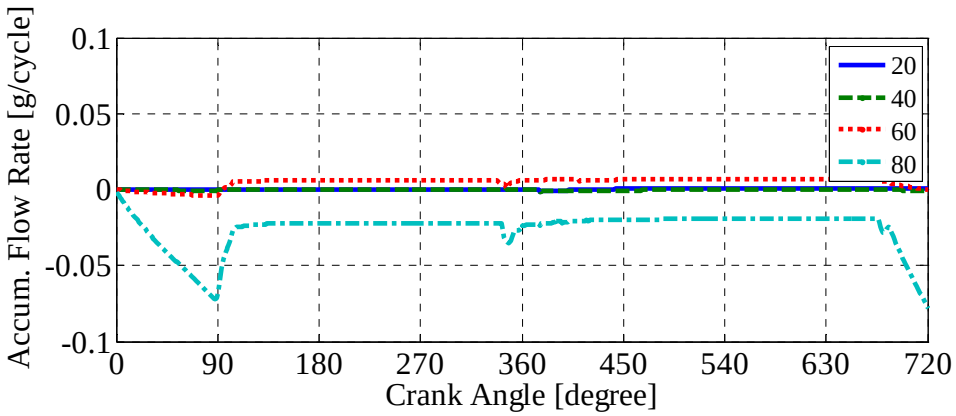

Figure 3-58 Accumulated oil flow rates at the BOD2 (BOD2=20um~80um)

3.2.3 The Effects of the Oil Supply at the TOD2

In this section, the boundary condition TOD2 is set as 20um, 40um, 60um, and 80um separately. Figure 3-59 and Figure 3-60 show the ring flutter from the late compression stroke to the early expansion stroke diminishes with the increase of the TOD2 boundary condition. Even there is no flutter for the 2nd ring when TOD2 is 80um. The oil supply

drives the oil flow from the 2nd land to the 2nd ring groove and then to the 3rd land. The direction is the same as the direction of the driven force generated by the pressure difference between the 2nd land and the inside of the 2nd ring groove and the pressure difference between the inside of the 2nd ring groove and the 3rd land. The oil film thickness at TOD2 varies from 20um to 80um corresponding to TOD2 when the 2nd ring moves down as shown in Figure 3-61. When the oil is pumped into the upper 2nd ring groove, whether it may reach the TID2 or not depends on the oil supply at the TOD2. In Figure 3-62, it can be easily found that the oil pumped into the upper 2nd ring groove can reach the TID2 for 60um TOD2 and 80um TOD2 in the late intake stroke and the early compression stroke and for 40um TOD2 from the late expansion stroke on.

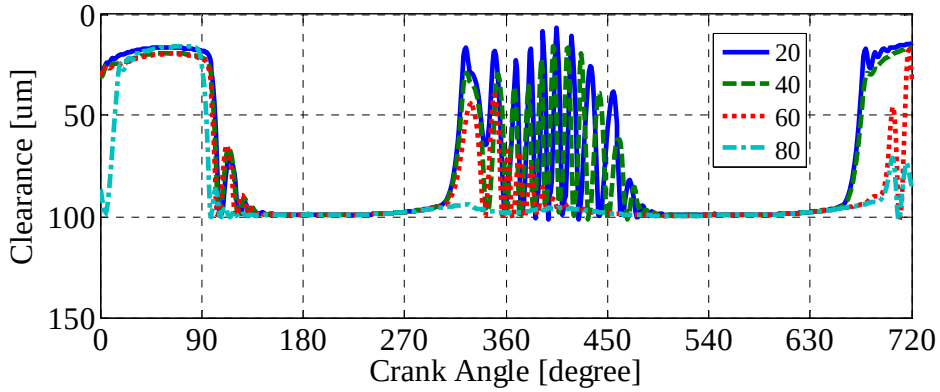

Figure 3-59 Clearance at the TOD2 (TOD2=20um~80um)

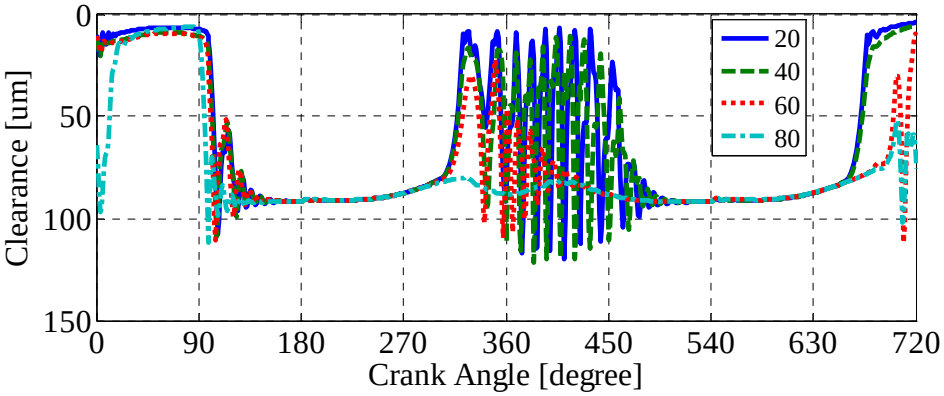

Figure 3-60 Clearance at the TID2 (TOD2=20um~80um)

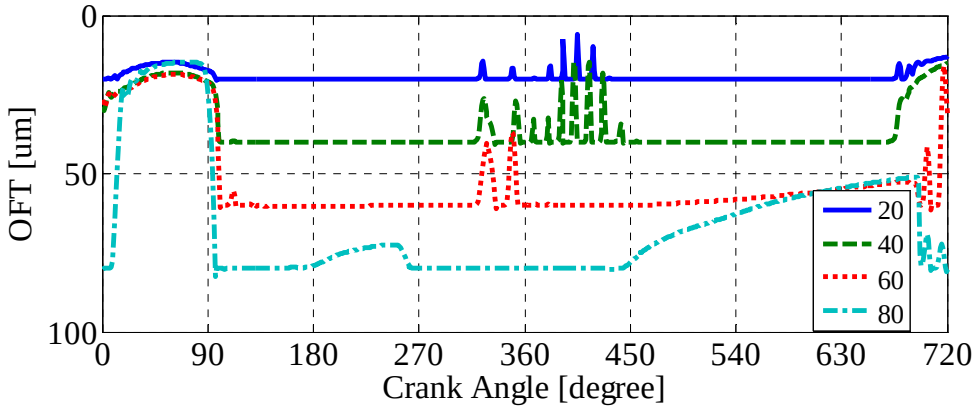

Figure 3-61 The oil film thickness at the TOD2 (TOD2=20um~80um)

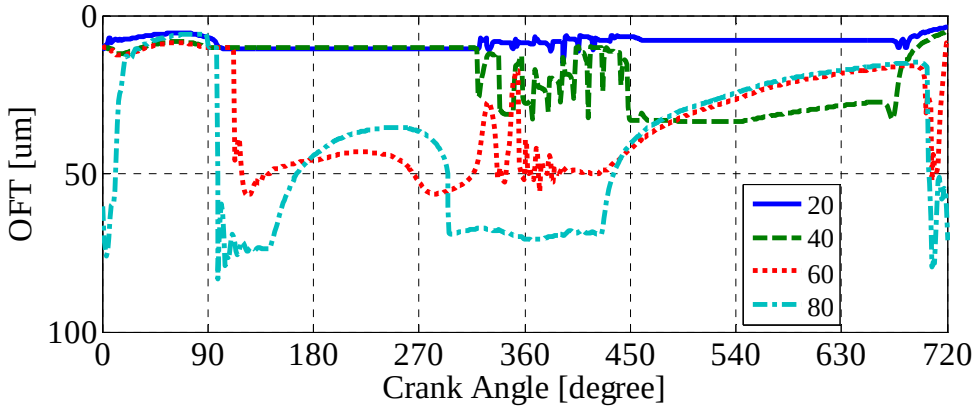

Figure 3-62 The oil film thickness at the TID2 (TOD2=20um~80um)

The evolution of the oil film in the upper 2nd ring groove and the 2nd ring motion throughout an engine cycle are shown in the following figures. In the following figures of this section, the yellow region is the 2nd ring, the green is the oil film, and the white is the gas channel. The vertical arrow at the top center indicates the direction of the 2nd ring motion, the horizontal arrow at the upper left corner shows the direction of the oil at TID2, and the horizontal arrow at the upper right corner shows the direction of the oil at TOD2.

The oil pumping phenomena in the late intake stroke are shown in Figure 3-63 (95 CAD) ~71 (114 CAD). Because of the sufficient oil supply for TOD2, the pumping process happens first for this boundary condition. Following, the oil is also pumped into the upper 2nd ring groove for 60um, 40um, and 20um TOD2.

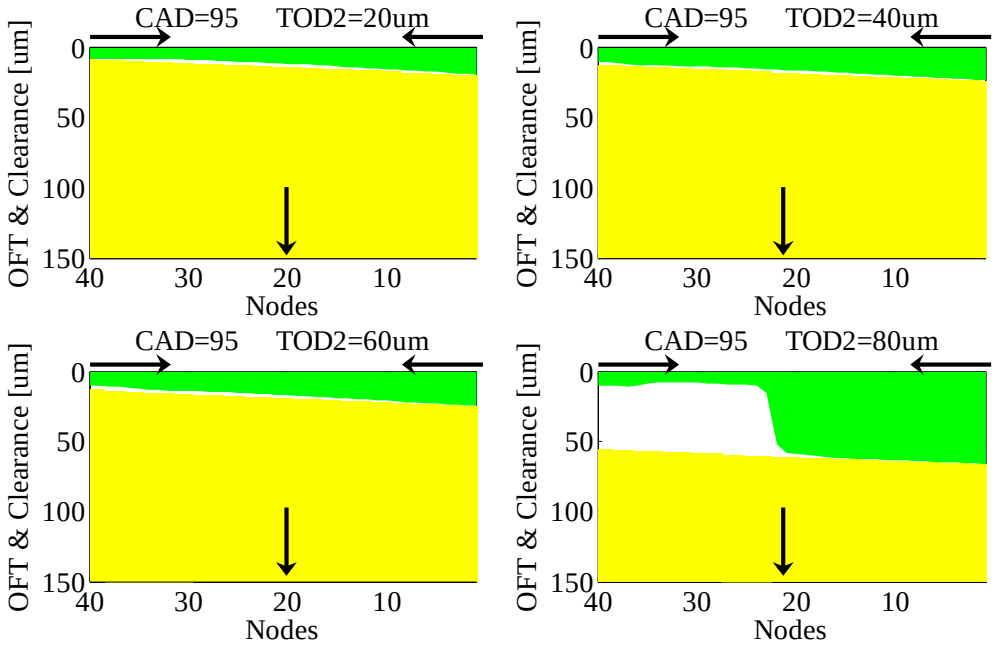

Figure 3-63 The oil film in the upper 2nd ring groove at CAD=95 (TOD2=20~80um)

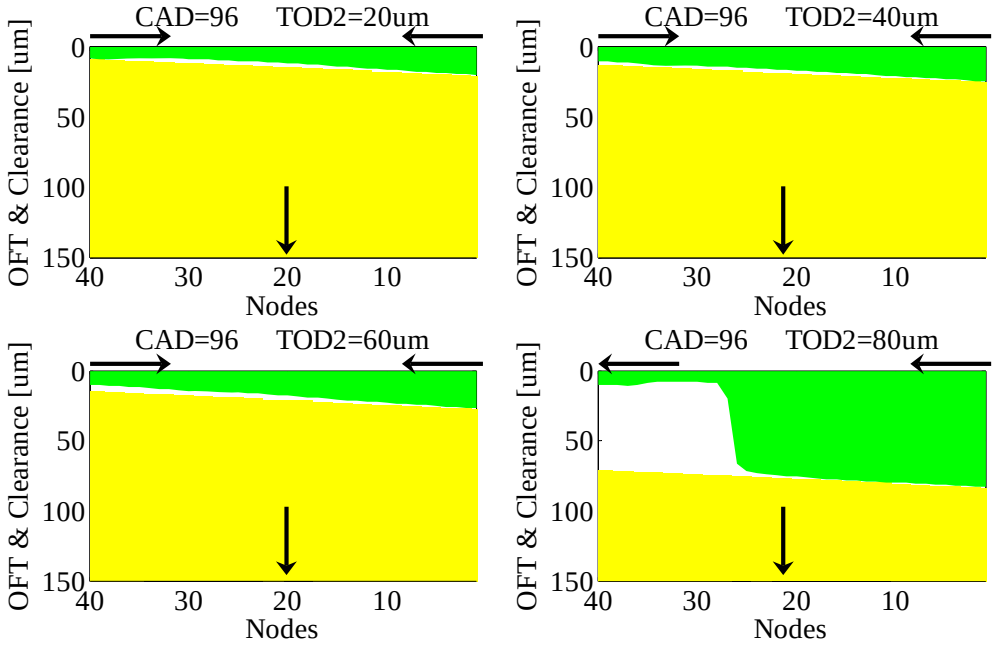

Figure 3-64 The oil film in the upper 2nd ring groove at CAD=96 (TOD2=20~80um)

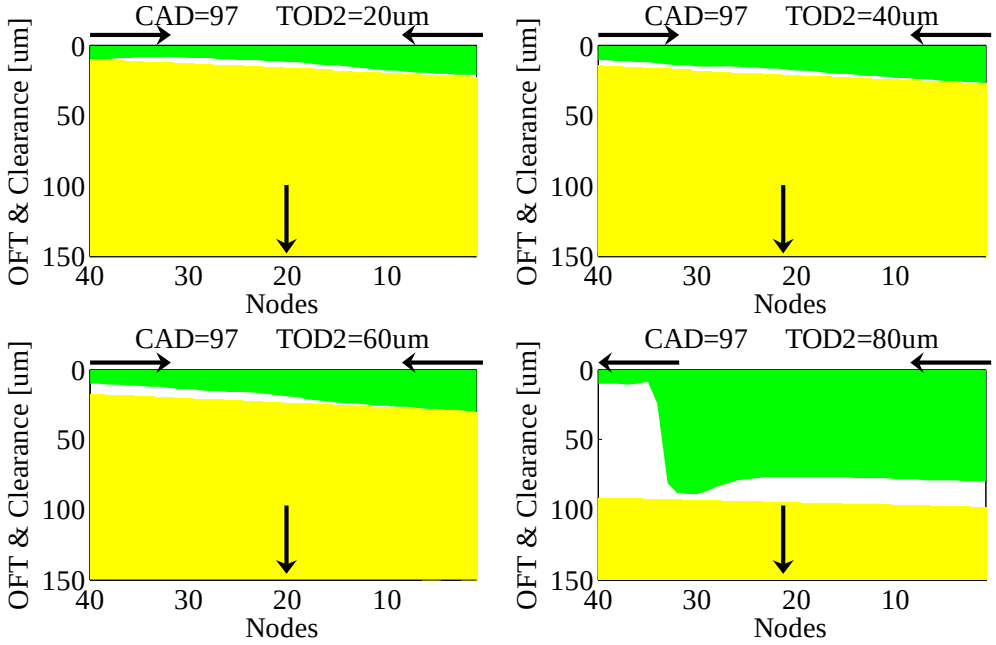

Figure 3-65 The oil film in the upper 2nd ring groove at CAD=97 (TOD2=20~80um)

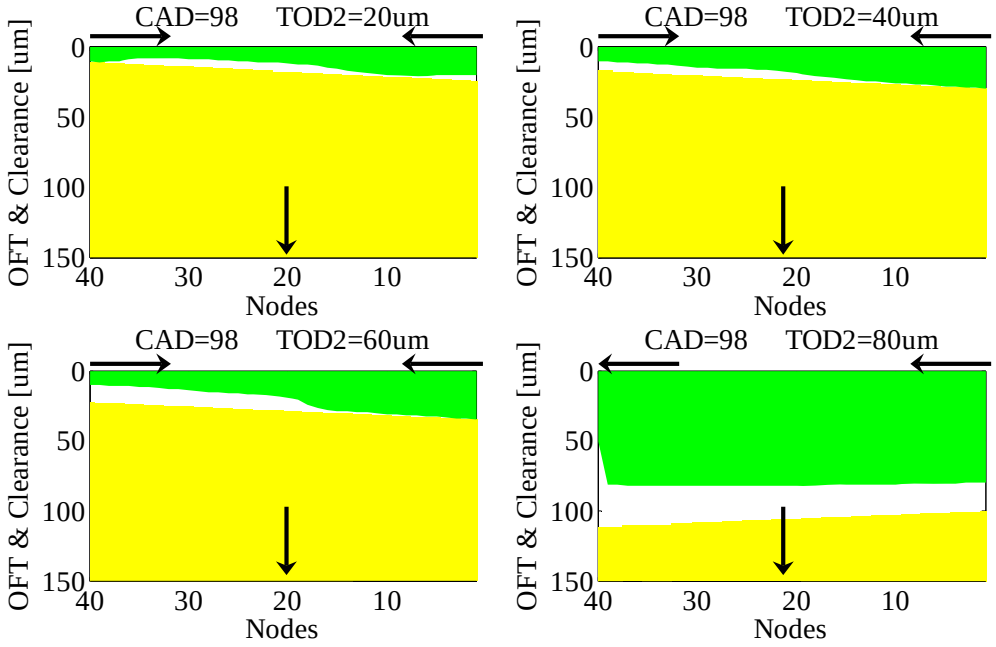

Figure 3-66 The oil film in the upper 2nd ring groove at CAD=98 (TOD2=20~80um)

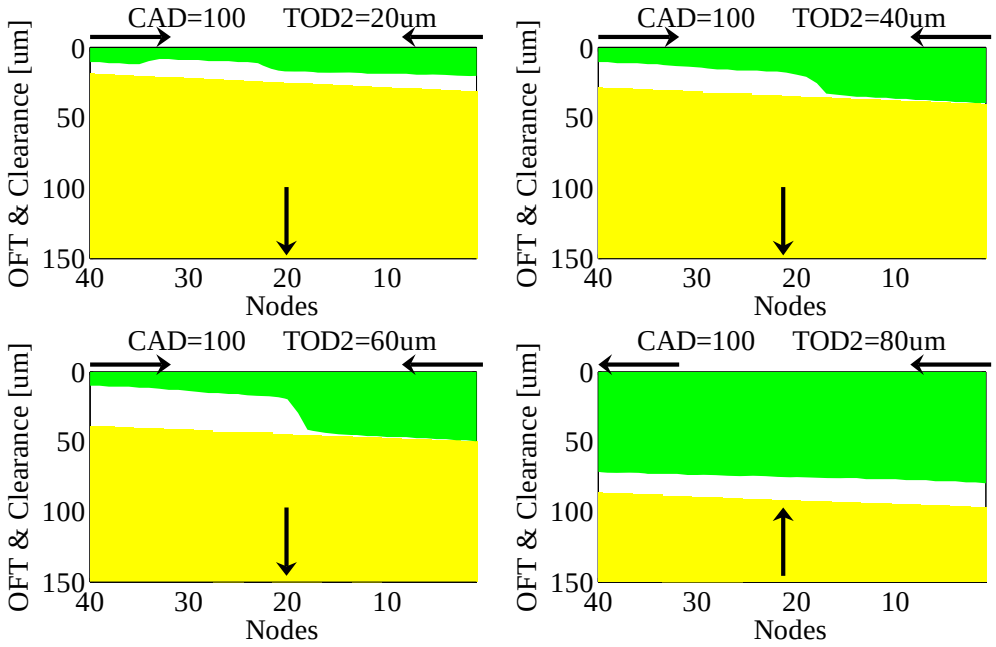

Figure 3-67 The oil film in the upper 2nd ring groove at CAD=100 (TOD2=20~80um)

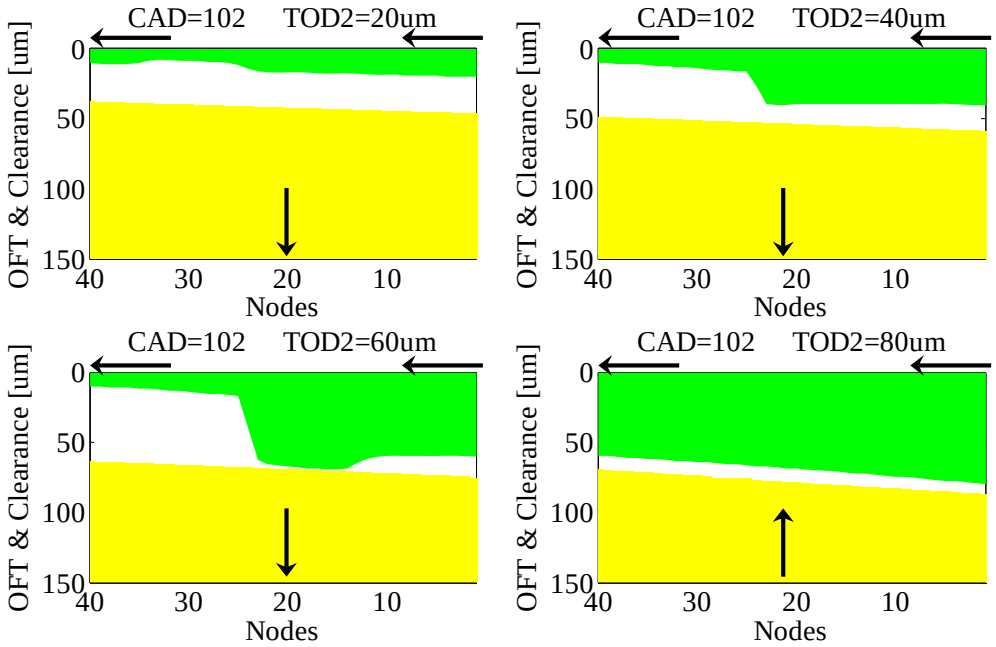

Figure 3-68 The oil film in the upper 2nd ring groove at CAD=102 (TOD2=20~80um)

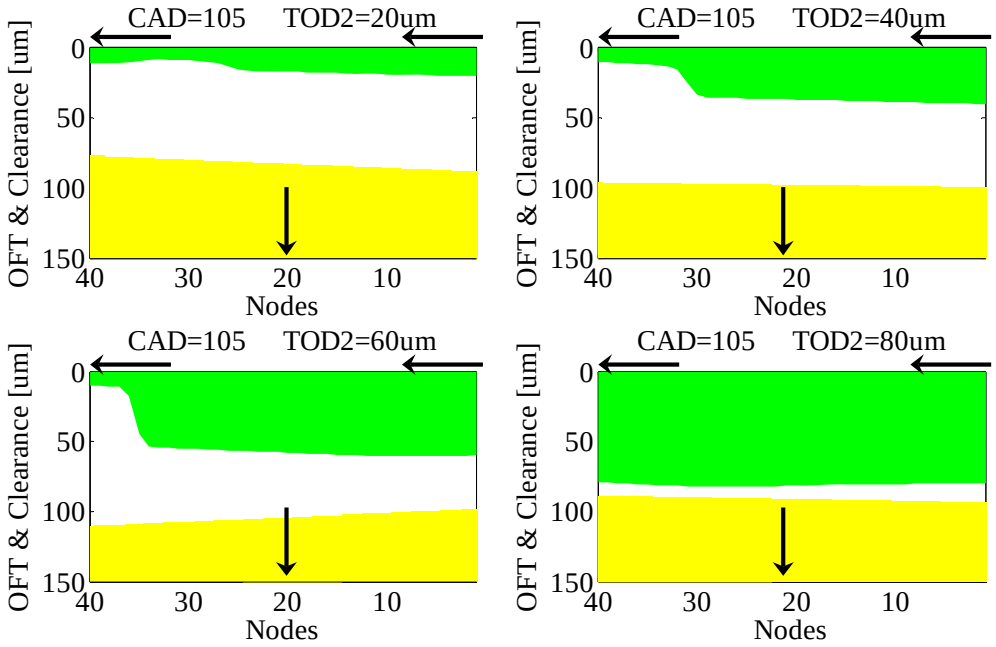

Figure 3-69 The oil film in the upper 2nd ring groove at CAD=105 (TOD2=20~80um)

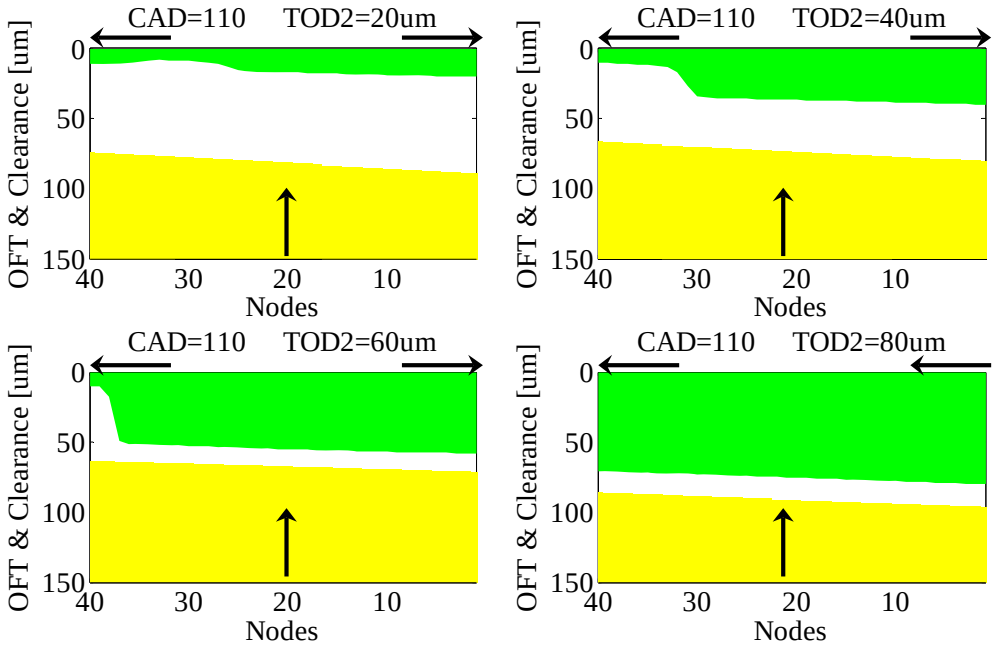

Figure 3-70 The oil film in the upper 2nd ring groove at CAD=110 (TOD2=20~80um)

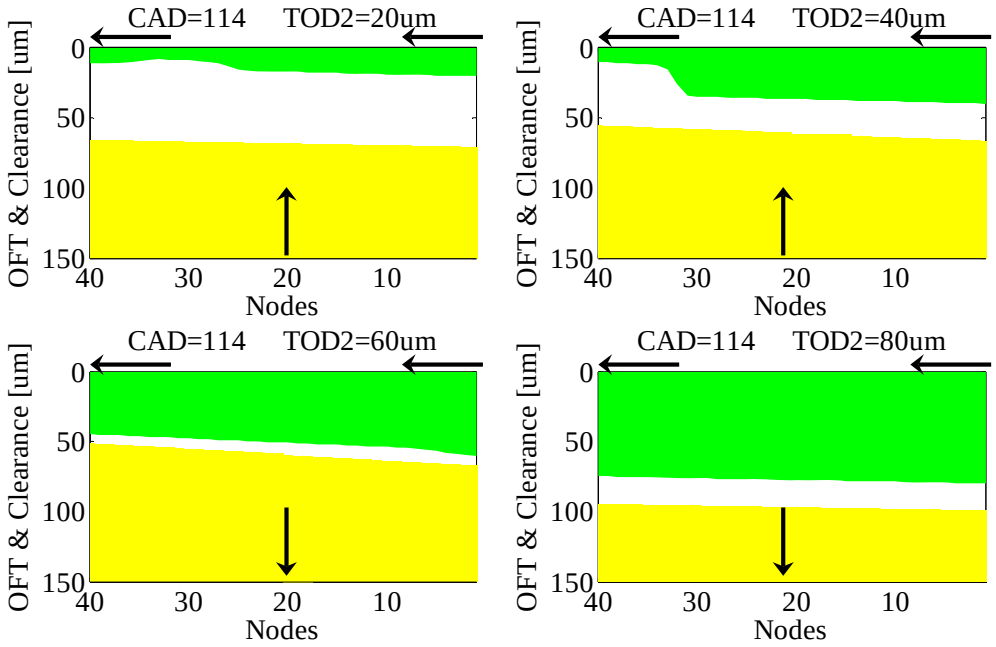

Figure 3-71 The oil film in the upper 2nd ring groove at CAD=114 (TOD2=20~80um)

The oil is pushed out of the upper groove by the 2nd ring at 180 CAD and 200 CAD, as shown in Figure 3-72 and Figure 3-73.

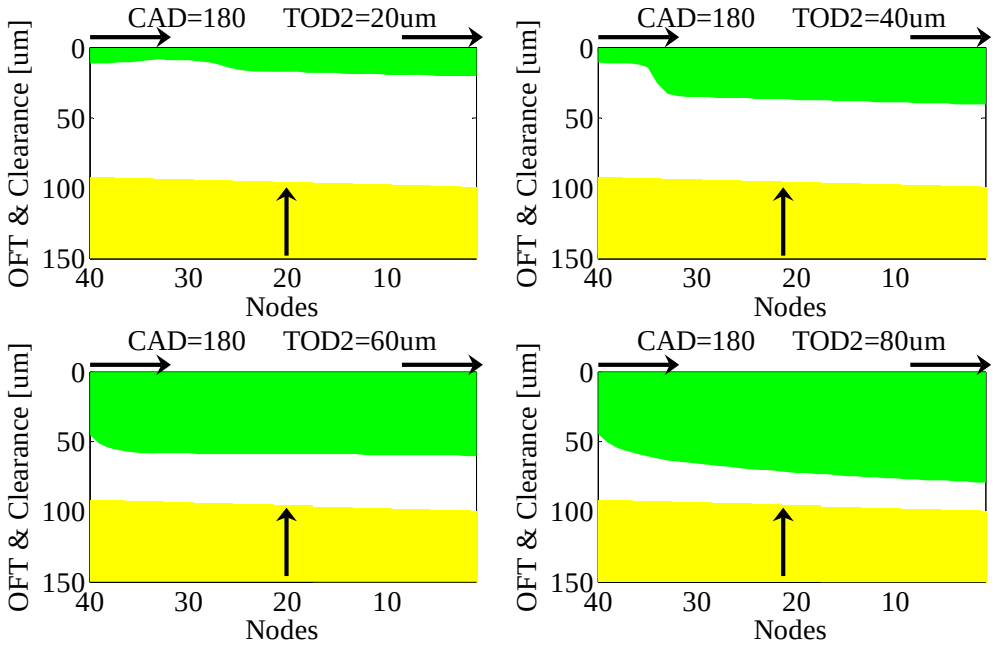

Figure 3-72 The oil film in the upper 2nd ring groove at CAD=180 (TOD2=20~80um)

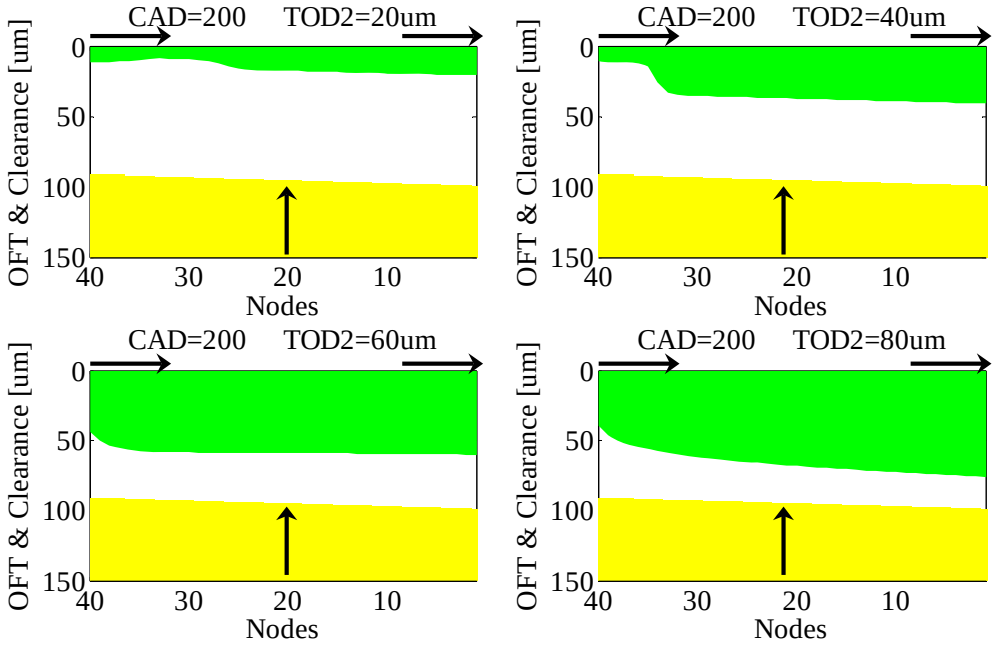

Figure 3-73 The oil film in the upper 2nd ring groove at CAD=200 (TOD2=20~80um)

For 20um, 40um, and 60um TOD2, the oil flows into the upper 2nd ring groove by the combined influence of pressure driven force and the 2nd ring motion. Because the large amount of oil is reserved in the groove for 80um TOD2, the oil flows out of the TOD2, as shown in Figure 3-74. However, after the oil amount decreases in the upper groove for 80um TOD2, the oil flows into the groove from the TOD2 again, as shown in Figure 3-75.

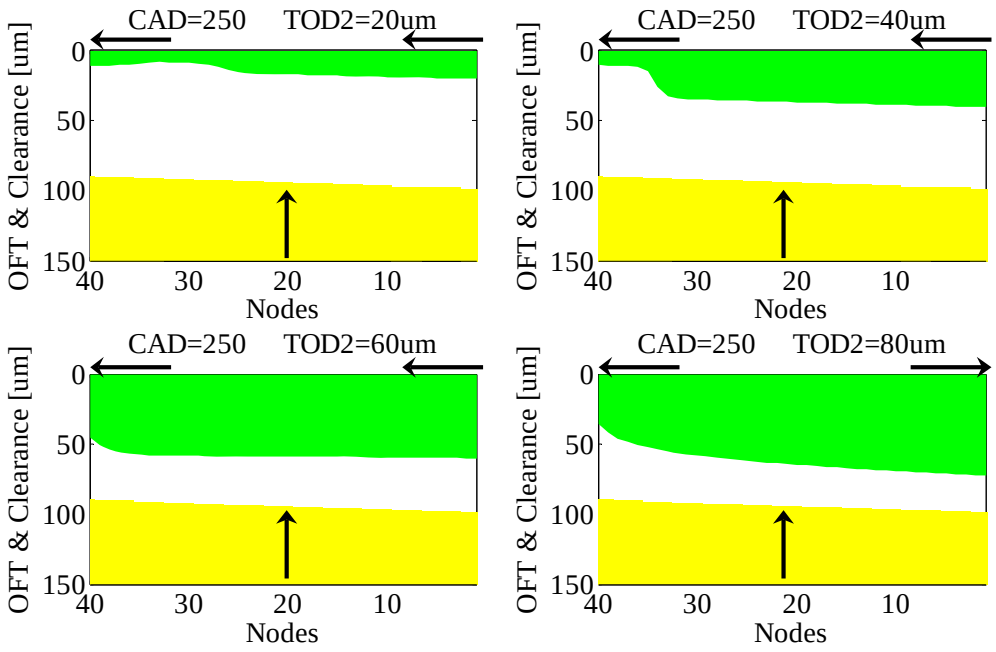

Figure 3-74 The oil film in the upper 2nd ring groove at CAD=250 (TOD2=20~80um)

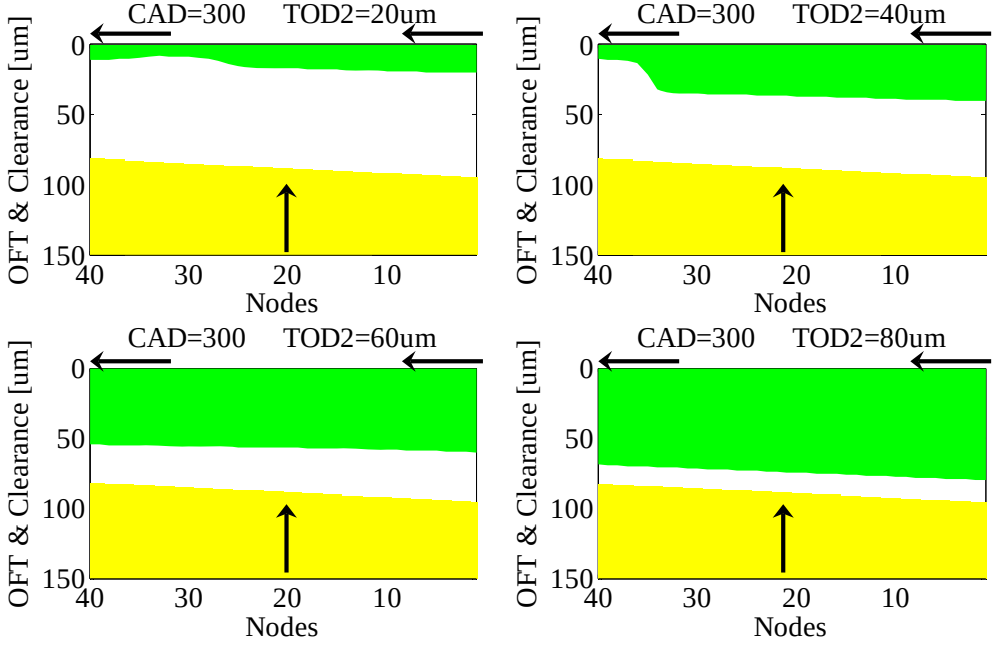

Figure 3-75 The oil film in the upper 2nd ring groove at CAD=300 (TOD2=20~80um)

Figure 3-76~81 show the stability of the 2nd ring by the influence of the thicken oil film in the upper ring groove for 80um TOD2. For other boundary conditions the 2nd ring motion has great effect on the upper oil film and therefore the direction of oil flow at both TOD2 and TID2.

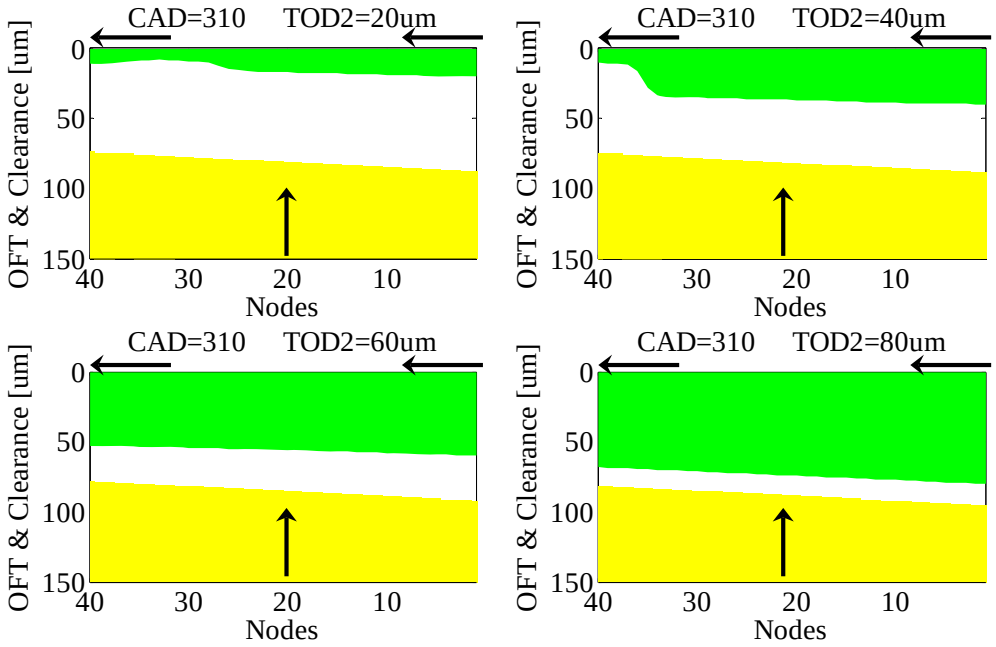

Figure 3-76 The oil film in the upper 2nd ring groove at CAD=310 (TOD2=20~80um)

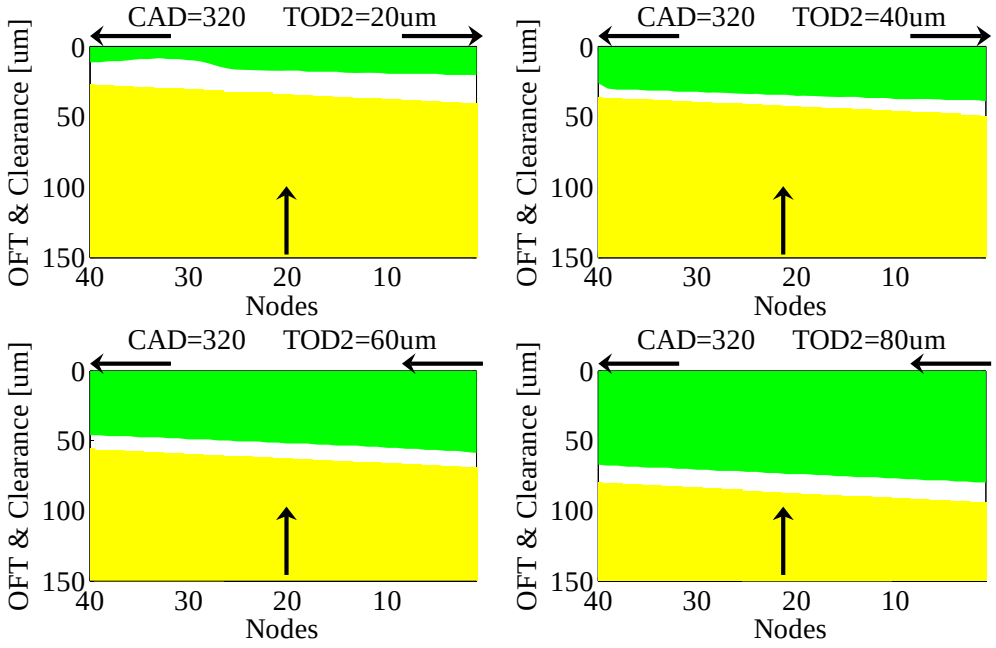

Figure 3-77 The oil film in the upper 2nd ring groove at CAD=320 (TOD2=20~80um)

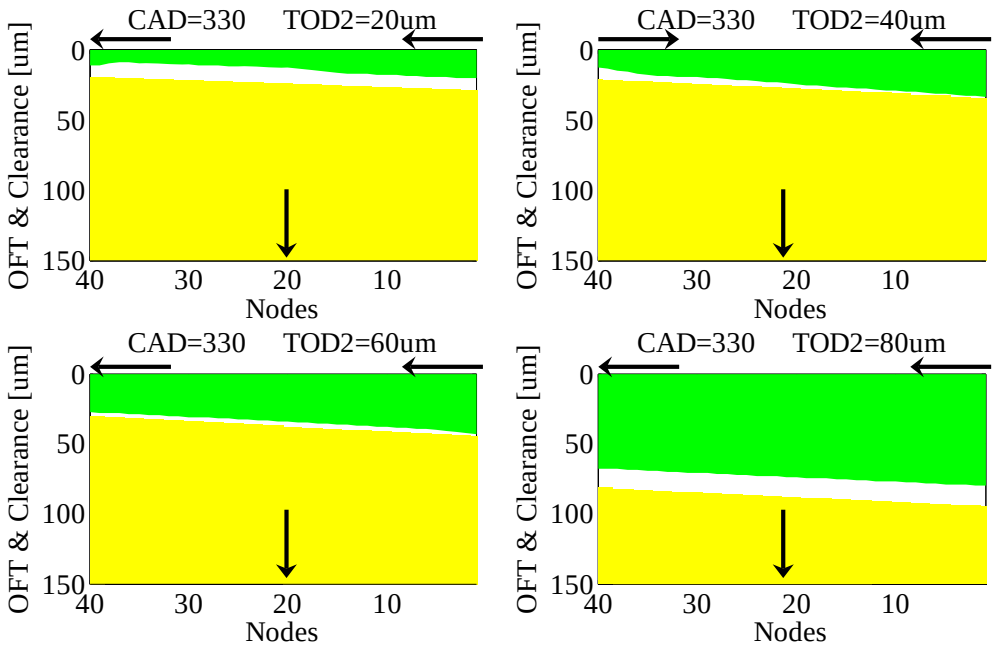

Figure 3-78 The oil film in the upper 2nd ring groove at CAD=330 (TOD2=20~80um)

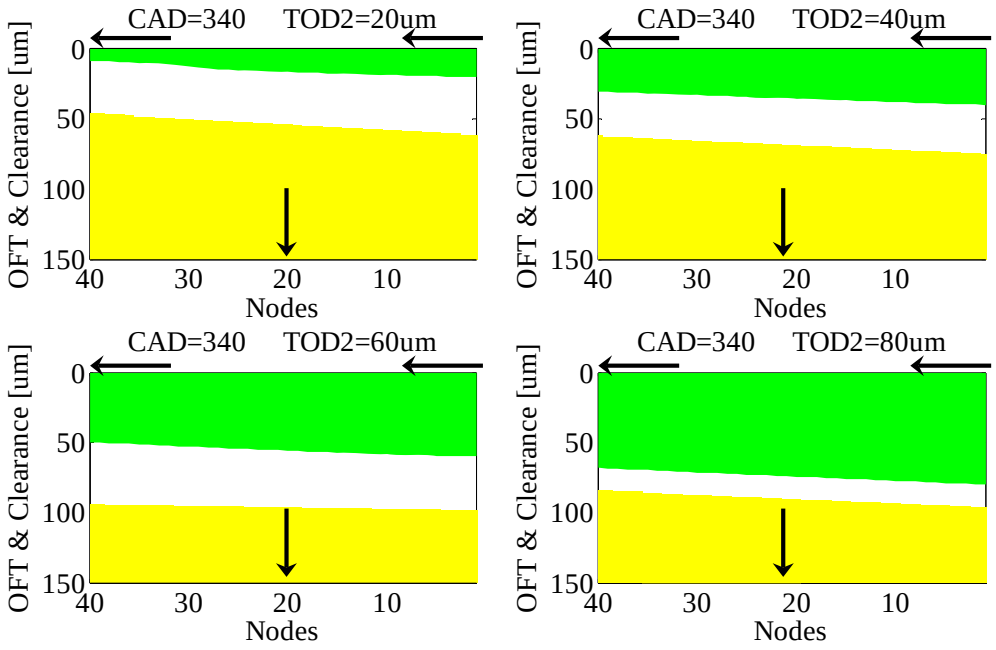

Figure 3-79 The oil film in the upper 2nd ring groove at CAD=340 (TOD2=20~80um)

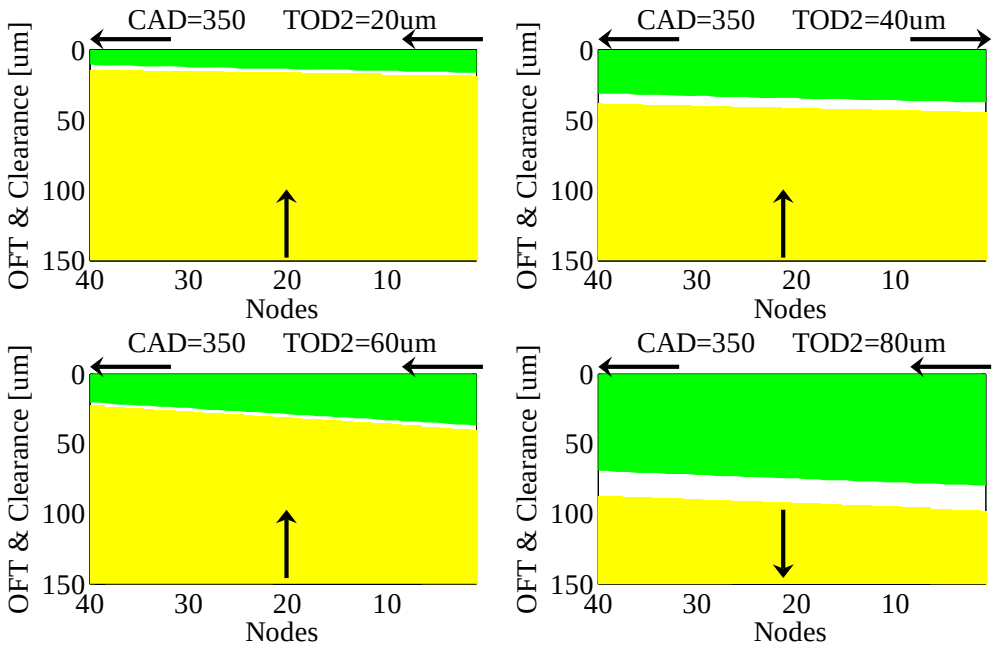

Figure 3-80 The oil film in the upper 2nd ring groove at CAD=350 (TOD2=20~80um)

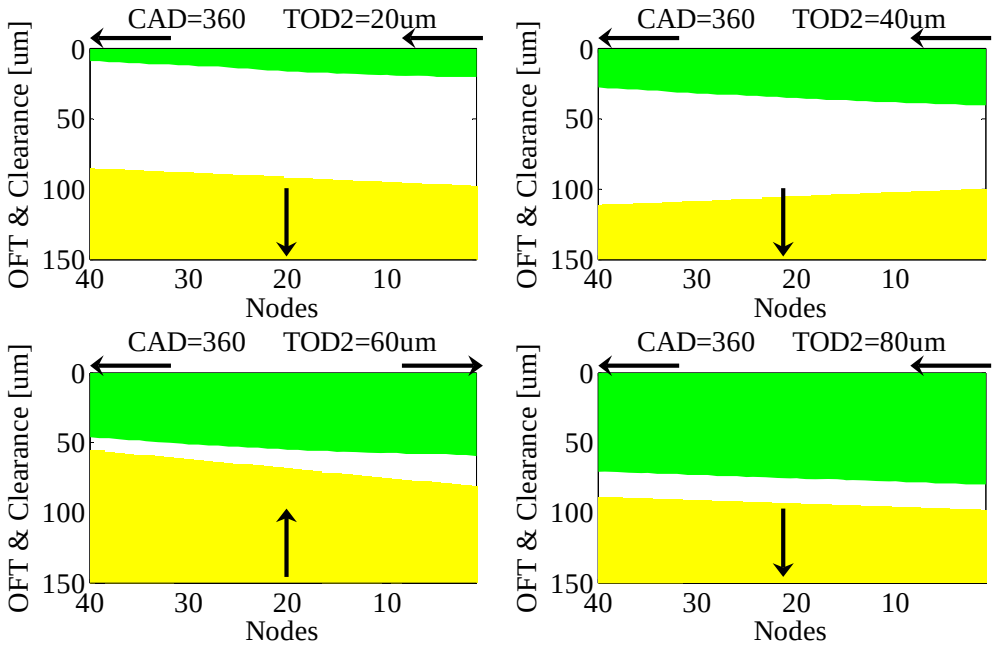

Figure 3-81 The oil film in the upper 2nd ring groove at CAD=360 (TOD2=20~80um)

The ring flutter and its effect on the upper oil film in the expansion stroke for 20um and 40um TOD2 are shown in Figure 3-82~91. At the same time, the oil keeps squeezing from the TOD2 for 60um and 80um TOD2.

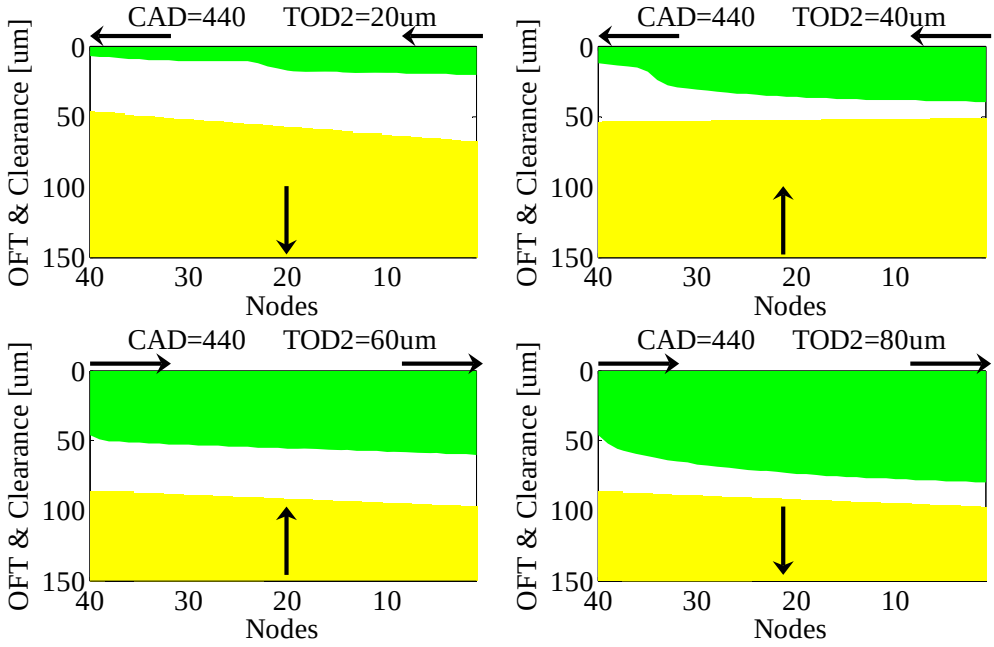

Figure 3-82 The oil film in the upper 2nd ring groove at CAD=440 (TOD2=20~80um)

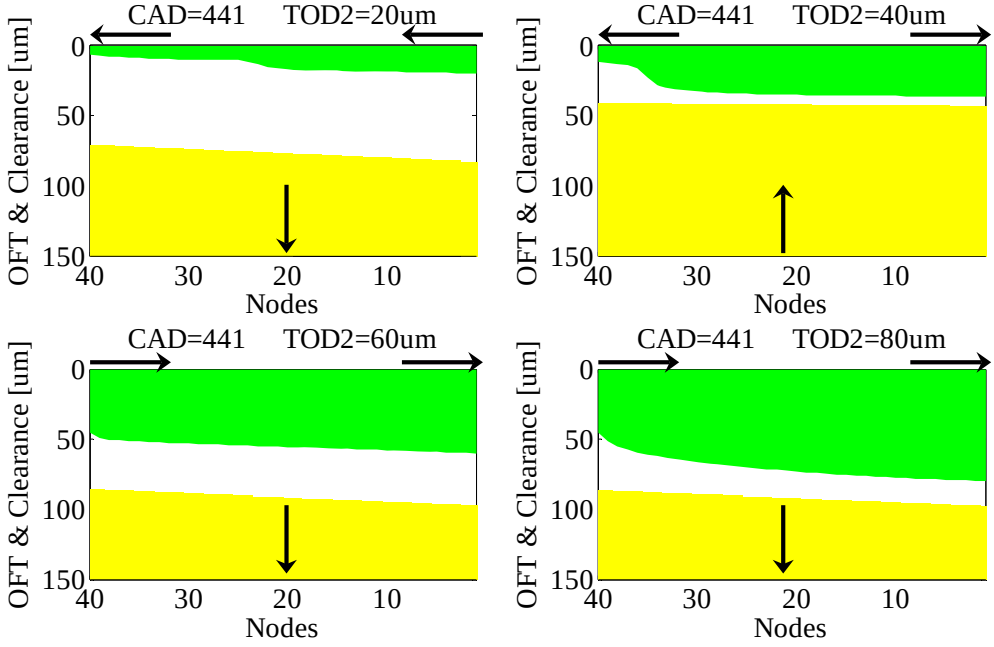

Figure 3-83 The oil film in the upper 2nd ring groove at CAD=441 (TOD2=20~80um)

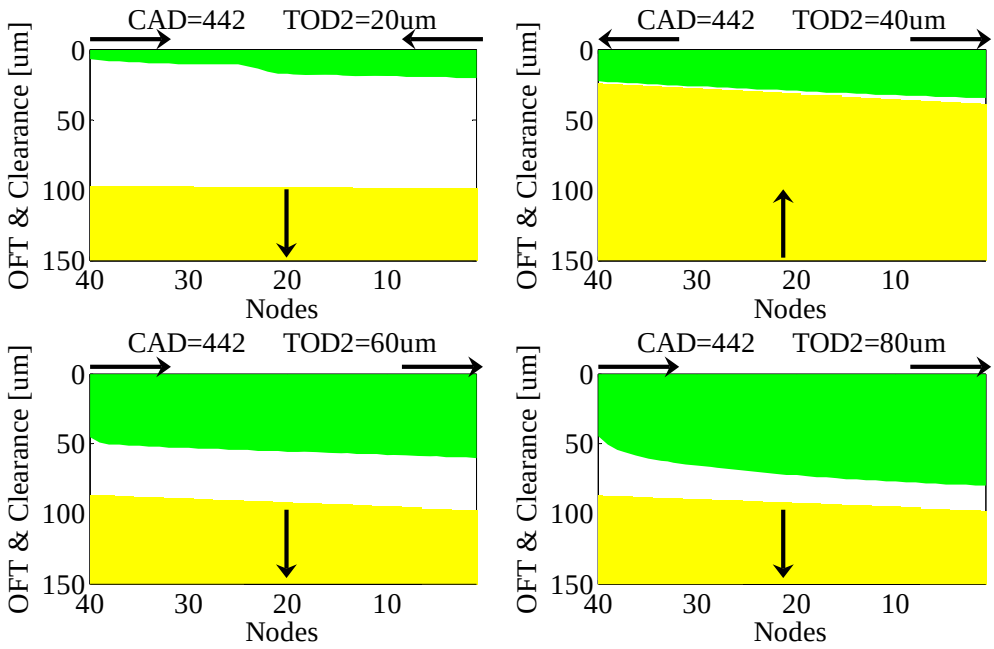

Figure 3-84 The oil film in the upper 2nd ring groove at CAD=442 (TOD2=20~80um)

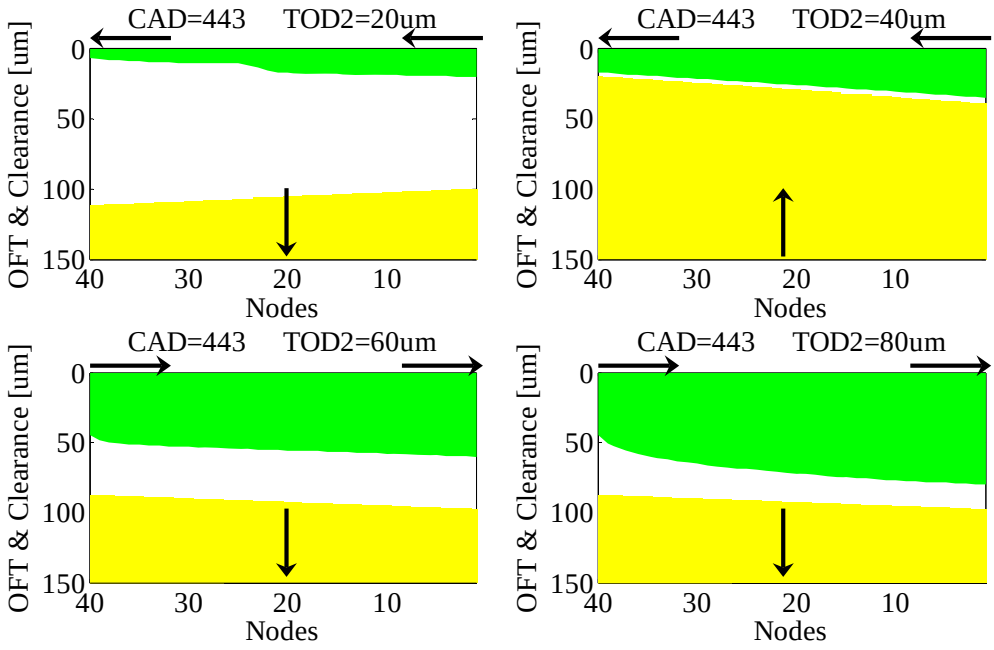

Figure 3-85 The oil film in the upper 2nd ring groove at CAD=443 (TOD2=20~80um)

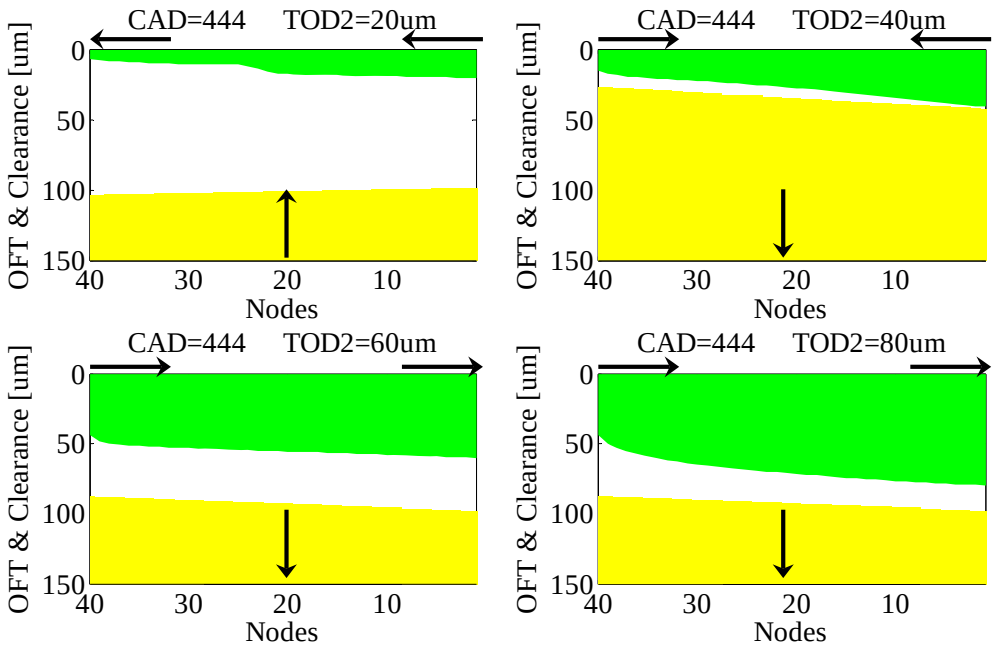

Figure 3-86 The oil film in the upper 2nd ring groove at CAD=444 (TOD2=20~80um)

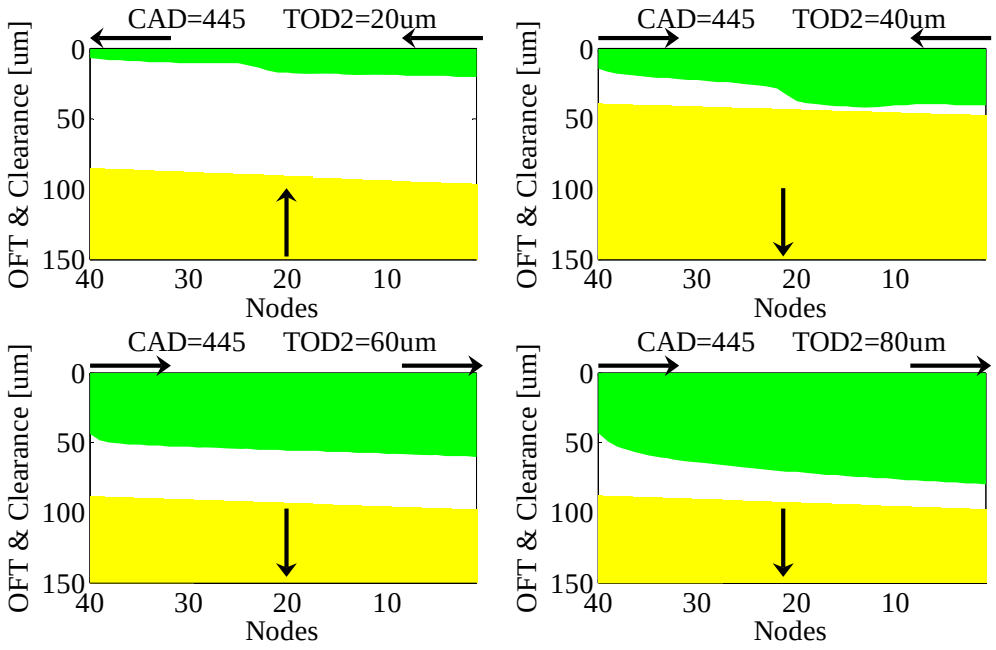

Figure 3-87 The oil film in the upper 2nd ring groove at CAD=445 (TOD2=20~80um)

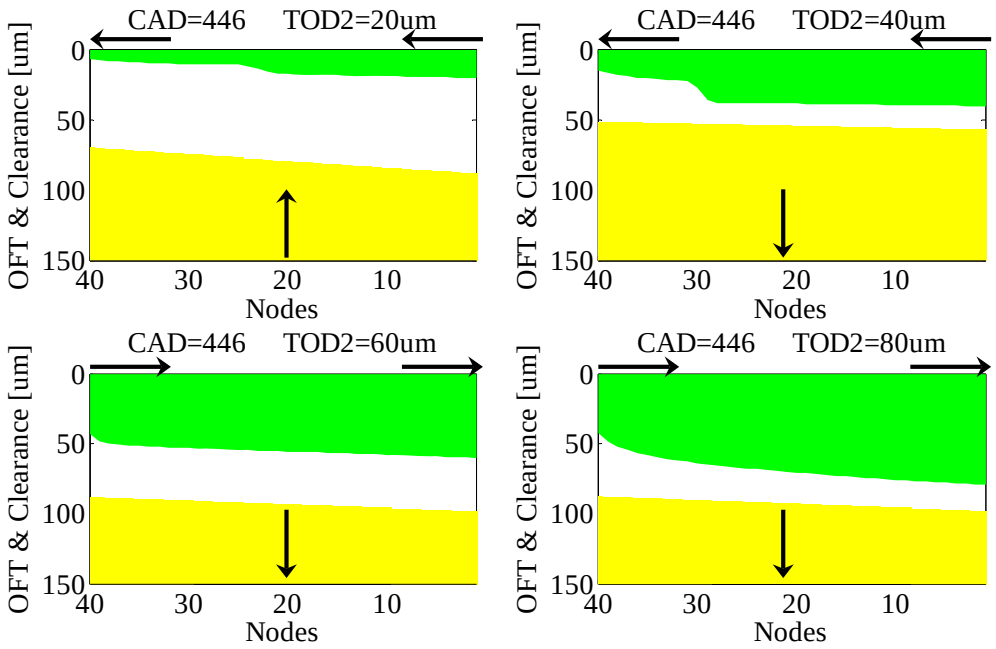

Figure 3-88 The oil film in the upper 2nd ring groove at CAD=446 (TOD2=20~80um)

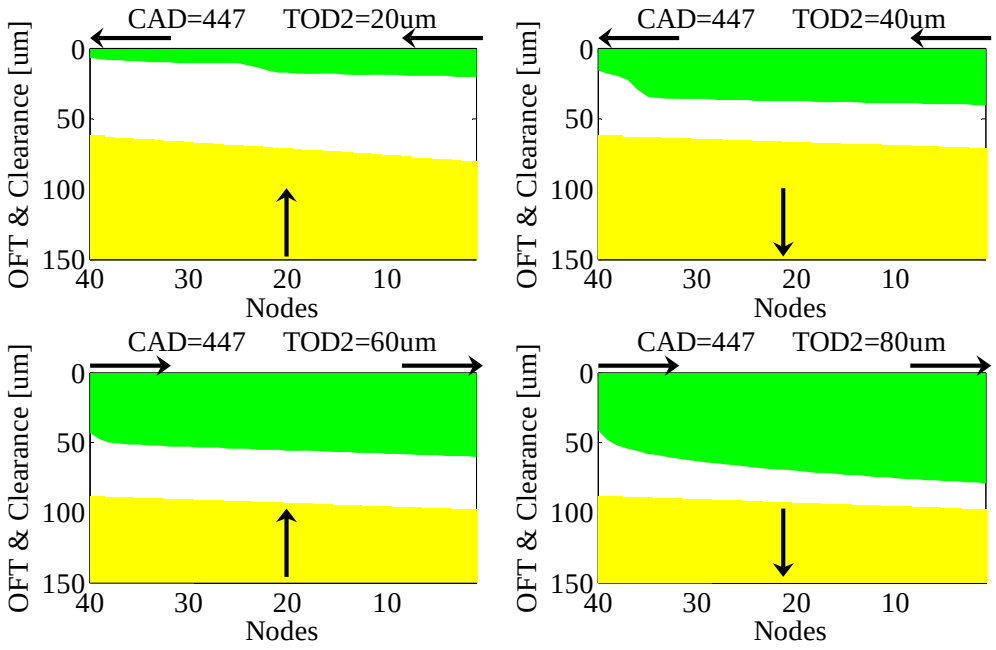

Figure 3-89 The oil film in the upper 2nd ring groove at CAD=447 (TOD2=20~80um)

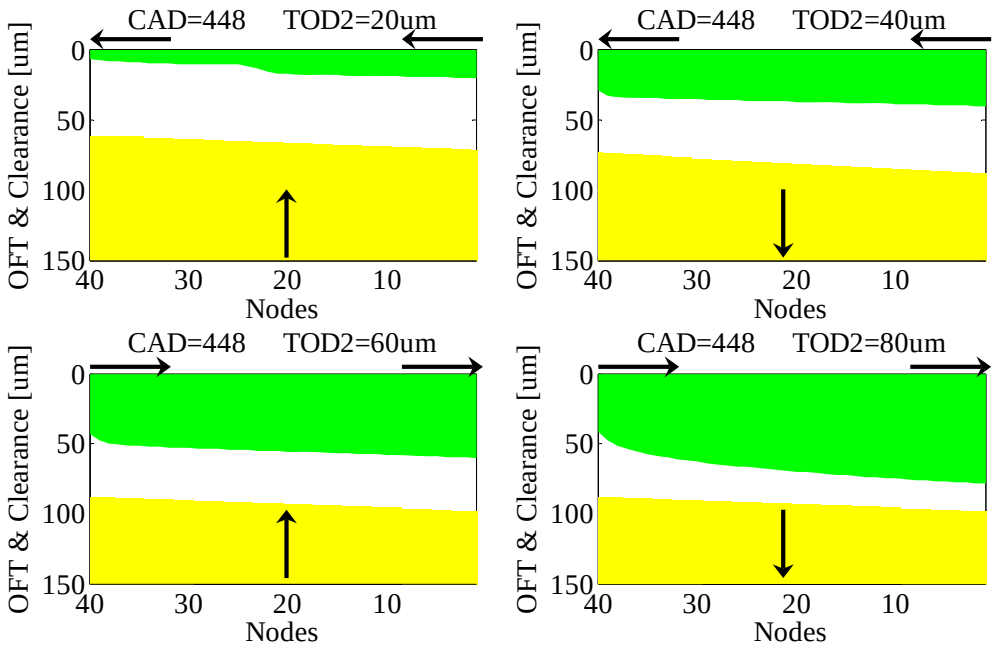

Figure 3-90 The oil film in the upper 2nd ring groove at CAD=448 (TOD2=20~80um)

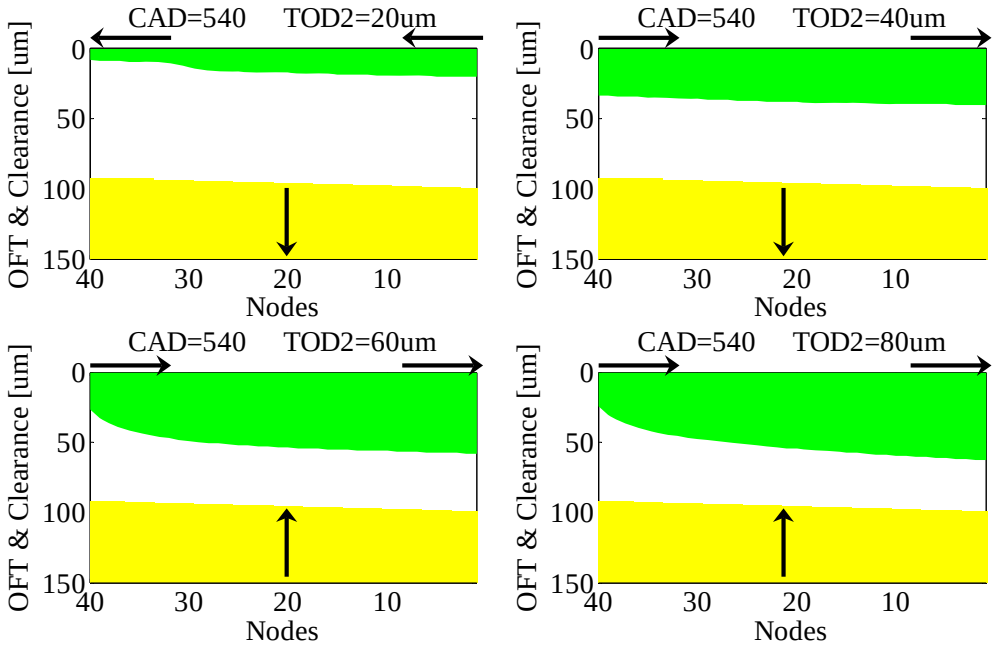

Figure 3-91 The oil film in the upper 2nd ring groove at CAD=540 (TOD2=20~80um)

Figure 3-92 shows the accumulated oil flow rates at the TOD2 (TOD2=20um~80um). The direction of the accumulated oil flow rate is from the 2nd land region to the inside of the 2nd ring groove, and the oil flow rate increases with the increase of the TOD2. This is

because more oil is pumped into the upper 2nd ring groove mainly at the late intake stroke and the early expansion stroke.

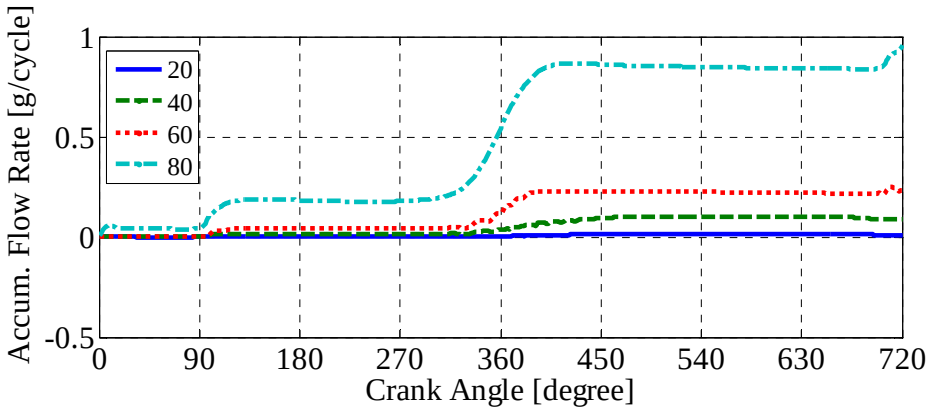

Figure 3-92 Accumulated oil flow rates at the TOD2 (TOD2=20um~80um)

3.3 Conclusion

The coupled model is applied to the analysis of a heavy duty diesel engine. Ring dynamics, force and moment balance of the rings, and gas and oil transport analysis are carried out. Emphasis has been placed on the variation of the oil film thickness due to the motion of the first two rings. The effect of oil supply on oil and gas transport in the 1st and 2nd ring grooves and on the pressure distribution in sub-regions of the ring-pack system was discussed.

At the operating condition studied here, the 1st ring always stays on the oil film attached on the piston flank of the lower 1st ring groove, and the 2nd ring moves up and down due to the inertial force from the axial acceleration/deceleration of the piston. The oil film distribution shown for these two rings demonstrates the oil pumping phenomena at different periods of the cycles. The force and moment balance analysis guarantees consistence between the motion of 1st and 2nd rings and the oil film distribution in their grooves.

The effect of the oil supply in the vicinity of the 2nd land and 3rd land on the oil flows in the 2nd ring groove was discussed: If the oil supply in the vicinity of the 3rd land reaches a specific amount, the oil can be pumped into the 2nd ring groove; The more oil is supplied in the vicinity of the 2nd land, the more oil flows into the 2nd ring groove; The evolution of the oil film in the upper 2nd ring groove and the 2nd ring motion throughout an engine cycle was also demonstrated.

(This page was intentionally left blank)

4. The Application of Coupled Model at Low Load in SI Engine

Oil consumption in engines is one of the primary interests for the automotive industry in order to control emissions and reduce service cost. The oil flow patterns and mechanisms lack understanding. Therefore it is extremely challenging to reduce the oil consumption from the ring pack system in SI engines. However, the oil consumption from the ring-pack systems significantly contributes to the total engine-out oil consumption.

The engine's load plays a major role in ring dynamics, oil transport and consumption, and blowby. The peak pressure inside the cylinder evolves dramatically from about 1bar manifold pressure at wide open throttle to a low load of around 150mbar at closed throttle. As such, the pressure inside the ring-pack system decreases accordingly, and the ring motion, including the linear and angular position and timing, changes as well due to the pressure driven forces and moments. The ring motion influences the clearances between ring and groove flanks and, therefore, the OFT distribution. Once again, the OFT distribution has an effect on the pressure distribution on the ring flanks and accordingly the ring dynamics. In conclusion, the engine's load plays more than a catalyst role in the oil consumption and blowby analysis.

Due to the reasons mentioned above, it is imperative to apply the coupled model to the low load analysis of SI engines. The specific roles of load in oil consumption and blowby studies can be demonstrated through detailed analysis of mass flow rates of oil and gas, OFT distribution and variation, and ring lift and twist timing and magnitude.

Unfortunately, experiments couldn't provide sufficient information regarding the oil flow rate into and out of the top ring groove. Therefore the oil pumping model was necessary to estimate the flow rate into and out of the top ring groove. The objective was to determine under what conditions oil could enter and exit the ring grooves, and the relative magnitude of the flow rates.

4.1 Steady State Analysis under High Intake Pressure

This model was applied to a spark-ignited engine, which comprises two compression rings and a U-flex oil-control ring. The specifications of the engine and the top two rings, as well as the operating conditions are presented in Table 4-1. This engine is the same as the one used by Przesmitzki, S. [38]. Figure 4-1 is the measured cylinder pressure at 3500 rpm under high intake pressure. The crankcase pressure remains near atmospheric pressure under all conditions. As can be seen in the figure, the peak pressure is around 19 bars.

In this section, the boundary conditions are varied to simulate the different situations of oil transport in the top ring groove as shown in Figure 4-2:

- oil starvation ((A));

- oil filling the lower groove ((B) and (C));
- oil filling the inside of the groove ((D));
- oil filling the upper groove ((E));
- oil flooded everywhere ((F)).

Table 4-1 Engine specifications

Bore Diameter	86.6mm
Stroke	88.0mm
Connecting Rod Length	158mm
Speed	3500RPM
Load	low

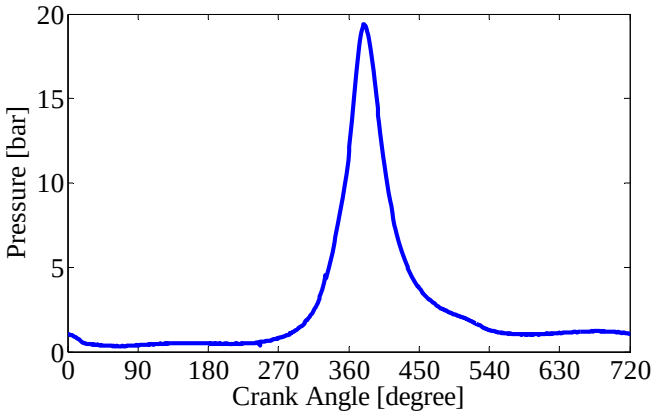

Figure 4-1 Cylinder pressure under 500mbar intake pressure at 3500 RPM

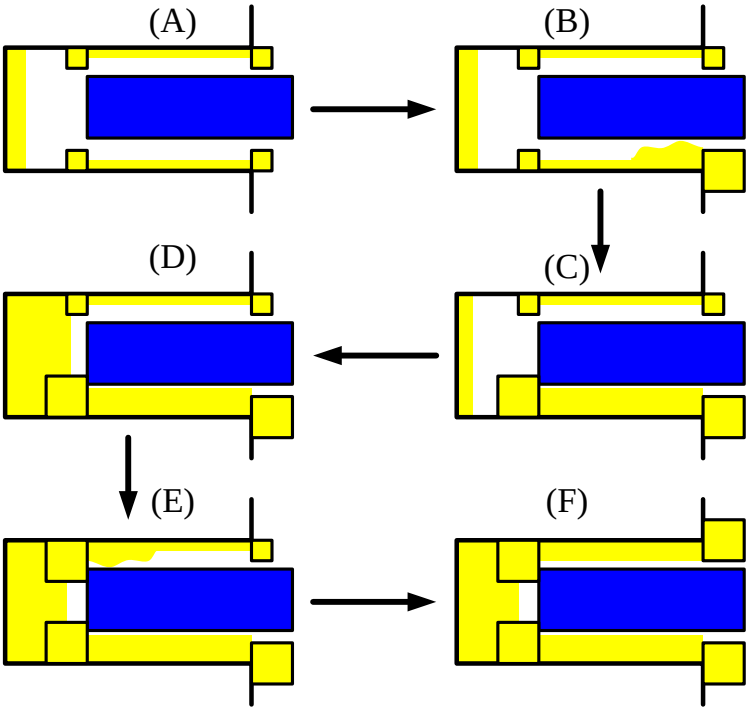

Figure 4-2 Flow chart of the oil filling process for the 1st ring groove

4.1.1 Oil Starvation in the First Ring Groove

First, the model was applied to a relatively starved condition as shown in Figure 4-3. The sizes of oil reservoirs for such condition are listed in Table 4-2 and the oil filling fraction inside the 1st ring groove is 10%. The oil film thickness and gas channel clearance in both the upper and lower 1st ring groove at the ID and OD are shown in Figure 4-4. The top red regions are oil films in the upper ring groove and the black regions below show oil films in the lower ring groove. The blue curve in both figures represents the clearance between the lower flank of the ring and groove at ID (left figure) and OD (right figure). The region between the upper oil film and the curve is the clearance for gas flow to go through the upper ring groove and the region between the curve and the lower oil film is also a gas channel.

At ID and OD of the top ring groove, the thickness of both the upper and lower oil film is less than 10um. Therefore, there is a large area for the top ring to lift upwards and downwards. The oil film thickness affects ring motion through the interaction of the ring flank with the upper oil film during the intake and compression strokes and the late exhaust stroke at the ID. The oil film thickness influences ring motion by the lower oil film from the late compression stroke to the late exhaust stroke at the OD. The effect of the oil film under this condition will be discussed later and be compared with the case shown in section 4.1.2.

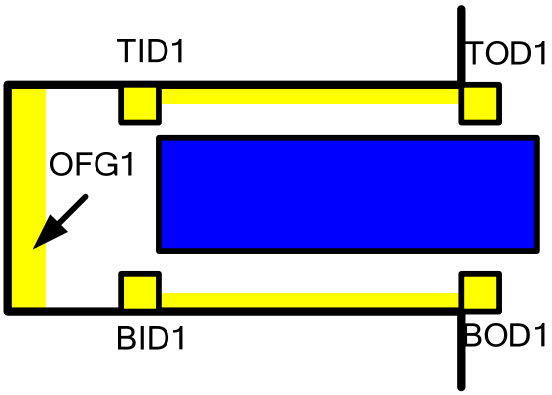

Figure 4-3 Schematic of oil starvation in the top ring groove

Table 4-2 Boundary conditions for oil starvation

Boundary Conditions	Value (um)
TOD1	10
TID1	10
OFG1	10%
BID1	10
BOD1	10

1st ring ID **1st ring OD**

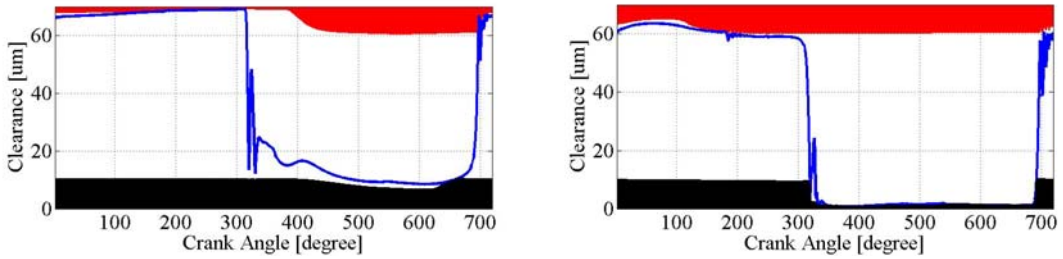

Figure 4-4 Oil film thickness and gas channel clearance at 1st ring ID and OD under 10-10-10%-10-10

4.1.2 Oil Filling the Lower First Ring Groove

To simulate the start of oil filling the lower 1st ring groove shown in Figure 4-5, only the BOD1 boundary condition has been changed from 10um to 40um, as shown in Table 4-3. Figure 4-6 shows the oil film thickness and gas channel clearance at the 1st ring IDs and ODs during this process. Everything is almost the same at 1st ring IDs as shown in section 4.1.1, but due to the variation of BOD1 the lower oil film thickness at BOD1 is much larger than that in Figure 4-4 and the gas channel at OD reduces when the OD of the top ring lifts upwards. Consequently, the oil flow rates increases at BOD1 as shown in

Figure 4-7. The oil flow rates at TID1 and TOD1 are very similar under 10-10-10-10-10% and 10-10-10-40-10%. Due to the BOD1's effect, more oil flows out in the vicinity of BOD1 at later compression stroke and is pumped into the lower 1st ring groove at later exhaust stroke under 10-10-10-40-10%. When the size of BOD1 becomes larger, more oil is pumped into the 1st ring groove in a whole cycle. In Figure 4-7, the positive flow rate means the oil flows along the 1st ring groove from TOD1 to BOD1, while the negative values are vice versa.

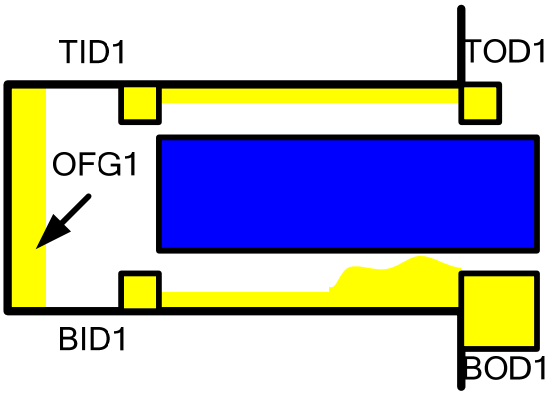

Figure 4-5 Schematic of oil filling the lower 1st ring groove

Table 4-3 Boundary conditions for oil filling the lower 1st ring groove

Boundary Conditions	Value (um)
TOD1	10
TID1	10
BID1	10
BOD1	40
IOFG1	10%

1st ring ID **1st ring OD**

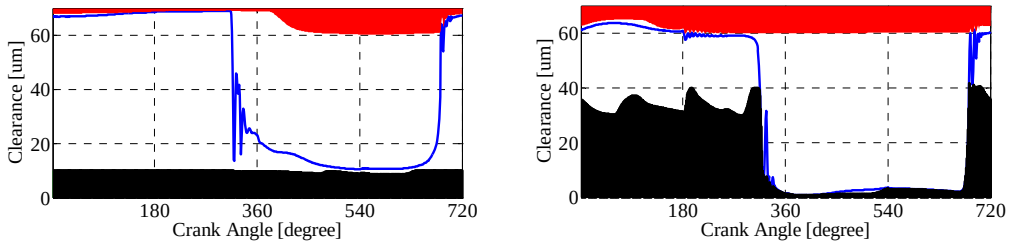

Figure 4-6 Oil film thickness and gas channel clearance at 1st ring IDs and ODs under 10-10-10-40-10%

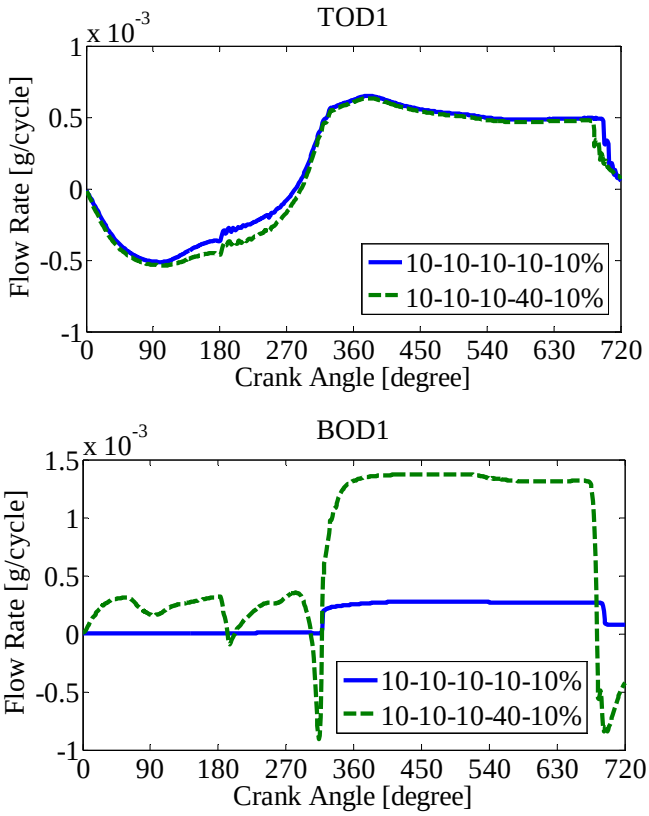

Figure 4-7 Accumulated oil flow rates at 1st ring TOD1 and BOD1 under 10-10-10-10-10% and 10-10-10-40-10%

The size of the oil reservoir at BID1 is set as 40um to simulate the phenomenon that the lower 1st ring groove is filled with oil, as shown in Figure 4-8. The boundary conditions for oil flooded in the lower 1st ring groove are listed in Table 4-4. Compared to Figure 4-6, the ring motion from later compression stroke to later exhaust stroke is severely affected by the variation of the oil film thickness at both IDs and ODs as shown in Figure 4-9. Because the space for the top ring to lift up and down diminishes, the lower ring flank comes into contact with the lower oil film in the late compression stroke. Large oil film thickness on the lower flank provides more damping when the ring travels toward the lower flank and results in much smoother ring motion trajectory than the previous case shown in Fig. 4-6. At both IDs and ODs, the lower gas channel space is very limited, and the lower ring flank attaches to the oil film tightly, thereby affecting the ring motion in the late exhaust stroke. The ring cannot lift up at that time, making the start point of the next cycle different for the top ring.

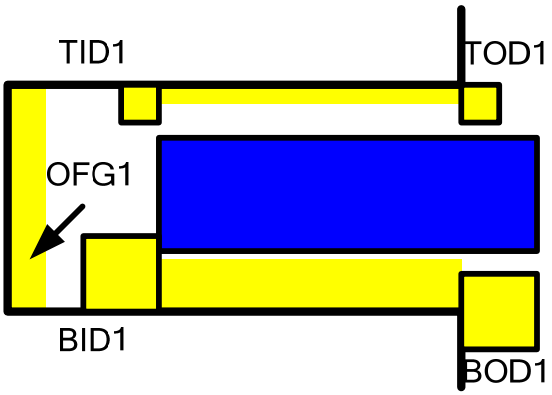

Figure 4-8 Schematic of oil flooded in the lower 1st ring groove

Table 4-4 Boundary conditions for oil flooded in lower 1st ring groove

Boundary Conditions	Value (um)
TOD1	10
TID1	10
BID1	40
BOD1	40
IOFG1	10%

1st ring ID **1st ring OD**

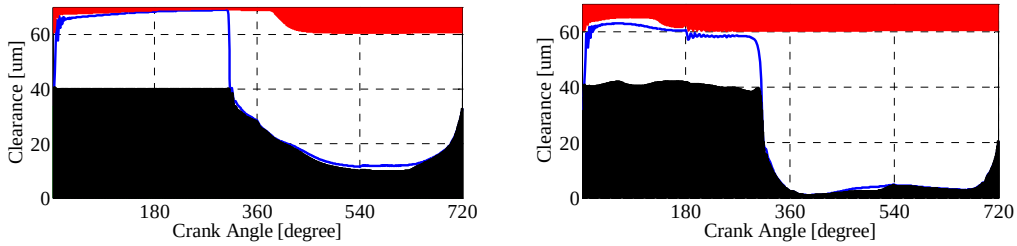

Figure 4-9 Oil film thickness and gas channel clearance at 1st ring ID and OD under 10-10-40-40-10%

For the oil flow rates in the 1st ring grooves, the ring dynamics plays a crucial role here. In Figure 4-10, at the beginning of a cycle, the 1st ring stays in the middle within the gas. Immediately, during the early intake stroke, the ring lifts upwards, which causes more oil to flow out of the upper 1st ring groove in the vicinity of TOD1 and more oil is pumped into the lower 1st ring groove at BOD1. The difference exists between this phenomenon and that the 1st ring remaining at a much higher position shown in Figure 4-6, which is due to the thickening of the oil film in the lower 1st ring groove. This increasing thickness influences the 1st ring dynamics. During the late exhaust stroke, there is no oil flow out of upper 1st ring groove at TOD1, but more oil is pumped into lower 1st ring groove at BOD1.

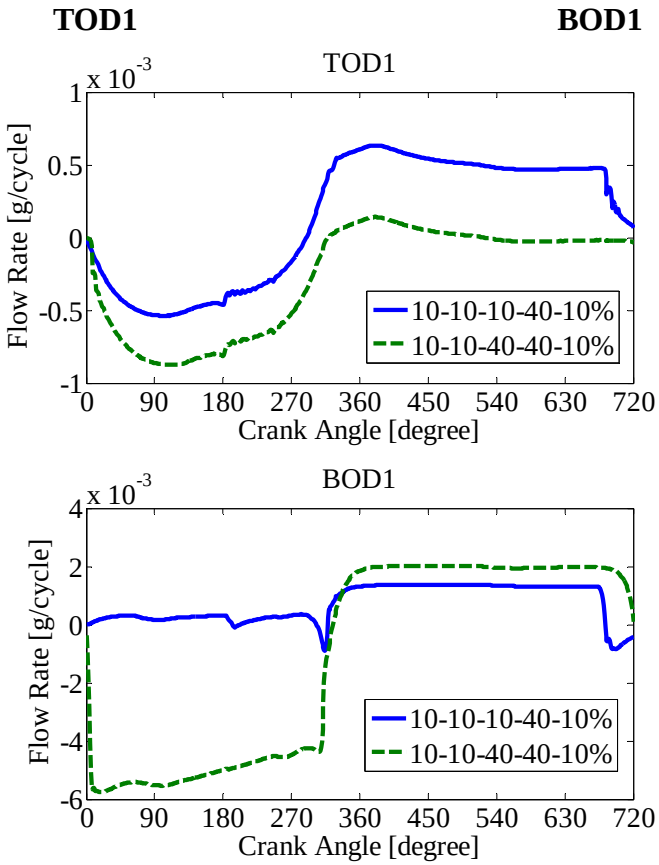

Figure 4-10 Accumulated oil flow rates at 1st ring TOD1 and BOD1 under 10-10-10-40-10% and 10-10-40-40-10%

4.1.3 Oil Filling the inside of the First Ring Groove

After the lower 1st ring groove is filled with oil, it is the time for the inside 1st ring groove to be occupied by oil in Figure 4-11. As shown in Table 4-5, the initial oil filling fraction becomes 90% to see what the differences are between this situation and the prior one. Figure 4-12 shows there is no explicit difference for the top ring motion and oil film distribution at both IDs and ODs. It can be explained that the oil film distribution in the 1st ring grooves is dominated by the boundary conditions at IDs and ODs. The tiny difference of oil flow rates at both TOD1 and BOD1 between 10-10-40-40-10% case and 10-10-40-40-90% case in Figure 4-13 comes from the gas dragging effect, which is affected by the oil filling fraction inside the 1st ring groove. The more oil inside the 1st ring groove, the less space for gas transport. Thus, less gas flows through 1st ring groove as well.

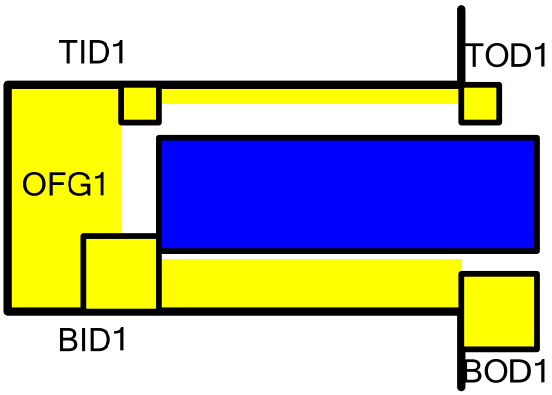

Figure 4-11 Schematic of oil filling the inside of the 1st ring groove

Table 4-5 Boundary conditions for oil filling the inside of the 1st ring grooves

Boundary Conditions	Value (um)
TOD1	10
TID1	10
BID1	40
BOD1	40
IOFG1	90%

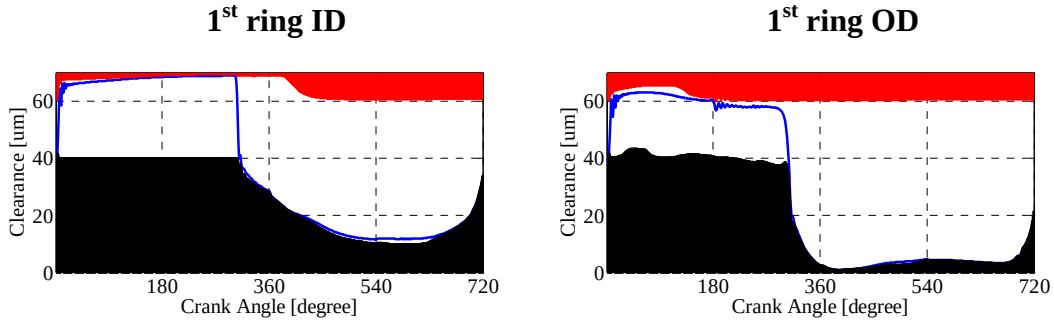

Figure 4-12 Oil film thickness and gas channel clearance at 1st ring ID and OD under 10-10-40-40-90%

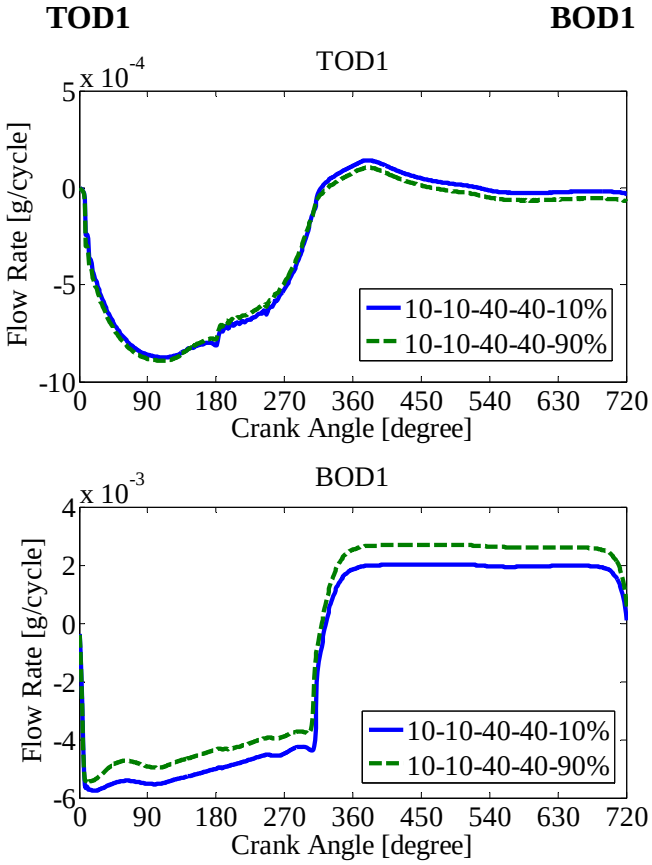

Figure 4-13 Accumulated oil flow rates at 1st ring TOD1 and BOD1 under 10-10-40-40-10% and 10-10-40-40-90%

4.1.4 Oil Filling the Upper First Ring Groove

In this section, oil begins to fill the upper 1st ring groove, as shown in Figure 4-14. In Table 4-6, BID1 is 40um. The ring dynamics shown in Figure 4-15 are totally different from those shown in Figure 4-4, Figure 4-6, Figure 4-9, and Figure 4-12 after the late compression stroke. The 1st ring continues to move downwards till the 1st ring stops in the vicinity of BOD1 and thus reaches the lower piston flank in the early expansion stroke. At this time, because the upper oil film thickness can surpass 40um and contact the upper flank of the 1st ring, blocking the gas channel in the upper 1st ring groove, the gas inside the 1st ring groove leaks through the lower 1st ring groove and therefore the 1st ring lifts up from the early expansion stroke on.

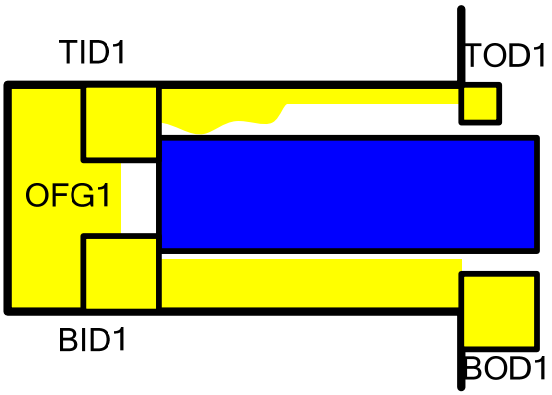

Figure 4-14 Schematic of oil filling the upper 1st ring groove

Table 4-6 Boundary conditions for oil filling the upper 1st ring groove

Boundary Conditions	Value (um)
TOD1	10
TID1	40
BID1	40
BOD1	40
IOFG1	90%

1st ring ID **1st ring OD**

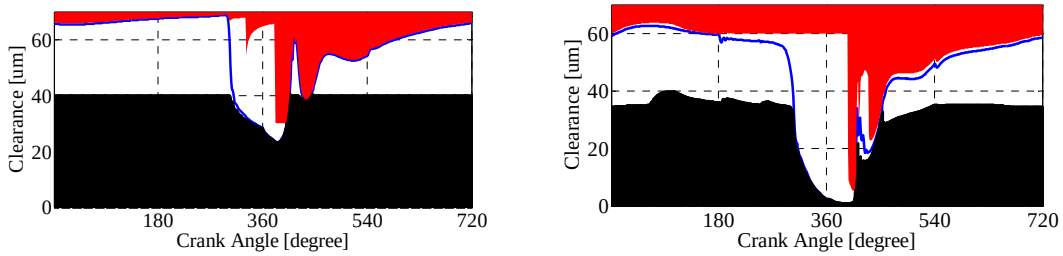

Figure 4-15 Oil film thickness and gas channel clearance at 1st ring ID and OD under 10-40-40-40-90%

The 1st ring's interaction with the upper oil film makes the oil flow out of the upper 1st ring groove increase dramatically as shown in Figure 4-16. Without the limitation of the 1st ring, the faster lower oil flow is driven by the larger pressure difference between inside of the 1st ring groove and on the 2nd land in the early expansion stroke. With the larger TOD1 and TID1 boundary conditions, and the more cycles that the program runs, the gas channel in the upper 1st ring groove is probably filled with oil in Figure 4-15.

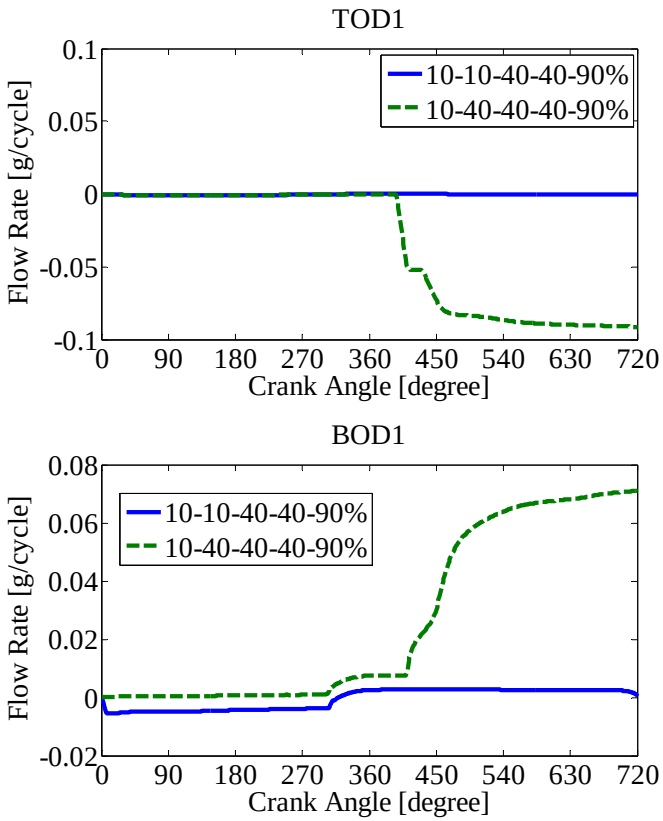

Figure 4-16 Accumulated oil flow rates at 1st ring TOD1 and BOD1 under 10-10-40-40-90% and 10-40-40-40-90%

4.1.5 Oil Flooded in the First Ring Groove

After a large amount of oil reaches the vicinity of TOD1, both the lower and upper 1st ring groove and inside the 1st ring groove are flooded with oil, as shown in 4-17. Under the boundary conditions in Table 4-7, the ring dynamics shown in Figure 4-18 are similar to that of the prior case. However, more oil fills the upper 1st ring groove during the compression stroke and early expansion stroke. At this time, cylinder pressure is higher than the pressure inside the 1st ring groove. Therefore, the larger BOD1 is, the more oil fills the upper 1st ring groove and affects the development of the whole upper oil film. The same explanation is given to the difference between the accumulated oil flow rates at the 1st ring TOD1 and BOD1 under 10-40-40-40-90% and 40-40-40-40-90% in Figure 4-19.

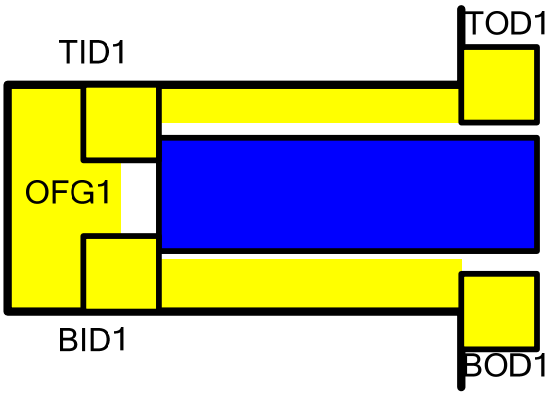

Figure 4-17 Schematic of oil flooded in the 1st ring groove

Table 4-7 Boundary conditions for oil flooded in the 1st ring groove

Boundary Conditions	Value (um)
TOD1	40
TID1	40
BID1	40
BOD1	40
IOFG1	90%

1st ring ID **1st ring OD**

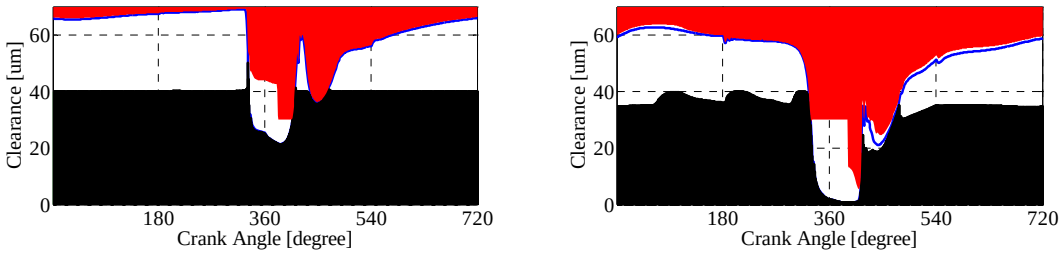

Figure 4-18 Oil film thickness and gas channel clearance at 1st ring ID and OD under 40-40-40-40-90%

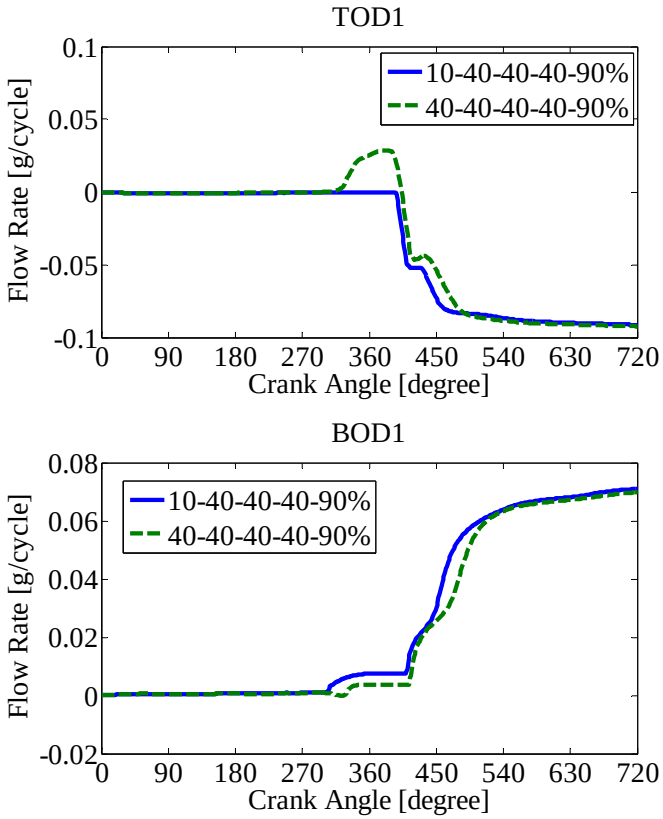

Figure 4-19 Accumulated oil flow rates at 1st ring TOD1 and BOD1 under 10-40-40-40-90% and 40-40-40-40-90%

4.1.6 Pressure Difference and Extra Blowby Gas

To clarify the effects of the boundary conditions on the extra blowby gas through the 1st ring groove, the cylinder pressure, pressure inside the 1st ring groove, and pressure on the 2nd land are compared in Figure 4-20 and Figure 4-21. The difference in the pressure curves in these two figures can be classified into two groups by considering the ring dynamics effect. One group recognizes that the 1st ring cannot lift from the early expansion stroke on. In this group, there is no significant difference between the pressure traces. Another group recognizes that the 1st ring can lift. The pressure inside the 1st ring groove is higher than cylinder pressure from the early expansion stroke on as shown in Figure 4-20. That is the reason why the 1st ring can lift under these boundary conditions. As discussed earlier, the oil film in the vicinity of TID1 blocks the gas channel, and thus the gas cannot leak through the upper 1st ring groove. This effect is also shown in Figure 4-21.

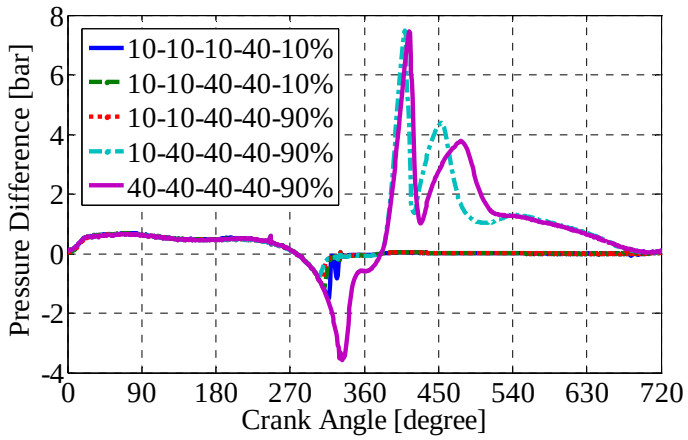

Figure 4-20 Differences between pressures inside the 1st ring grooves and cylinder pressure

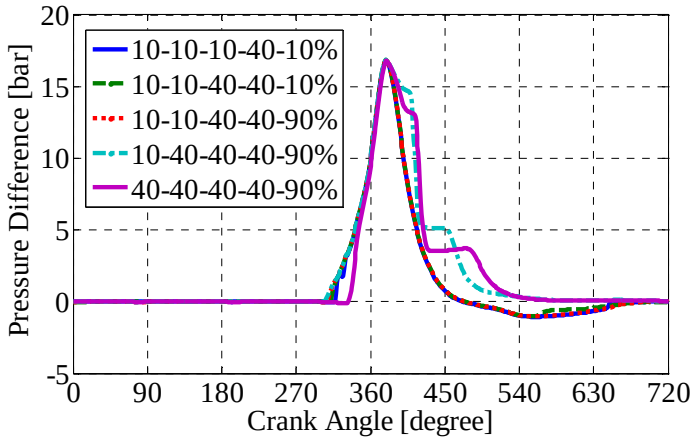

Figure 4-21 Pressure differences between inside the 1st ring grooves and on the 2nd land

4.2 Steady State Analysis under Lower Intake Pressure

Similar steady state analysis presented in section 4.1 is performed under lower intake pressure. In this section, Figure 4-22 is the Cylinder pressure under 150mbar intake pressure at 3500 RPM with the engine not firing. Such a condition would be typical of a moderate speed deceleration when the fuel is shut off to assist engine braking. As can be seen in Figure 4-22, under motored conditions, the peak pressure is approximately around 3.2 bars at closed throttle. This is comparable to the crankcase pressure, which remains near atmospheric pressure under all conditions.

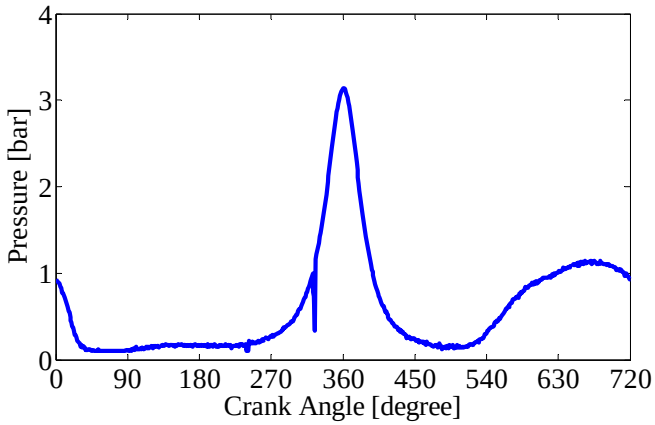

Figure 4-22 Cylinder pressure under 150mbar intake pressure at 3500 RPM

As shown from Figure 4-23 to Figure 4-26, the effect of the oil film thickness for low load conditions on 1st ring dynamics is not as obvious as that was presented for high loading in section 4.1. Due to the small pressure differences shown in Figure 4-27 and Figure 4-28, the 1st ring always stays attached with the upper oil film. The pressure distribution in both the upper and lower 1st ring groove is shown in Figure 4-29 and Figure 4-30. The balance of forces and moments for the 1st ring is analyzed and proves the stability of the 1st ring, as shown in Figure 4-31 and Figure 4-32. The accumulated oil flow rates at the 1st ring TOD1 and BOD1 are also not very sensitive to boundary conditions, as shown in Figure 4-33. In fact, the oil flow in the vicinity of BOD1 is greater than at TOD1, and, thus, the oil keeps filling the 1st ring groove. Because of the small pressure differences, the stability of the 1st ring is clearly demonstrated here, however, the dynamic oil filling process inside the 1st ring groove will be observed explicitly in sect 4.3.

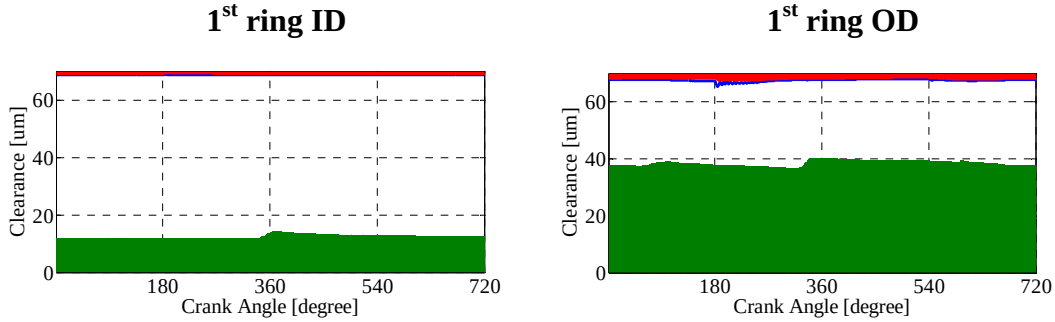

Figure 4-23 Oil film thickness and gas channel clearance at 1st ring ID and OD

under the 10-10-10-40-10% condition

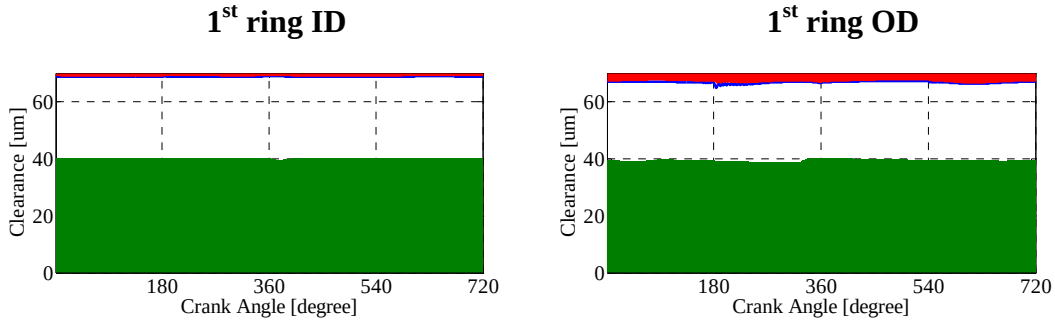

Figure 4-24 Oil film thickness and gas channel clearance at 1st ring ID and OD under the 10-10-40-40-10% condition

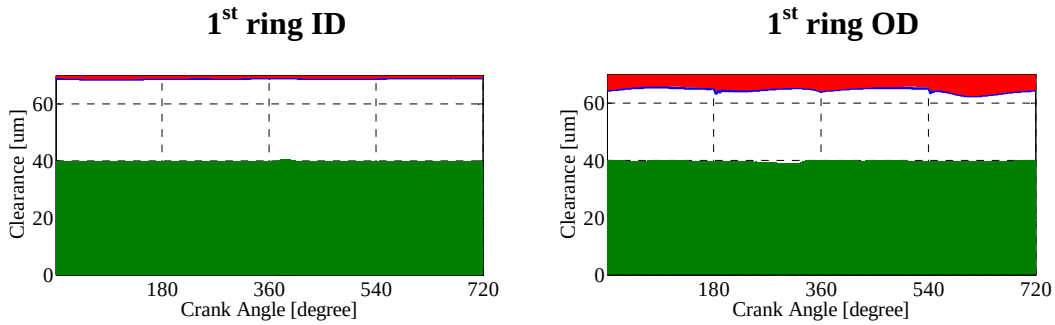

Figure 4-25 Oil film thickness and gas channel clearance at 1st ring ID and OD under the 10-10-40-40-90% condition

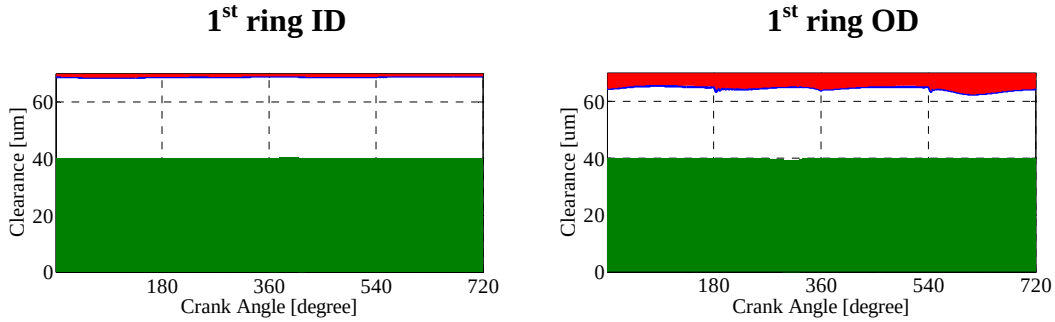

Figure 4-26 Oil film thickness and gas channel clearance at 1st ring ID and OD under the 40-40-40-40-90% condition

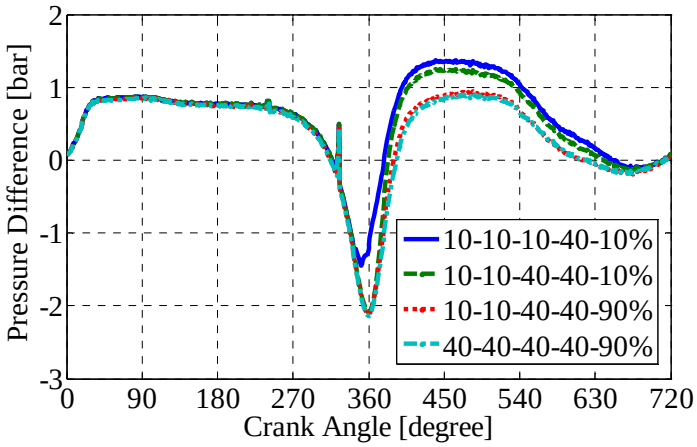

Figure 4-27 Differences between the pressure inside of the 1st ring groove and the cylinder

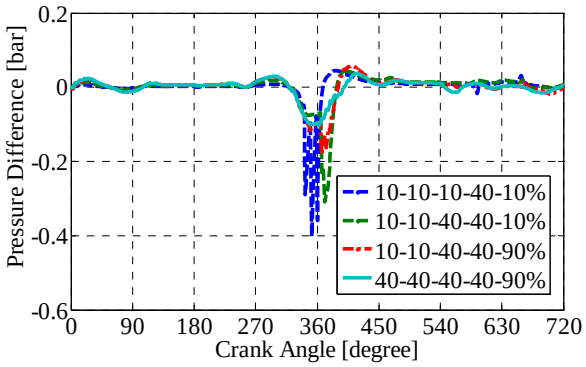

Figure 4-28 Pressure differences between the inside of the 1st ring groove and on the 2nd land

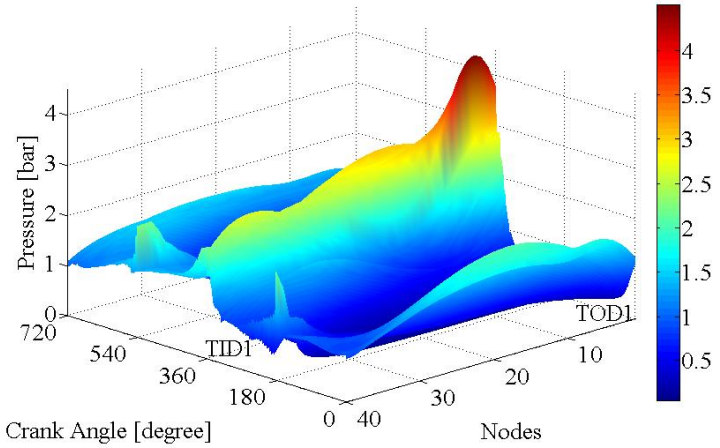

Figure 4-29 Pressure distribution in the upper 1st ring groove

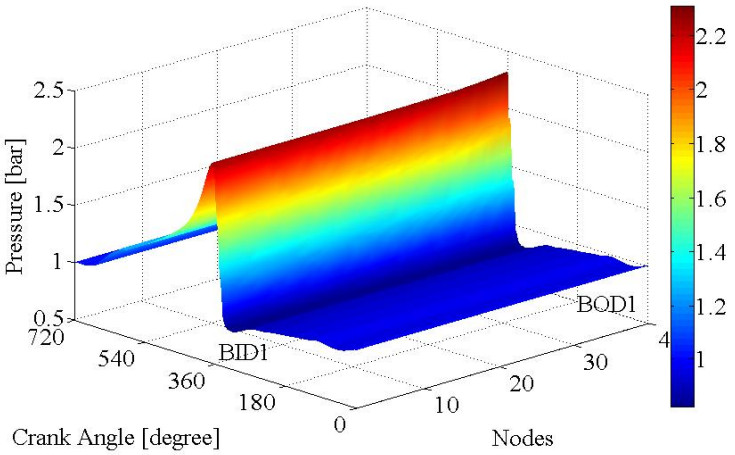

Figure 4-30 Pressure distribution in the lower 1st ring groove

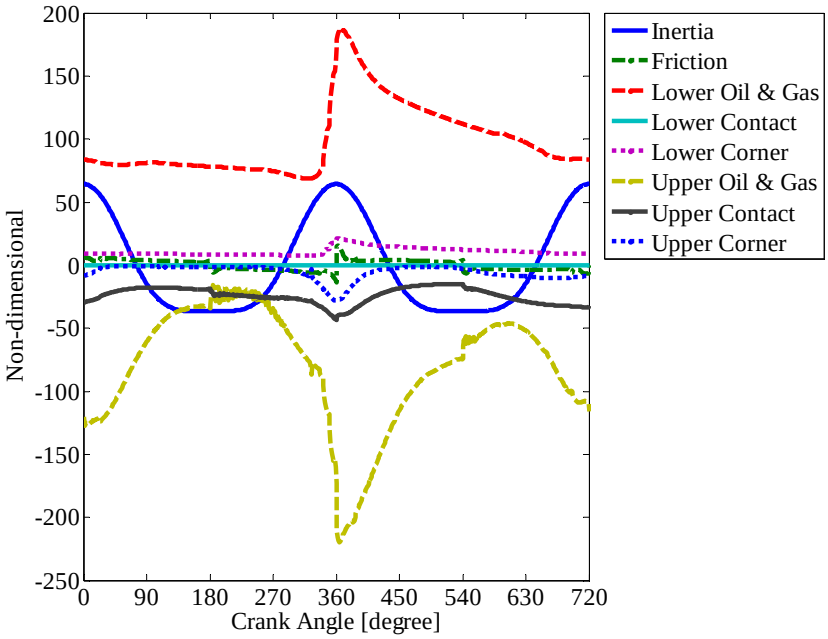

Figure 4-31 Force balance for the 1st ring

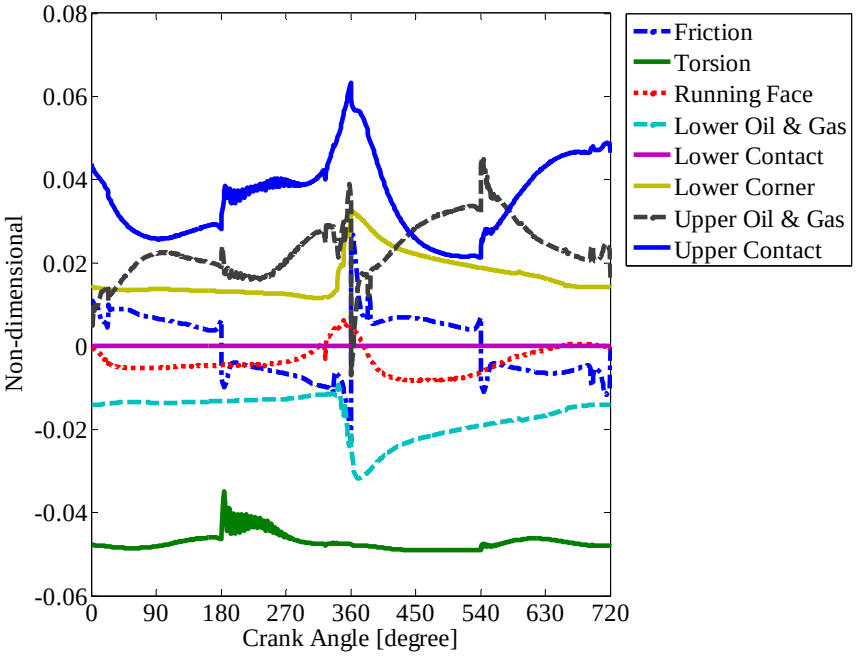

Figure 4-32 Moment balance for the 1st ring

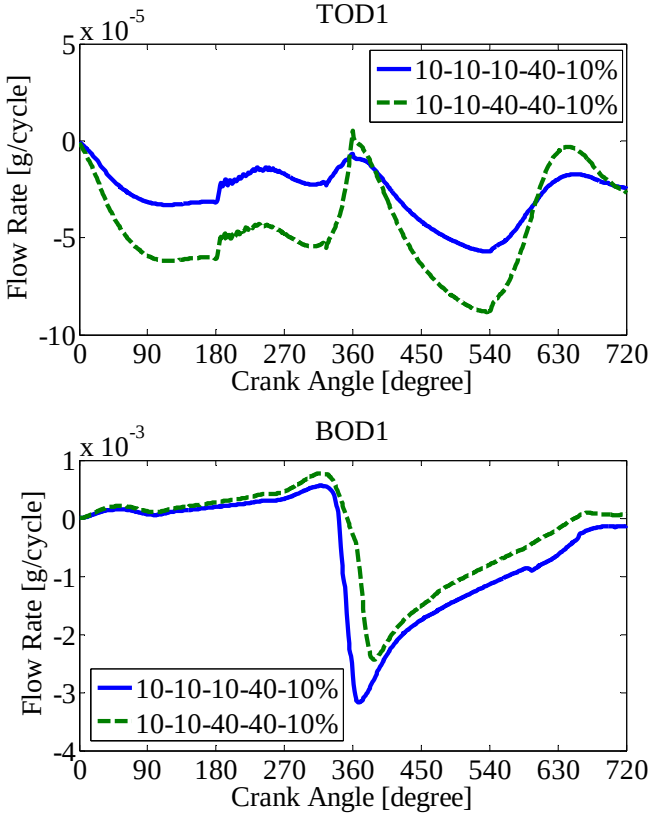

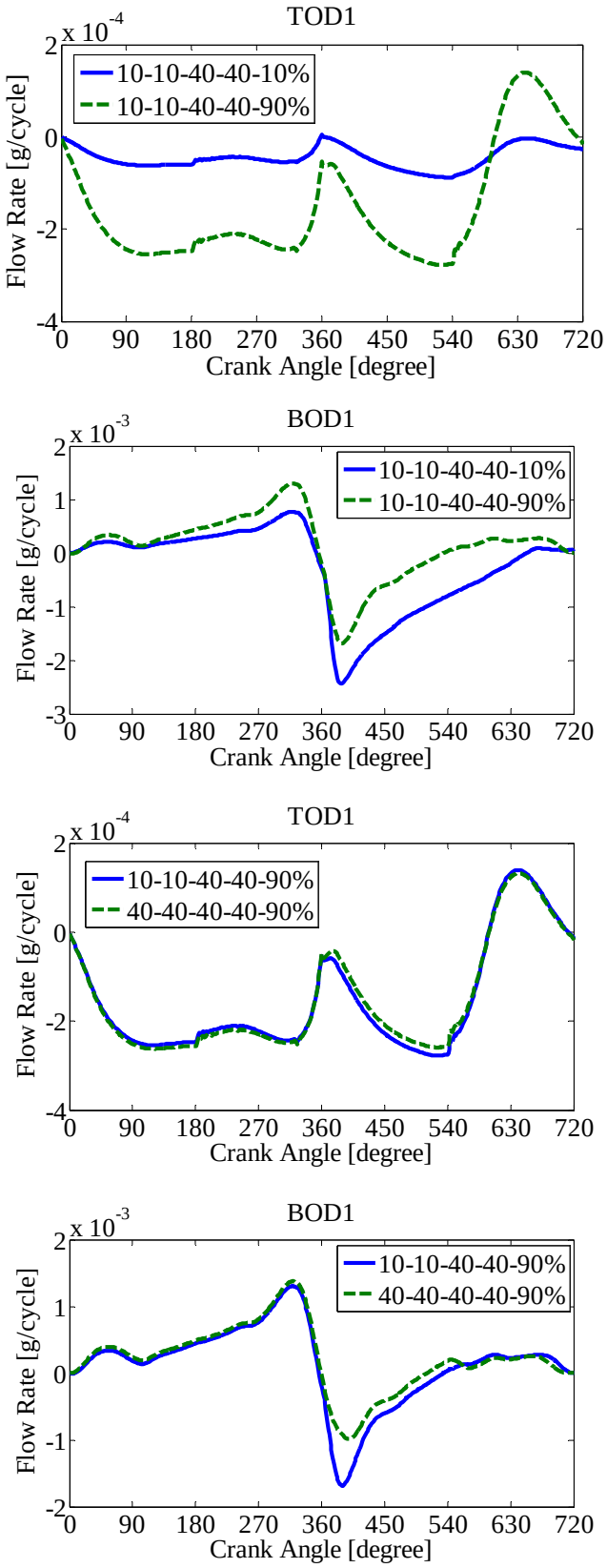

Figure 4-33 Accumulated oil flow rates at 1st ring TOD1 and BOD1 under different boundary conditions

4.3 Transient State Analysis

Analysis of the transient state, that is, transitioning from higher to lower intake pressure, or vice versa, is performed in this section. In the first case, the intake pressure is 110mbar, and the cylinder pressure trace as well as the 2nd land pressure trace is shown in Figure 4-34. The engine specifications are the same as in Table 4-1 and the boundary conditions are shown in Table 4-10.

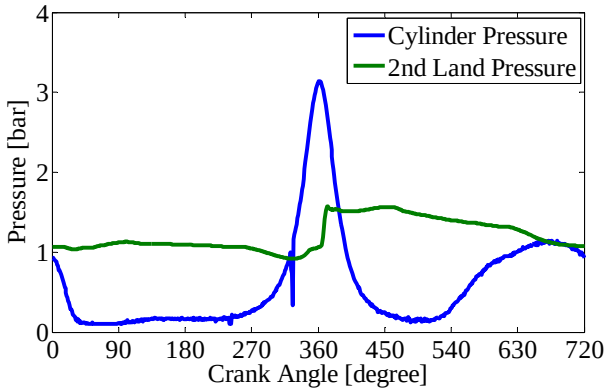

Figure 4-34 Cylinder and 2nd land pressure under 110mbar intake pressure at 3500 RPM

Table 4-8 Boundary conditions for transient state analysis under 110mbar intake pressure

Boundary Conditions	Value (um)
TOD1	5
TID1	5
BID1	5
BOD1	40

Due to the difference between the cylinder pressure and the 2nd land pressure shown in Figure 4-35, oil flows from the top ring groove bottom OD to the upper OD. Therefore, the boundary condition BOD1 decides the amount of oil flow into the top ring groove.

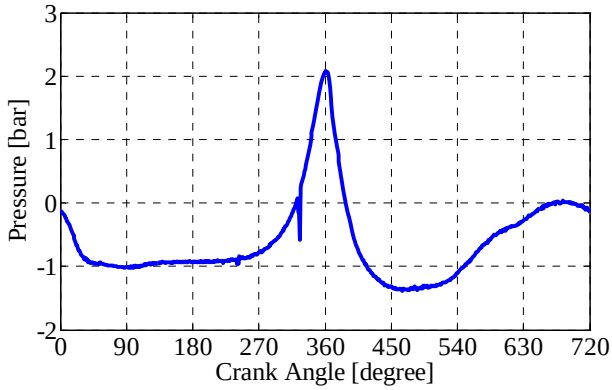

Figure 4-35 Pressure difference under 110mbar intake pressure at 3500 RPM

The transient oil filing process in the 1st ring groove is shown in Figure 4-36. The upper line in each graph is the lower 1st ring flanks and the curve under it is the upper bounds of oil film. The explanation of this process is given as follows:

- The 1st cycle: the ring can move down to the lower ring groove flank during the expansion stroke. There is less oil at the BOD1 and therefore the ring experiences negative twists at the bottom;
- The 2nd cycle: the ring moves down to the lower ring groove flank during the expansion stroke, but there is more oil at the BOD1 and therefore the negative twist angle is reduced;
- The 3rd cycle: the ring cannot move down as in the cycle before due to the addition of oil, that filled at BOD1;
- The 5th cycle: more oil accumulates from BOD1 to BID1;
- The 10th cycle: lower ring groove has almost been filled;
- The 100th cycle: lower ring groove has been completely filled.

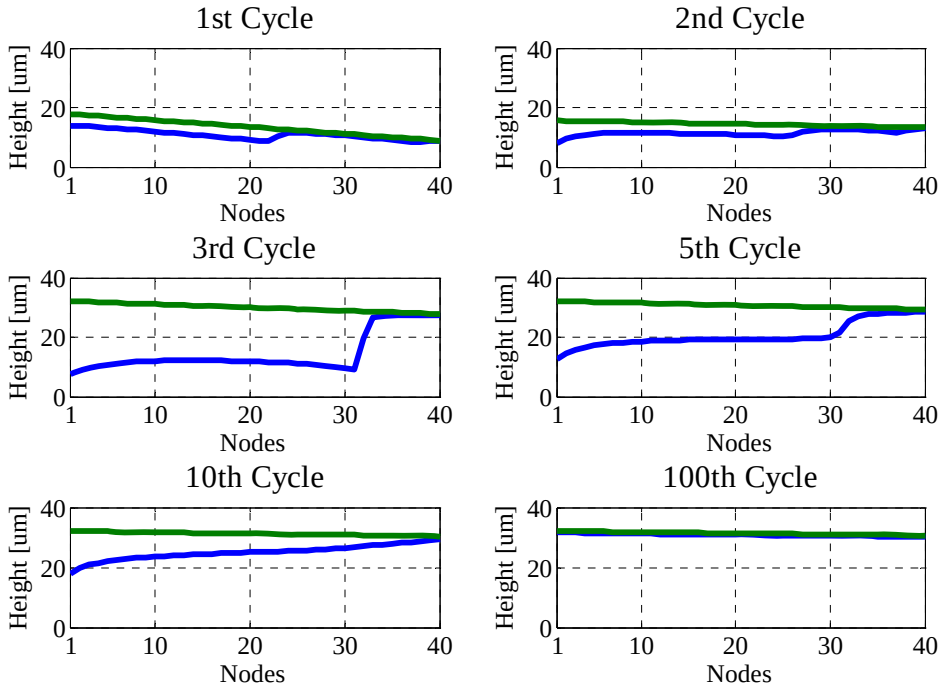

Figure 4-36 Clearance and oil film thickness in the lower 1st ring groove at 363 CAD

Figure 4-37 demonstrates the whole transient oil filling process inside the 1st ring grooves from the 1st cycle to around the 125th cycle.

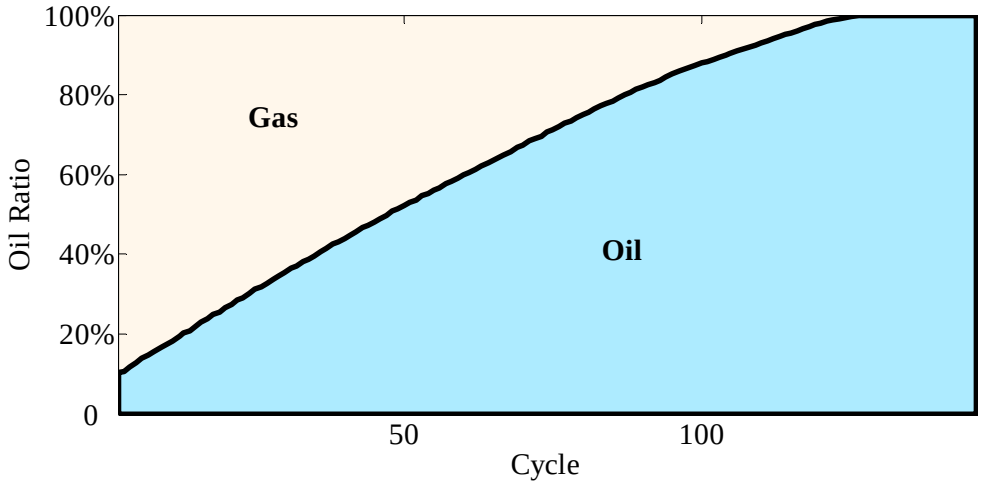

Figure 4-37 Transient oil filling process inside the 1st ring grooves under 110mbar intake pressure

For the next case, the intake pressure is 500mbar, and the cylinder pressure as well as the 2nd land pressure is shown in Figure 4-1. The engine specifications are the same as in Table 4-1 and the boundary conditions are shown in Table 4-3. Figure 4-38 indicates that the oil keeps leaking out of the 1st ring groove from a 90% oil occupation ratio to around 10%. This is a result of the pressure difference between the sub-regions before the early expansion stroke in every cycle. In this computation, the boundary conditions for TID1

and BID1 do not change with the amount of oil accumulated inside the 1st ring groove. These parameters should increase or decrease at the same rate. If so, after the effect of the upper oil film on the 1st ring dynamics described in 4.1.4 is considered, the oil leakage rate is probably higher than shown in Figure 4-38.

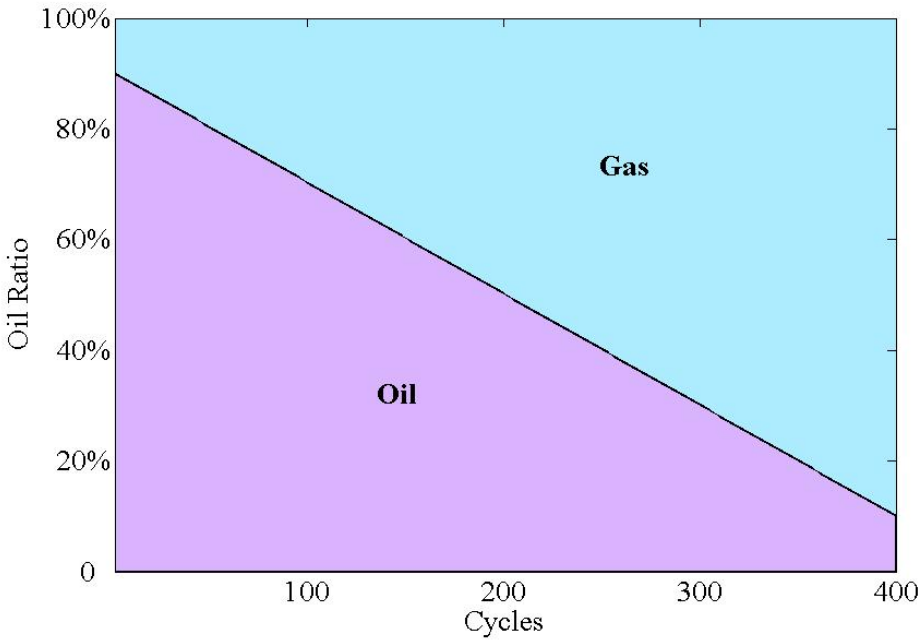

Figure 4-38 Transient oil filling process inside the 1st ring grooves under 500mbar intake pressure

4.4 Conclusion

The coupled model is applied to analyze the oil and gas transport in the first ring grooves at low load in SI engine in this chapter. Both steady state and transient state analyses are performed to clarify the effect of the oil film present in the 1st ring groove on oil consumption and blowby gas.

In the steady state analysis, five boundary conditions for the 1st ring groove were changed to demonstrate the following phenomena: oil starvation; oil filling the lower groove, inside the groove, and upper groove; and oil flooded everywhere. Under higher intake pressure, the oil film thickness in the lower 1st ring groove dictates the magnitude when the 1st ring moves down and therefore dictates the size of the gas channel. The oil film thickness in the upper 1st ring groove strongly affects the ring's dynamics from the early expansion stroke on, increasing both the oil consumption and blowby gas. However, under lower intake pressure, the effect of the oil film thickness on oil consumption and blowby gas is not the same intensity as under higher intake pressure. This is due to the smaller pressure differences between the different sub-regions.

In the transient state analysis, the dynamic oil filing process inside the 1st ring groove under lower intake pressure was demonstrated. Due to the lower cylinder pressure, after several cycles, the space inside 1st ring groove is filled with oil. However, under higher intake pressure, the oil inside 1st ring groove flows through the lower 1st ring groove.

(This page was intentionally left blank)

Chapter 5 Summary

The thesis was intended to be a modeling work on the interaction between ring dynamics and oil and gas transport along ring-pack systems under steady and transient state in internal combustion engines. A 2-D coupled ring dynamics and gas and oil transport model was developed. In this coupled model, oil in the ring grooves and on the lands, oil pumping between a ring and its groove, asperity contact between ring and piston flanks, gas flow through a ring gap, and other specifications for piston and ring design are considered.

Then, the coupled model is applied to the analysis of a heavy duty diesel engine. Ring dynamics, force and moment balance of the rings, and gas and oil transport analyses are carried out. The 1st ring always stays on the oil film attached to the piston flank of the lower 1st ring groove, and the 2nd ring moves up and down due to the inertial force of the axial acceleration/deceleration of the piston. The oil film distribution shown for these two rings demonstrates the oil pumping phenomena at different portions of the 4-stroke cycle. The 2nd ring cannot flutter when its lower groove is flooded with oil, which causes the pressure inside the 2nd ring groove to exceed the 2nd land pressure during the early expansion stroke.

In addition, the coupled model is applied to analyze the oil and gas transport in the first ring grooves at low load operation in an SI engine. In the steady state analysis, under high intake pressure, the oil film thickness in the lower 1st ring groove decides the magnitude of which the 1st ring moves down and, thus, decreases the size of the gas channel there. The oil film thickness in the upper 1st ring groove can strongly affect the 1st ring dynamics from the early expansion stroke on. This increases both the oil consumption and blowby gas, both of which do not occur under low intake pressure. In the transient state analysis, under low intake pressure, the 1st ring groove is filled with oil, but under high intake pressure, the oil in the 1st ring grooves flows through the lower 1st ring groove.

Results from the coupled model correlate well with experimental measurements that have been previously conduct. Such correlation indicates the practical value of these tools.

(This page was intentionally left blank)

References

1. Nakada, M., "Piston and Piston Ring Tribology and Fuel Economy," Proceedings of Internal Tribology Conference, Yokohama, 1993.
2. Heywood, J. B., Internal Combustion Engine Fundamentals, McGraw-Hill, 1988.
3. Tian, T., 2002, "Dynamic Behaviors of Piston Rings and Their Practical Impact. Part 1: Ring Flutter and Ring Collapse and Their Effects on Gas Flow and Oil Transport," Proc IMechE, Part J: Journal of Engineering Tribology, Vol. 216, pp. 209-227
4. Tian, T., 2002, "Dynamic Behaviors of Piston Rings and Their Practical Impact. Part 2: Oil Transport, Friction, and Wear of Ring/Liner Interface and the Effects of Piston and Ring Dynamics," Proc IMechE, Part J: Journal of Engineering Tribology, Vol. 216, pp. 229-247
5. Tian, T., Noordzij, L. B., Wong, V. W., and Heywood, J. B., 1998, "Modeling Piston-Ring Dynamics, Blowby, and Ring-Twist Effects," ASME Transaction - JOURNAL OF ENGINEERING FOR GAS TURBINES AND POWER, Vol.120, pp.8 43 -85 4.
6. Tian, T., Rabute, R., Wong, V. W., and Heywood, J. B., 1997, "Effects of Piston-Ring Dynamics on Ring/Groove Wear and Oil Consumption in a Diesel Engine," SAE Paper 970835
7. Tian, T., Wong, V. W., and Heywood, J. B., 1996, "A Piston Ring-Pack Film Thickness and Friction Model for Multigrade Oils and Rough Surfaces," SAE Paper 962032.
8. Liu, L., Tian, T., and Rabute, R., 2003, "Development and Application of an Analytical Tool for Piston Ring Design," SAE Paper 2003-01-3112.
9. Liu, L. and Tian, T., 2005, "Modeling Piston Ring-Pack Lubrication with Consideration of Ring Structural Response," SAE Paper 2005-01-1641.
10. Liu, L., Tian, T., 2004, "A Three-Dimensional Model for Piston Ring-Pack Dynamics and Blow-by Gas Flow," ASME ICE Fall Technical Conference, ICE 2004-968.
11. Liu, L., Tian, T., 2005, "Implementation and Improvements of a Flow Continuity Algorithm in Modeling Ring/Liner Lubrication," SAE Paper 2005-01-1642.
13. Tian, T., 1997, "Modeling the Performance of the Piston Ring-Pack in Internal Combustion Engines," Ph.D. Thesis, MIT.
14. Yilmaz, E., 2003, "Sources and Characteristics of Oil Consumption in a Spark-Ignition Engine," Ph.D. Thesis, MIT.
15 Furuhama, S.; Hiruma, M.; Tsuzita, M.: "Piston Ring Motion and Its Influence on Engine Tribology," SAE Paper 790860, 1979.
16 Stecher, F.: "Analysis of Piston Ring Packs for Combustion Engines," SAE Paper 790863, 1979.
17 McGeehan, J. A.: "A Survey of the Mechanical Design Factors Affecting Engine Oil Consumption," SAE Paper 790864, 1979.
18 Thirouard, B.; Tian, T.: "Oil Transport in the Piston Ring Pack (Part II): Zone Analysis and Macro Oil Transport Model," SAE Paper 2003-01-1953. 2003.
19 Ariga, S.: "Observation of Transient Oil Consumption with In-Cylinder Variables," SAE Paper 961910, 1996.

20 Tian, T.: "Dynamic behaviours of piston rings and their practical impact. Part 1: ring flutter and ring collapse and their effects on gas flow and oil transport," Proc. Instn Mech Engrs, Vol. 216, Part J, Journal of Engineering Tribology, pp. 209-228, 2002.
21 Vokac, A.; Tian, T.: "An Experimental Study of Oil Transport on the Piston Third Land and the Effects of Piston and Ring Designs," SAE Paper 2004-01-1934, 2004.
22 McGeehan, J. A.: "A Survey of the Mechanical Design Factors Affecting Engine Oil Consumption," SAE Paper 790864, 1979.
23 Yoshida, H.; Yamada, M.; Kobayashi, H.: "Diesel Engine Oil Consumption Depending on Piston Ring Motion and Design," SAE Paper 930995, 1993.
24. Thirouard, B., 2001, “Characterization and modeling of the fundamental aspects of oil transport in the piston ring pack of internal combustion engines”, Ph.D. Thesis,
Department of Mechanical Engineering, MIT, June 2001
25. Thirouard, B., Tian, T., 2003, “Oil Transport in the Piston Ring Pack (Part I): Identification and Characterization of the Main Oil Transport Mechanisms”, SAE Paper 2003-01-1952.
26. Thirouard, B., Tian, T., 2003, “Oil Transport in the Piston Ring Pack (Part II): Zone Analysis and Macro Oil Transport Model”, SAE Paper 2003-01-1953. 27. Artzner, D., “Investigation of Oil Consumption Mechanisms in a Spark-Ignition Engine”, M.S. Thesis, Department of Mechanical Engineering, MIT, May 1996.
27. Keribar, R., Dursunkaya, Z., Flemming, M.F., 1991, “An Integrated Model of Ring Pack Performance”, Transactions of ASME, Journal of Engineering for GAas Turbines and power, Vol. 113, pp 382-389.
28. Dursunkaya, Z., Keribar, R., Richardson, D., 1993, “Experimental and Numerical Investigation of Inter-Ring Gas Pressures and Blow-by in a Diesel Engine”, SAE Paper 930792.
29. Ariga, S., 1996, “Observation of Transient Oil Consumption with In-Cylinder Variables”, SAE Paper 961910.
30. Zelenka, P., Kriegler, W., Herzog, P. L., Cartellieri, 1990, “Ways Toward the Clean Heavy Duty Diesel”, SAE Paper 900602.
31. Ejakov, M. A., Schock, H. J., Brombolich, L. J., Carlstrom, C. M., and Williams, R. L., 1997, "Simulation Analysis of Inter-Ring Gas Pressure and Ring Dynamics and Their Effect on Blow-by,", ASME Paper 97-ICE-50
32. F. M., White, 2003, Fluid Mechanics, McGraw-Hill, Fifth Edition.
33. Press, W. H., Teukolsky, S. A., Vetterling, W. T., and Flannery, B., 1992, Numerical Recipe, Cambridge University Press, Second Edition.
34. Greenwood, J. A. and tripp, J. H., "The Contact and Two Nominally Flat Surfaces," Proc. Inst. Mech. Engrs., Vol. 185, p. 625.
35. Hu, Y., Cheng, H.S., Arai, T., Kobayashi, Y. and Aoyama, S., 1993, "Numerical Simulation of Piston Ring in Mixed Lubrication – A Nonaxisymmetrical Analysis," ASME Journal of Tribology, 93-Trib-9.
36. Shapiro, A. H., "The Dynamics and Thermodynamics of Compressible Fluid Flow," Vol. I, the Ronald Press Company, New York, 1953
37. http://crd.lbl.gov/~xiaoye/SuperLU/
38. Przesmitzki, S., "Characterization of Oil Transport in the Power Cylinder of Internal

Combustion Engines during Steady State and Transient Operation," Ph.D. Thesis, Department of Mechanical Engineering, MIT, June 2008
39. Liu, L, "Development of a 2D Model for Oil Transport in Piston/Ring Packs" Consortium on Lubrication in IC Engines, MIT, October 2005